EFFECTS OF VERTICAL COMPONENT AND SPATIAL VARIATION OF GROUND MOTIONS ON BASE ISOLATED STRUCTURES

by

Cem Yılmaz

B.S., Civil Engineering, Istanbul Technical University, 2005

M.S., Structural Engineering, Istanbul Technical University, 2008

Submitted to the Institute for Graduate Studies in
Science and Engineering in partial fulfillment of
the requirements for the degree of
Doctor of Philosophy

Graduate Program in Civil Engineering

Boğaziçi University

2023

ACKNOWLEDGEMENTS

I would like to express my deep gratitude to my supervisor, Prof. Serdar Soyöz for his invaluable guidance and encouragement. This PhD thesis would not have been possible without his support and direction.

I would also like to thank to Prof. Kutay Orakçal and Prof. Ufuk Yazgan who provided me with assistance during the process of my thesis work. Their ideas, critiques, and contributions greatly contributed to the development of my thesis.

Last but not least, I am very thankful to my wife, Tuğçe Sezaioğlu Yılmaz. Her endless support, patience, and understanding helped me overcome all challenges during my studies. My dear wife, thank you again for your unwavering faith, love, and support throughout my thesis work. And, my son, Tuna who was born in the middle of thesis is one of my greatest inspirations. I hope I will be an inspiration for him.

ABSTRACT

EFFECTS OF VERTICAL COMPONENT AND SPATIAL VARIATION OF GROUND MOTIONS ON BASE ISOLATED STRUCTURES

In this study, the effects of vertical component and spatial variation of ground motions on base isolated structures with friction pendulum type of seismic isolators were investigated. The base isolated structures can have relatively long plan dimensions. The long plan dimensions are mainly preferred because of two reasons. Firstly, base isolated structures can be more tolerant to thermal expansions compared to conventional fix-based buildings. Increasing thermal expansions depending on the length of the building can be tolerated in base isolated structures. Secondly, operational difficulties may arise when seismic expansion joints are created between base isolated blocks due to the requirement of a significant seismic gap distance between the blocks. However, structures with longer plan dimensions require the examination for additional issues. The spatial variation of ground motion which occurs as a result of increasing foundation dimension can cause the structure to be subjected to nonuniform ground motion. In the common approach, it is assumed that the ground motion is uniform at every point below the structure. However, as the foundation length of the structure increases, the effect of the spatial variation becomes more significant and induce nonuniform motion under the structure. In this study, the effect of nonuniform ground motion on base isolated structures with friction pendulum type of isolators was investigated. The vertical component of earthquakes is a determinant factor in the design of friction type seismic isolators and the magnitude of horizontal loads to be transferred to the structure. Therefore, the effects of both uniform and spatially varying distribution of the vertical component of earthquakes were separately examined.

ÖZET

DEPREM DÜŞEY BİLEŞENİNİN VE DEĞİŞEREK YAYILAN YER HAREKETİNİN TABAN YALITIMLI BİNALAR ÜZERİNDEKİ ETKİLERİ

Bu çalışmada, uzayda değişerek yayılan yer hareketleri ve yer hareketlerinin düşey bileşenin sürtünmeli tip sismik izolatörler ile deprem yalıtımı sağlanmış yapılar üzerindeki etkileri incelenmiştir. Sismik izolatörler ile deprem yalıtımını sağlanan yapıların plan uzunlukları çok fazla olabilmektedir. Plan uzunluklarının fazla olması temel olarak iki sebebe dayanmaktadır. İlk olarak, deprem yalıtımlı yapılar, tabana ankstre konvansiyonel binalara kıyasla ısıl genleşmelere karşı daha toleranslı olabilmektedir. Bina uzunluğuna bağlı olarak artan ısıl genleşmeler sismik izolatörlü binalarda tolere edilebilmektedir. İkinci olarak, eğer sismik izolasyonlu dilatasyonlu bloklar oluşturulursa bloklar arasındaki sismik boşluk mesafe gereksinimin çok fazla olması nedeniyle operasyonel zorluklar ortaya çıkabilmektedir. Ancak, plan boyutları uzun olan yapılar bazı ilave konuların irdelenmesi ihtiyacını doğurmaktadır. Deprem dalgalarının mesafe bağlı olarak uzaysal değişime uğraması yapının düzgün olmayan yer hareketine maruz kalmasına sebep olmaktadır. Yaygın yaklaşımda, yer hareketinin yapının altındaki her noktada eşit olduğu kabul edilmektedir. Ancak, yapının temel boyutları uzadıkça yer hareketinin uzaysal değişimi önemli bir hale gelmekte ve yapı altında düzgün olmayan harekete sebep olmaktadır. Bu çalışma kapsamında, düzgün olmayan yer hareketinin sürtünmeli tip izolatörler ile deprem yalıtımı sağlanmış yapılar üzerindeki etkisi incelenmiştir. Deprem düşey bileşeni, sürtünmeli tip sismik izolatörlerin tasarımında ve yapıya aktarılacak yatay yükün büyüklüğünde belirleyici bir etken olmaktadır. Bundan dolayı deprem düşey bileşininin düzgün ve uzayda değişerek dağılımının etkileri ayrı ayrı incelenmiştir.

TABLE OF CONTENTS

LIST OF FIGURES

LIST OF TABLES

LIST OF SYMBOLS

A_b	Foundation area
A_{ik}	Fourier coefficients
$A^*_{s\beta}$	Best linear unbiased estimate
B	Foundation halfwidth
B_{ik}	Fourier coefficients
$B^*_{s\beta}$	Best linear unbiased estimate
c	Shear wave velocity
C_k	Covariance matrix
C_{aa}	Covariance matrix between known points
$C_{\alpha\beta}$	Covariance matrix between known and unknown points
$C_{\beta\beta}$	Covariance matrix between unknown points
d_{max}	Maximum displacement demand of isolator
d_t	Resultant displacement of isolator
d_x	Isolator displacement along X direction
d_y	Yield displacement of isolator
d_y	Isolator displacement along Y direction
f_c	Corner frequency
f_{ck}	Characteristic compressive strength of concrete
F_y	Yield force of isolator
g	Acceleration of gravity
G	Shear modulus of soil
$G(\omega_k)$	Power spectral density function
H_0	Filter amplitude threshold
kN	Kilonewton
K_1	Initial stiffness of isolator
K_2	Post-yield stiffness of isolator
K_x	Longitudinal direction stiffness of soil
K_y	Transverse direction stiffness of soil

K_z	Vertical direction stiffness of soil
L	Foundation semi-length
MPa	Megapascal
N	Total number of spatial location point
P	Axial load on column and isolator
R_e	Equivalent effective radius of curvature
r_{ij}	Relative distance
s	Distance scale parameter
T	Duration of time series
t	Time
T_{eff}	Effective stiffness of isolation system
V_s	Shear wave velocity of soil
w_t	Discrete frequency
x_i	Position vector
$Z_i(t)$	Known time series
α_k	Coefficients of autoregressive process
μ_e	Friction coefficient of pendulum isolator
ξ_{eff}	Effective damping
$\rho_{\omega k}(r_{ij})$	Coherency function
σ^2	One step prediction variance
ω_u	Cut-off frequency
φ_k	Independent random phase angles
Δt	Time step
$\Delta\omega$	Frequency step
ϑ	Poisson's ratio

LIST OF ACRONYMS/ABBREVIATIONS

AR	Autoregressive Model
BLUE	Best Linear Unbiased Estimator
FEM	Finite Element Model
FFT	Fast Fourier Transform
MESA	Maximum Entropy Spectral Analysis
PSDF	Power Spectrum Density Function
SGM	Strong Ground Motion
SS-1	Structure 1
SS-2	Structure 2
SVGM	Spatially Varying Ground Motion

1. INTRODUCTION

Earthquake is an important natural disaster in many parts of the world. When designing structures against earthquakes, engineers aim to create a structural system that can withstand the loads to be transferred to the superstructure due to ground motion. In addition, as an alternative to the conventional design, it can be aimed to dissipate the seismic energy that will occur due to ground motion. In this alternative approach, seismic isolators can be an important equipment.

However, in the structural design with seismic isolators, it is necessary to consider further issues beyond those in conventional design. This research aims to investigate effects of vertical component and spatial variation of strong ground motion on base isolated structures.

1.1. Objective

In this thesis, the vertical component of earthquakes and spatially varying ground motion have been investigated, which have significant effects on the structural design with friction pendulum isolators.

The horizontal load generated by the friction pendulum isolators is directly correlated with the axial load on the isolator. When the vertical component of the earthquake acts in the direction of gravity, the axial load on the isolators increases. As a result of the increase in the axial force, the amount of horizontal load acting on the isolators also increases. This leads to an increase in the total horizontal load transferred to the superstructure. Herewith, both the axial loads on the isolator and the horizontal loads transferred to the superstructure increase due to the vertical component of the earthquake.

Due to the difficulty of covering seismic gaps, structures with seismic isolators are usually designed as a single block. These structures, which are designed as a single block, can be quite long in plan. With an additional approach, seismic isolator structures can be deliberately designed as a single block since the additional stresses created by the thermal effects in the base isolated structures are less than conventional structures and the torsion can be eliminated by adjusting isolator effective stiffnesses in the base isolated structures. However, in these long structures designed as a single block, it is necessary to consider the spatial varying ground motion. The non-uniform distribution of ground motion can influence the horizontal loads transferred to the superstructure, isolator axial loads, column axial loads and isolator displacement demands.

By integrating the two issues described above (the vertical component of the earthquake and the spatially varying ground motion), the effects of these two issues on the structural design and isolator responses have been examined together.

1.2. Literature Review

1.2.1. Base Isolation Development

Although the first patented works were made at the end of the 1800s, academic and practical engineering studies have made important progress in the late 1970s and early 1980s. The Pestalozzi Elementary School in Macedonia and the Law and Justice Center in California can be cited as some examples of which have been designed during this period. In this period, elastomeric isolators were used for the base isolation technique. Early friction pendulum bearings did not produce restoring force and therefore started to be used after elastomeric bearings.

Kelly (1994) has conducted a study on the Implementation of base Isolation in the United States. The author gives a summary about development of base isolation. Moreover, he mentioned that the base isolation is also an effective technique for retrofit

of existing buildings. Furthermore, he indicated base isolated building with elastomeric bearings had provided expected performance at experienced earthquakes.

Tan and Weng (1996) investigated dynamic properties of isolated structures. The authors proposed a bilinear hysteretic model and applied it to mathematical model of Law and Justice Center building. They compared the results of mathematical model and accelerometers records instrumented before Upland Earthquake (1990). They concluded the suggested model is a feasible approach.

Some researchers carried out experimental study on seismic isolators. Anoop Mokha, Constantinou (1991) performed quarter-scale shake table test on a six-story building. They concluded that the structure remained elastic while peak table acceleration was about 1g. Bhasker Rao and Jangid (2001) performed shake table tests to evaluate performance of base isolated systems with elastomeric bearing and sliding bearing separately. They found a good agreement between analytical and experimental results. They concluded that both base isolation methods were effective to reduce dynamic responses. Moreover, they indicated that the sliding bearings should be associated with restoring force.

1.2.2. Studies on Vertical Component of Earthquake

After a better understanding of isolator dynamic properties, the effects of vertical excitation of strong ground motion on seismic isolators began to be investigated.

Ryan and Dao (2015) performed full scale shake table test for base isolated 5-story moment frame building. They consider three components of earthquake excitation. They observed horizontal and vertical coupling effect. Moreover, they indicated that vertical component effect would be an important issue for design of nonstructural components.

Moreover, Landi, Grazi and Diotallevi (2015) studied effects of sliding velocity and vertical component of earthquake on responses of base isolated system with friction pendulum bearings. They used a set of near field ground motion records and observed an increase of 15% in horizontal force.

Loghman, Khoshnoudian and Banazadeh (2015) investigated the effect of vertical component of earthquake on base isolated system with triple concave friction pendulum with numerical studies. They observed an increase of 29.5% in horizontal force when the vertical component was considered.

These studies mainly investigate the horizontal and vertical excitations coupling effects on base isolated systems. According to their experimental and analytical studies the significant effects of vertical excitation on building and isolator responses have been demonstrated.

1.2.3. Studies on Spatially Varying Ground Motion

Two different approaches are used to simulate spatially varying ground motion: conditional and unconditional. In the conditional approach, a stochastic model is used to generate earthquake time histories at different locations. The model is conditioned on the available earthquake recordings at selected stations to capture the spatial variation of ground motion. On the other hand, the unconditional approach does not consider the available recordings and generates earthquake time histories independently at each location using a stochastic model.

Shinozuka (1972) has carried out first studies for multidimensional, multivariate and nonstationary simulations. Shinozuka and Deodatis (1991) and Deodatis (1996) introduced a method to generate acceleration time histories which are compatible with prescribed acceleration response spectrum. In their studies, firstly stationary acceleration records were generated and then records converted to non-stationary form using modulating functions. Furthermore, more comprehensive investigations have been car-

ried out utilizing the data acquired from the SMART-1 array located in Taiwan. The researchers proposed coherency models, which were then evaluated based on the accuracy of the SMART-1 array data.

Vanmarcke and Zavoni (1993) carried out studies on conditional simulation of spatially correlated earthquake ground motion. A known earthquake acceleration history has been used as reference record to generate acceleration histories at targeted points.

Zerva (2002) conducted an extensive review of simulation techniques to investigate spatially varying ground motion and compared them to each other. Additionally, Zerva examined the effects of spatially varying ground motion on various types of structures, including long foundations, dams, and bridges. The study aimed to provide a comprehensive understanding of the behavior of these structures under spatially varying ground motion and to identify the limitations and challenges associated with simulating such ground motion. The results of the study were valuable for improving the design and analysis of structures subjected to spatially varying ground motion.

Both approaches were used to generate a set of earthquake ground motion time histories that were applied as input to the finite element model of the structure. These time histories were then analyzed to evaluate the dynamic response of the building under multi-support excitation effects.

1.3. The Scope of Thesis

This thesis consists of five chapters. Chapter 1 of this thesis serves to provide an introduction to the research topic, detailing the underlying motivations and justifications for the study. It includes literature review that summarizes the current state of knowledge related to the topic. The chapter also outlines the scope and objectives of the research, which provide a framework for the subsequent chapters.

Chapter 2 gives general information on seismic isolators. The requirement of seismic gap construction in the base isolated structures is explained. In addition to that, preliminary design of friction pendulum to be used in finite element models is presented.

In Chapter 3 of the thesis, the simulation of spatially correlated ground motion is discussed in detail. The chapter begins by explaining the mathematical background of the simulation. This includes the concept of spatial correlation, which refers to the degree to which ground motion at one location is related to ground motion at another location. The chapter then goes on to explain the process of simulating spatially correlated ground motion, which involves generating a set of random variables that represent ground motion at different locations. The simulation results are then presented, which show the effect of spatial correlation on ground motion parameters such as peak ground acceleration and time delay.

Chapter 4 provides a detailed description of the finite element models used to investigate the effects of the vertical component and spatially varying ground motion on base isolated structures. The chapter includes information on the finite element model geometry, material properties, and the analysis method used to simulate the seismic response. Additionally, the chapter presents the numerical results of the analysis in terms of total base shear, isolator axial load level, column axial load level, and isolator displacement demand. The results are discussed in detail, and an interpretation of the findings with respect to the design of base isolated structures is provided.

Chapter 5 provides a summary of the analytical studies conducted in Chapter 4, where the effects of the vertical component and spatially varying ground motion on base isolated structures were investigated. The chapter presents the conclusions drawn from the results and discusses their implications for the design of base isolated structures. Lastly, this chapter highlights some recommendations for future research on this topic to further improve the understanding of the behavior of base isolated structures under non-uniform ground displacement conditions.

2. BASE ISOLATION

2.1. The Basic Concept of Base Isolation

Seismic base isolation is a technique used to protect structures and their components from the damaging effects of earthquakes. Seismic isolators are devices that are installed between the building's foundation and superstructure to provide isolation from ground motion. These isolators are designed to absorb and dissipate the energy of an earthquake, reducing the seismic forces transmitted to the structure and minimizing the risk of structural damage or collapse. The primary goal of base isolation is to decrease the effects of earthquake forces on structures, not to increase the strength of the structure. This is achieved by modifying the natural period of the system and adding damping through the use of seismic isolators. The lateral stiffness of elastomeric bearings or the geometrical properties and friction coefficient of friction pendulum isolators can be used to shift the natural period of the system. Target damping can also be achieved by determining the yield force level and cyclic behavior of the isolator. By reducing the effects of earthquake forces, base isolation can significantly improve the seismic performance of structures and protect them from damage.

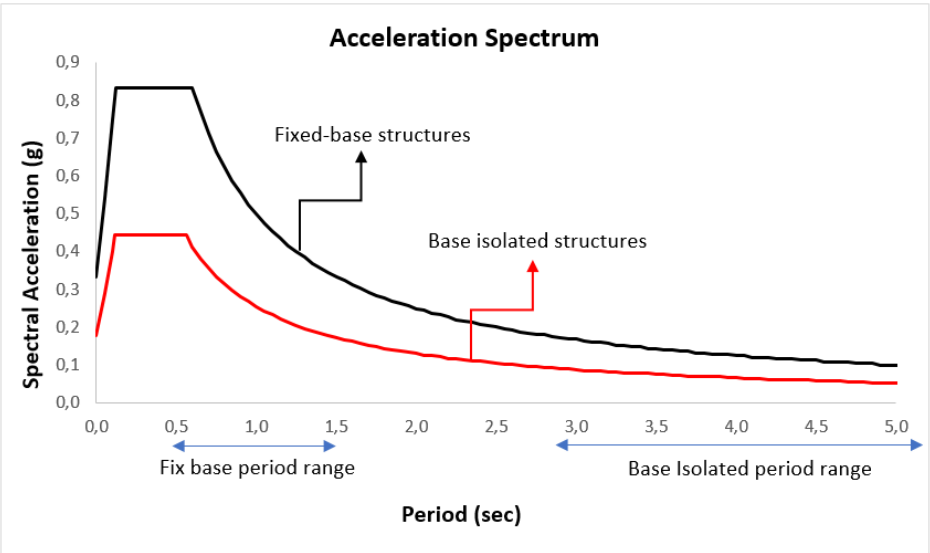

Figure 2.1. Representative acceleration spectrums.

The first applications of base isolation in very basic form have been constructed very long times ago in the regions (Turkey, Iran, etc.) having high seismic activities. This very basic form of base isolation systems has been usually constructed with sand layers, marble surfaces or rollers which have been expected to be provided sliding surface to protect the monumental structures against earthquake hazards. Figure 2.2. depicts Çemberlitaş Tower, which is one of these examples, featuring a cubic marble base placed on bronze feet and supported by marble orthostat stones (Naderzadeh, 2009).

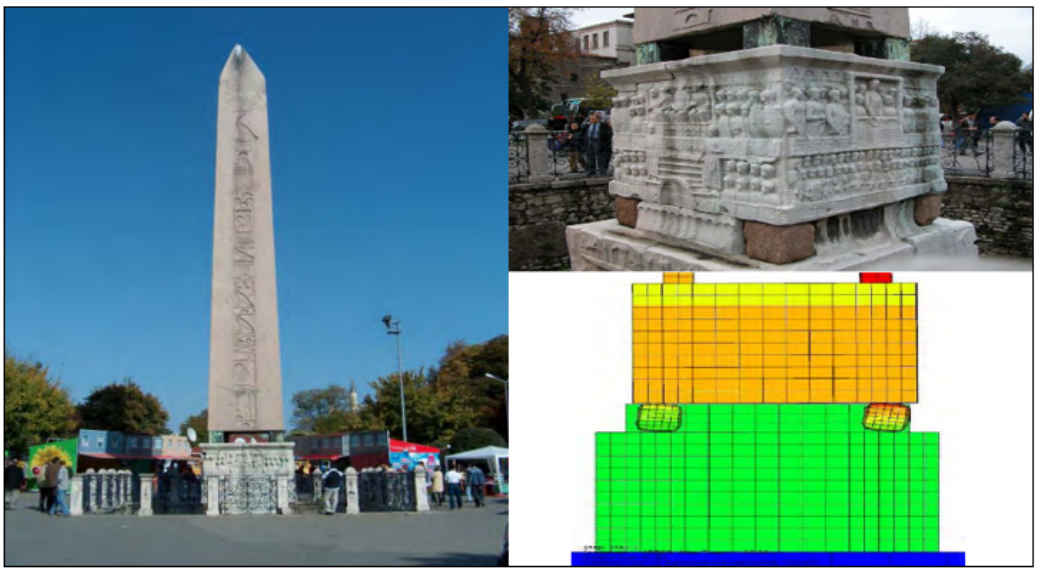

Figure 2.2. The obelisk of theodosius in İstanbul.

The seismic base isolation is an important tool to make structure remain elastic or nearly elastic. Elastic or nearly elastic design limits the floor accelerations and inter-story drifts thus it contributes to achieve operational or fully operational performance level even if dealing with irregular buildings.

Rubber-based (elastomeric) and friction pendulum isolators are the most commonly used and well-known types of isolators. These isolators are designed to mitigate the effects of seismic activity on structures such as buildings and bridges.

Elastomeric isolators, also known as rubber-based isolators, consist of layers of rubber or similar elastomeric material encased between metal plates. The rubber layers provide flexibility and damping properties, allowing the isolators to absorb and dissipate seismic energy. The metal plates help distribute the load and provide stability to the structure. Rubber-based isolators are effective in reducing the transmission of seismic forces to the superstructure, thereby protecting it from damage.

Friction pendulum isolators, on the other hand, work based on the principle of friction and pendulum motion. These isolators typically consist of a sliding bearing with a curved surface that rests on a flat surface. The sliding bearing allows the superstructure to move horizontally during an earthquake, while the pendulum motion allows the bearing to oscillate and dissipate energy. Friction pendulum isolators are highly effective in isolating structures from seismic vibrations and reducing the transfer of forces.

Both rubber-based and friction pendulum isolators provide advantages in seismic isolation. They ensure a high level of energy dissipation, which helps protect the structure and its occupants from the damaging effects of earthquakes. These isolators also provide flexibility, allowing the structure to move and deform without undergoing significant damage. By reducing the transfer of seismic forces, they help increase the overall resilience and safety of structures in seismically active regions.

Figure 2.3 and Figure 2.4 likely provide illustrations of different types of isolators, along with examples of their representative hysteresis loops. A hysteresis loop is a graphical representation of the relationship between stress and strain in a material. In the context of isolators, it shows how the isolator responds to ground motion by deforming and absorbing energy, and how it releases that energy when the motion reverses direction.

Figure 2.3a (Alireza, 2015), Figure 2.3b (Bridgestone, 2022), and Figure 2.3c (Oiles, 2022) respectively show a schematic representation of the lead rubber bearing

isolator, an actual image of the high-damping rubber bearing isolator, and a representation of the natural rubber bearing isolator.

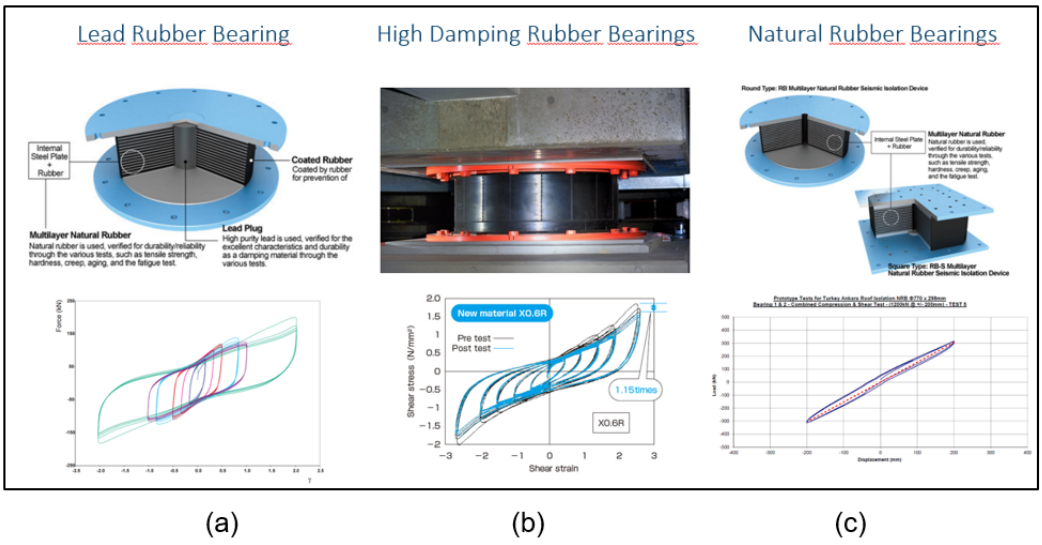

Figure 2.3. Elastomeric isolator types and representative hysteresis loop.

Figure 2.4a-Figure 2.4b (EPS, 2022) depict the single-double surface friction pendulum type isolator, while Figure 2.4c (Dacheng Rubber, 2022) shows a sliding type isolator.

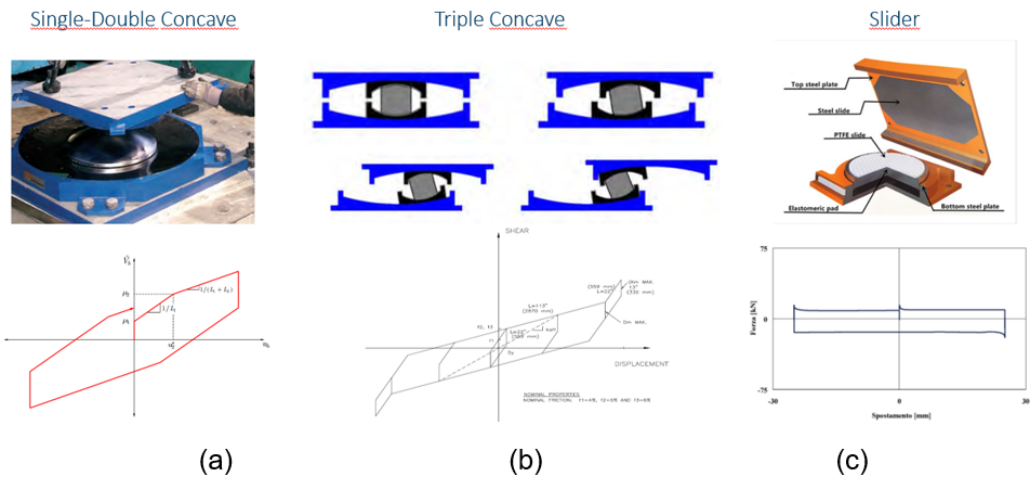

Figure 2.4. Friction pendulum types and representative hysteresis loop.

2.2. Seismic Gap Requirements at Base Isolated Buildings

Seismic isolators used in base isolation systems are designed to have a certain amount of displacement demand to absorb seismic energy and reduce the load transferred to the structure. The isolators should be able to move freely to meet displacement demand. Therefore, a properly designed seismic gap is crucial to prevent adjacent structures from colliding or pounding into each other during earthquakes. The size and shape of the gap are determined based on the expected displacement demands of the isolators and the proximity of adjacent structures.

The seismic gap should allow the motion not only in the longitudinal direction but also in the transverse direction. However, it may be difficult to cover the gaps in a way that will not prevent the bi-directional seismic movement. Furthermore, the cover of seismic gaps should not interrupt operational functionality.

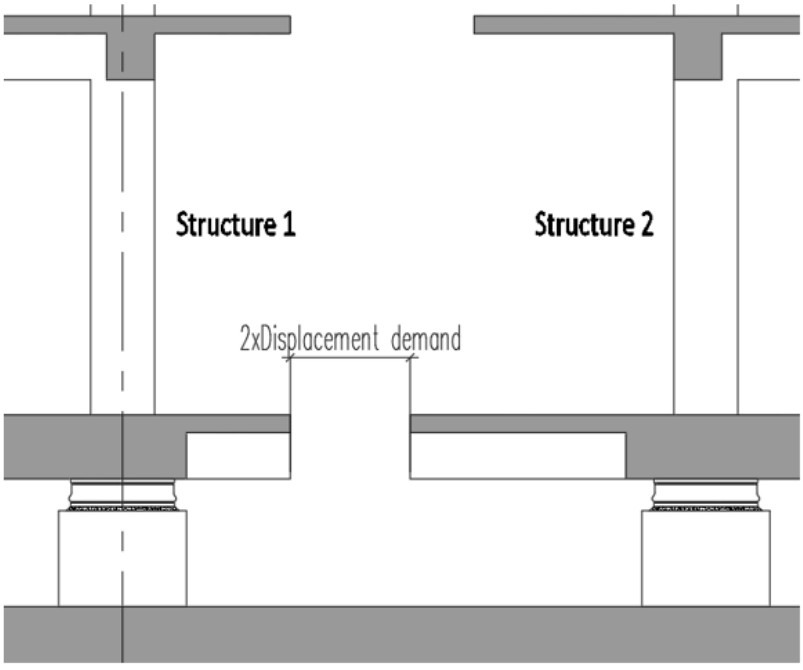

Figure 2.5. Schematic demonstration of seismic gap.

As an alternative approach, the multi blocks can be constructed on a common isolation plane to reduce seismic gap distance.

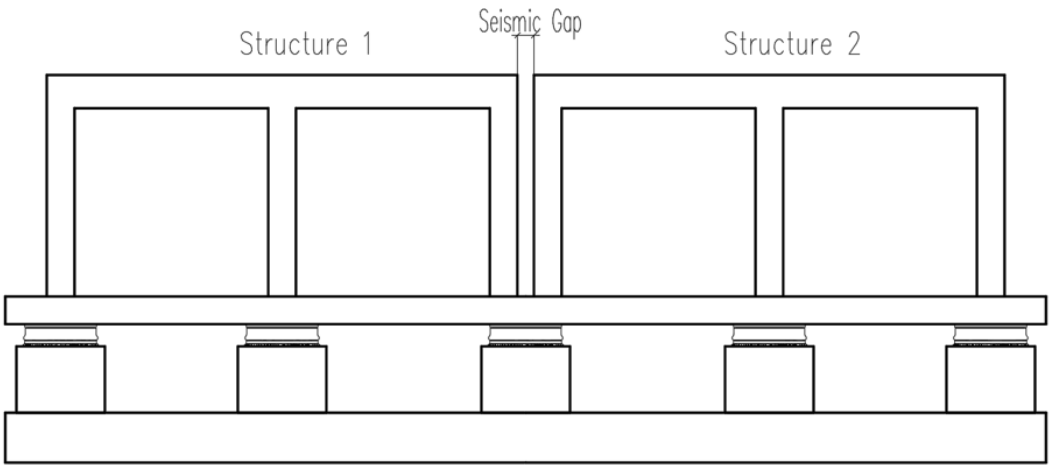

Figure 2.6. Schematic demonstration multi-blocks on common isolation plane.

However, in this approach, the structures designed independently from each other can interact dynamically due to being constructed on common isolation plane. The dynamic interaction between the structures with different physical properties prevents to design of structures independently. The one block design also eliminates the structural behavior complexity of multi blocks constructed on common isolation plane. In order to minimize the number of seismic gaps required and avoid potential pounding effects, base isolated buildings are typically designed as a single block, resulting in longer building lengths in the plan.

2.3. Design of Friction Pendulum Isolator

Friction pendulum is a type of seismic isolation bearings used in structures to increase their seismic safety. It consists of a steel concave sliding surface and a spherical convex surface. Two surfaces are separated by a layer of material with low friction.

During an earthquake, the steel concave surface slides along the spherical convex surface, generating frictional resistance which dissipates the energy of the earthquake and reduces the impact on the structure.

Friction pendulum isolators are a type of seismic isolation device that utilize a convex sliding surface on top of a concave surface to allow the isolator to move in any

direction during an earthquake. This motion dissipates the energy of the earthquake and reduces the seismic forces transmitted to the superstructure. Additionally, the concave surface of the isolator allows it to re-center the structure after the earthquake has stopped, ensuring that the structure returns to its original position and reducing the potential for residual deformations. This re-centering capability is particularly important for structures that may experience multiple earthquakes over their design life.

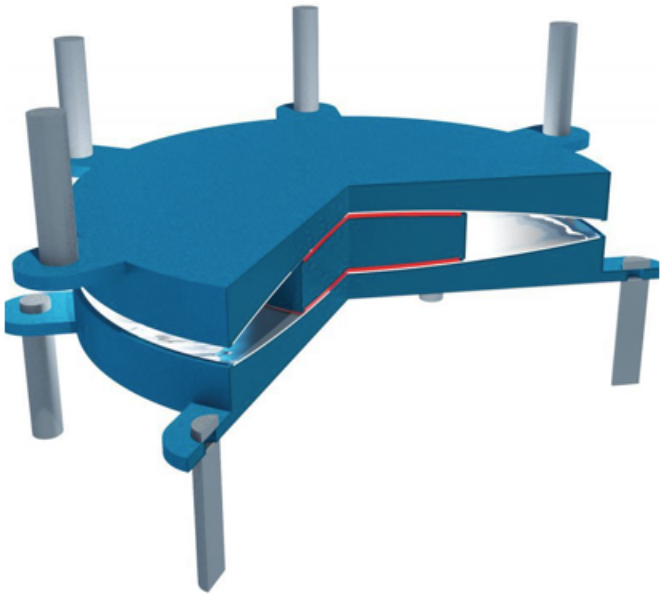

Figure 2.7. Friction pendulum isolator and components (TIS Corp.).

The dynamic properties of friction pendulum isolators are dependent on several factors, including the equivalent radius of curvature, friction coefficient, and axial load magnitude acting on the isolators. These properties play an important role in the overall behavior of the isolated structure during an earthquake. Additionally, the axial load level has a significant impact on the friction coefficient of the isolators, as the friction coefficient is a function of the pressure on the sliding material.

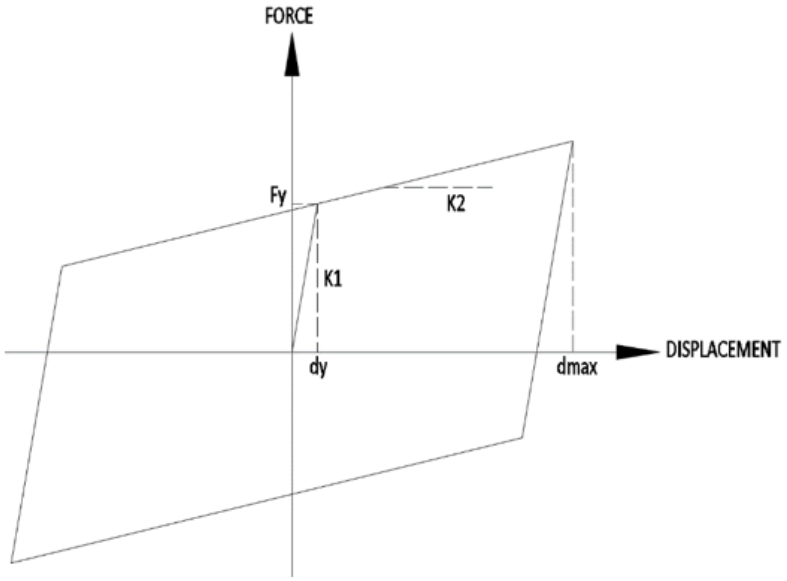

Figure 2.8. Friction pendulum isolators hysteresis loop.

The dynamic properties of a friction pendulum isolator shown in Figure 2.8, are calculated as

$$F_y = \mu_e x P, \tag{2.1}$$

$$K_1 = F_y/d_y, \tag{2.2}$$

$$K_2 = P/R_e, \tag{2.3}$$

$$T_eff = 2\pi\sqrt{\frac{R_e}{g} x \frac{d_{max}}{d_{max} + \mu_e x R_e}}, \tag{2.4}$$

$$\xi_{eff} = \frac{2}{\pi} x \frac{\mu_e x R_e}{d_{max} + \mu_e x R_e}. \tag{2.5}$$

In this study, friction coefficient of 0.04 and an equivalent radius of curvature of 4.5 meters have been selected.

3. SIMULATION OF SPATIALLY CORRELATED GROUND MOTION

Spatially varying ground motion refers to the phenomenon where the seismic ground motion recorded at one location can differ significantly from the ground motion recorded at another location, even if the two locations are relatively close to each other. Spatial variation in ground motion can be caused by a number of factors.

One of the main factors contributing to spatially varying ground motion is coherency loss. Coherency loss refers to the reduction in correlation between the ground motion recorded at two points as the distance between the points increases. This can happen because seismic waves are affected by scattering, diffraction, and other phenomena that cause them to lose energy and change direction as they travel through the ground.

Another factor contributing to spatially varying ground motion is the wave passage effect. The wave passage effect is a phenomenon that occurs when seismic waves travel through different layers of soil, causing the velocity of the waves to change as they pass through layers of soil. This can cause time delay in ground motion even for locations that are relatively close to each other.

Finally, local site effects can also contribute to spatially varying ground motion. Different types of soil layers can have different dynamic properties, which can change the amplitude of bedrock motion.

As a result, spatially varying ground motion can result multi-support excitation, which can have significant implications for the structural design of large base isolated structures. Multi-support excitation refers to the situation where different parts of a structure are subjected to different ground displacement due to spatial variation. This can lead to undesirable interactions between different components of the structure,

making the analysis and design more challenging. Therefore, it is important to consider spatially varying ground motion effects in the seismic design of base isolated large structures.

3.1. Simulation Procedure

In the present study, the conditional simulation method is implemented using a known acceleration history as a reference record. Specifically, conditional simulations are a widely used simulation technique that enable the generation of synthetic ground motion records that exhibit statistical compatibility with the recorded ground motions at nearby locations. Through this process, a set of synthetic ground motions can be generated that closely resemble the reference acceleration history in terms of their statistical properties, such as amplitude, frequency content, and duration.

The studies published by Vanmarcke, Fenton and Zavoni, (1996) is followed to implement spatially correlated ground motion simulations. A known acceleration history of strong ground motion at a certain location can be expressed as Fourier series, that can be written as

$$Z_i(t) = \sum_{k=0}^{K-1}, [A_{ik}cos(w_t t) + B_{ik}sin(w_t t)], \tag{3.1}$$

$$A_{ik} = \frac{1}{k}\sum_{j=0}^{K-1} Z_i(t_j)cos(\frac{2\pi k_j}{K}), \tag{3.2}$$

$$B_{ik} = \frac{1}{K}\sum_{j=0}^{K-1} Z_i(t_j)sin(\frac{2\pi k_j}{K}), \tag{3.3}$$

where ω is discrete frequency, $\Delta\omega$ is frequency step, and A_{ik}, B_{ik} are the Fourier coefficients.

For each frequency step, covariance matrix, C_k and frequency specific covariance matrix can be construced as

$$C_{ij}(w_k) = \begin{cases} \frac{1}{2}\rho_{\omega k}(r_{ij})G(\omega_k)\Delta w, & for\ k = 0 \\ \frac{1}{4}\{\rho_{\omega k}(r_{ij})G(\omega_k) + \rho_{wK-k}(r_{ij})G(\omega_{K-k})\}, & for\ k = 1, ...\frac{K}{2} - 1\ , \\ \rho_{\omega k}(r_{ij})G(\omega_k)\Delta w, & for\ k = K/2 \end{cases} \quad (3.4)$$

$$C_k = \begin{bmatrix} C_{\alpha\alpha} & C_{\alpha\beta} \\ C_{\alpha\beta}^T & C_{\beta\beta} \end{bmatrix}, \quad (3.5)$$

where $C_{\alpha\alpha}$ is the covariance matrix between known points, $C_{\beta\beta}$ is the covariance matrix between unknown points, and $C_{\alpha\beta}$ is the covariance matrix between known and unknown points, at all frequencies ω_k.

The admissible spatial correlation function and spectral density function, $\rho_{\omega k}(r_{ij})$ and $G(\omega_k)$ and the matrix C_k are positive and can be expressed as the product of lower triangular matrix L_x and its transpose by means of Cholesky decomposition, that can be written as

$$C_k = L_k L_k^T. \quad (3.6)$$

Firstly, unconditioned Fourier coefficients, A_s, B_s, are calculated as

$$A_s = L_k U_k\ and\ B_s = L_k V_k. \quad (3.7)$$

Then, Best Linear Unbiased Estimators (BLUE), A_α^* and B_α^*, can be computed as

$$A_\alpha^* = C_{T_{\alpha\beta}}^* C_{\alpha\alpha}^{-1} A_\alpha, B_\beta^* = C_{\alpha\beta}^T C_{\alpha\alpha}^{-1} B_\alpha, \quad (3.8)$$

Similarly, to produce motions which are conditioned on the recordings at points x_α, a set of Best Linear Unbiased Estimators (BLUE) must be employed for each of the unknown points x_β (Heredia-Zavoni, 1993). $A_{s\beta}^*$ and $B_{s\beta}^*$ are the best linear unbiased estimates of the simulated Fourier coefficients at the unknown target points and can be calculated as

$$A^*_{s\beta} = C^*_{T_{\alpha\beta}} C^{-1}_{\alpha\alpha} A_{s\alpha}, B^*_{s\beta} = C^T_{\alpha\beta} C^{-1}_{\alpha\alpha} B_{s\alpha}. \tag{3.9}$$

Finally, the conditional Fourier coefficients at the unknown points A_c and B_c computed as

$$A_c = A^*_\beta + A_{s\beta} - A^*_{s\beta}, B_c = B^*_\beta + B_{s\beta} - B^*_{s\beta}. \tag{3.10}$$

Relative distance, r_{ij} is between the known point and the point at which simulation is to be performed. G_{ij} represents the spectral density function of known earthquake and ρ_{ij} represents frequency dependent coherency function.

Once the Fourier coefficients of the unknown points are obtained through the conditionally simulated ground motion data, they can be used to compute time histories of ground motion at these points. This can be done by using the Fourier coefficients to perform an inverse Fourier transform. The inverse Fourier transform converts the frequency domain representation of the ground motion into its corresponding time-domain representation.

3.2. Coherency Loss Function

The subject of coherency loss in spatially varying ground motion has been one of the topics of interest for researchers in the field of earthquake engineering. To address this phenomenon, various researchers have proposed different functions and models to quantify and simulate the loss of coherency in ground motion. These models typically take into account factors such as the spatial correlation between ground motion signals at different points, the frequency content of the signals, and the effects of wave passage and site-specific characteristics.

To evaluate the spatial correlation of ground motion across the structure's base, this study utilized the frequency dependent coherency function. The coherency func-

tion, which was proposed by Vanmarcke in 1994, accounts for the variation of coherence with frequency and distance, which are critical factors in assessing the spatial correlation of ground motion. By employing this function, the study aimed to obtain more accurate estimations of the spatial variation of ground motion and its effects on the seismic response of base-isolated structures. The coherency function is determined as

$$\rho_{\omega K}(r_{ij}) = exp\left(-\frac{w_k|r_{ij}|}{2\pi cs}\right), \tag{3.11}$$

where r_{ij} is the distance between the points, c is the wave shear velocity and s is the distance scale parameter.

Figure 3.1 illustrates the effect of both the distance between two points and the shear wave velocity of the medium on coherency loss.

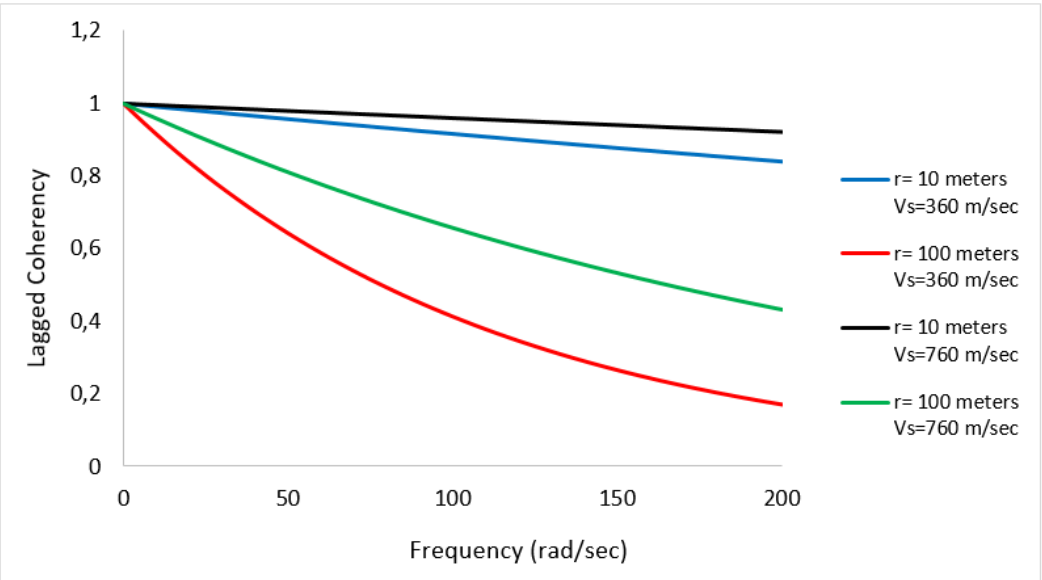

Figure 3.1. Coherency loss function.

3.3. Reference Earthquake Events

In this study, Kahramanmaras earthquake (Turkey, 2023) and Hector Mine (1999) were selected as the known earthquakes. The deta.iled information regarding the known strong ground motion data is presented in Table 3.1 below.

Table 3.1. The detail of reference ground motion data.

SGM ID	**Strong Ground Motion Name**	**Magnitude**	R_{JB}	V_{s30}
3134	Kahramanmaraş, Turkey	7.8	28 km	374 m/s
4628	Kahramanmaraş, Turkey	7.8	82 km	337 m/s
3137	Kahramanmaraş, Turkey	7.8	82 km	688 m/s
1776	Hector Mine, California	7.1	56 km	359 m/s
1795	Hector Mine, California	7.1	50 km	686 m/s

To gain a better understanding of the effect of shear wave velocity, multiple recordings of the same earthquake with varying shear wave velocities were selected for simulation of spatially varying ground motion. This was done to ensure that the potential variations in shear wave velocity among recordings were accounted for in the analysis, allowing for a more accurate assessment of the shear wave velocity's impact on spatial variation.

In order to capture the effects of both horizontal and vertical incoherencies on the structural behavior, spatially correlated simulations of strong ground motion were conducted using three components, namely longitudinal, transverse, and vertical. The acceleration histories were simulated for points separated by a distance of 10 meters from each other to achieve a higher degree of accuracy.

3.4. Construction of Power Spectral Density Function

Power spectral density (PSD) function is used to define distribution of energy in time series as a function of frequency. In the context of spatial variation of strong ground motion, PSD function is a useful tool for analyzing the frequency content of ground motion and its spatial variation. By estimating the PSD function of ground motion at different locations, one can gain insights into the frequency-dependent characteristics of seismic waves and their changes over distance.

Before the construction of PSD function of known earthquake, the recorded acceleration data is divided to subwindows to increase accuracy of simulation.

The maximum entropy spectral analysis which is proposed by Burg (1975) is carried out to construct one-sided power spectrum density function.

In the present study, the maximum entropy spectral analysis (MESA) method, which was proposed by Burg in 1975, is carried out to construct one-sided power spectrum density function. MESA is a popular technique for estimating power spectral density functions of time series data. MESA is based on the principle of maximum entropy, which states that the best estimate of an unknown probability density function is the one that maximizes the entropy subject to any constraints that are imposed by the available data.

In the context of seismic data analysis, MESA can be used to construct one-sided power spectral density functions of ground motion records.

The one-sided power spectral density function describes how the energy in the ground motion is distributed across different frequencies, and it is a fundamental tool for understanding the frequency content of seismic signals. PSD can be calculated as

$$G(\omega) = \frac{\sigma^2 \Delta t}{|1 + \sum_{k=1}^{M} \alpha_k e^{-ik\omega\Delta t}|^2}, \tag{3.12}$$

where Δt is the sampling interval, σ^2 is the one-step prediction variance and α_k are the coefficients of autoregressive model. The parameters of autoregressive model were calculated by minimizing the final prediction error.

Figure 3.2, Figure 3.3, Figure 3.4, Figure 3.5, Figure 3.6 show the subwindows of known strong ground motion and Figure 3.7, Figure 3.8, Figure 3.9, Figure 3.10, Figure 3.11 represent power spectral density functions of each subwindow.

The figures below were prepared for horizontal components for each known strong ground motion. The same procedures are applied for the transverse and vertical components.

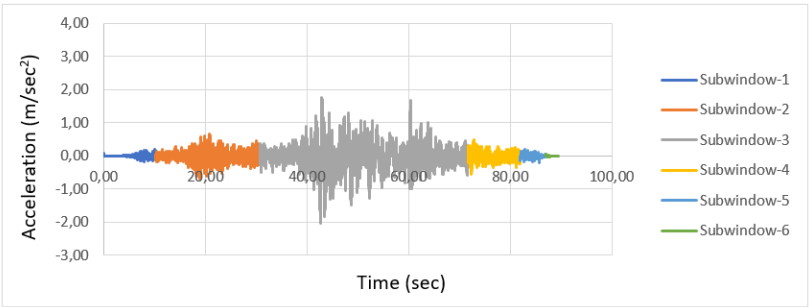

Figure 3.2. The subwindows of known acceleration history (SGM ID: 3134).

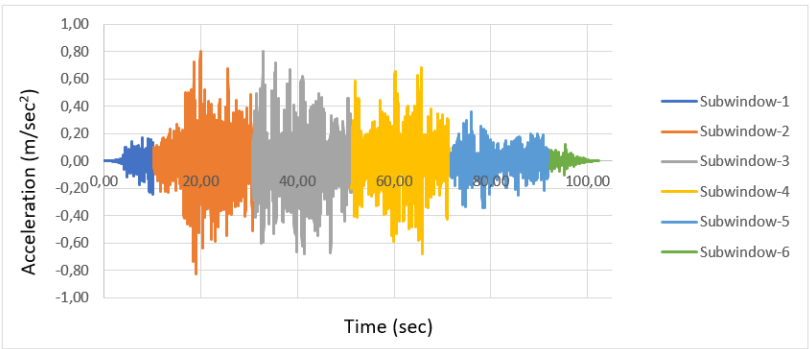

Figure 3.3. The subwindows of known acceleration history (SGM ID: 4628).

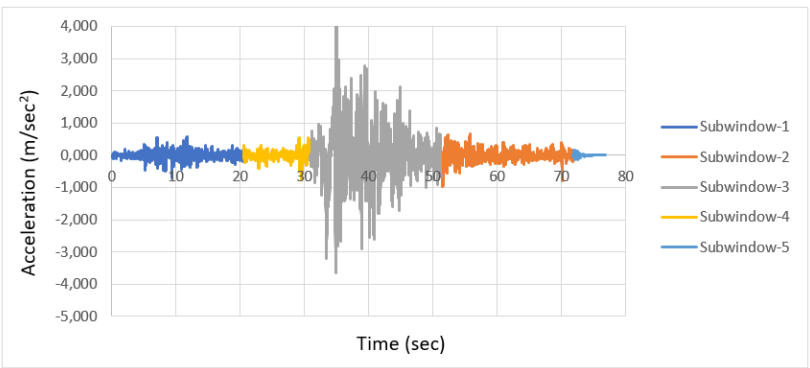

Figure 3.4. The subwindows of known acceleration history (SGM ID: 3137).

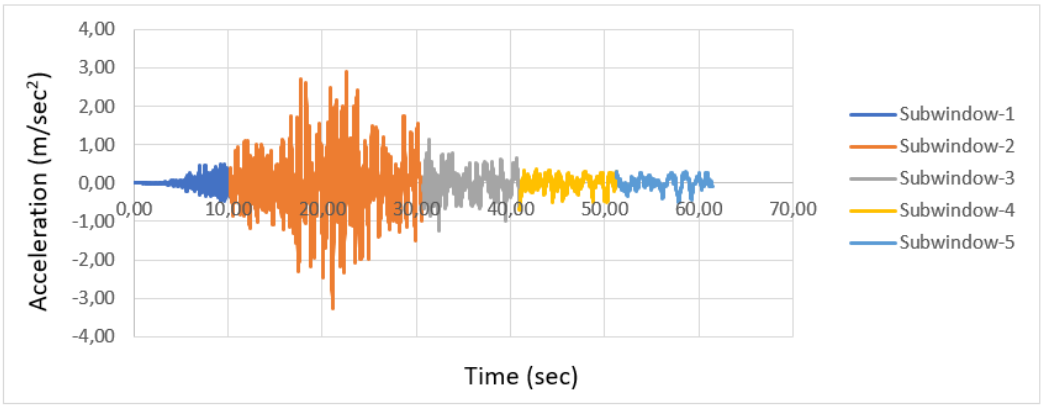

Figure 3.5. The subwindows of known acceleration history (SGM ID: 1776).

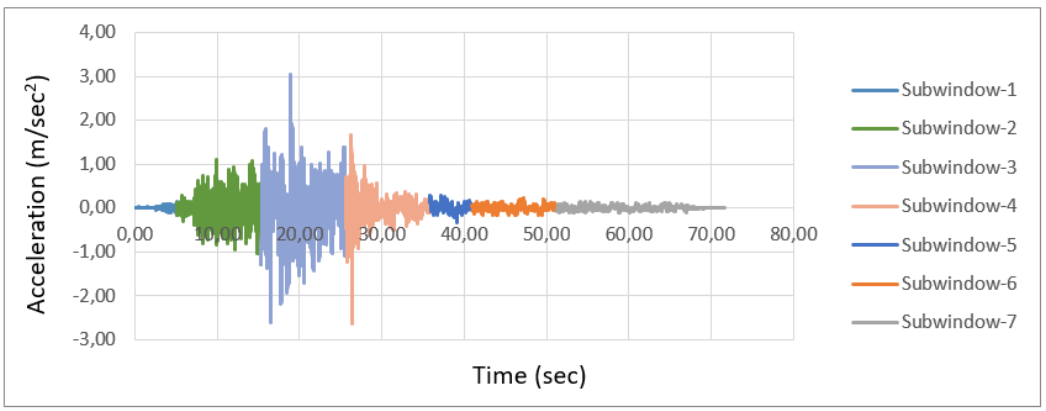

Figure 3.6. The subwindows of known acceleration history (SGM ID: 1795).

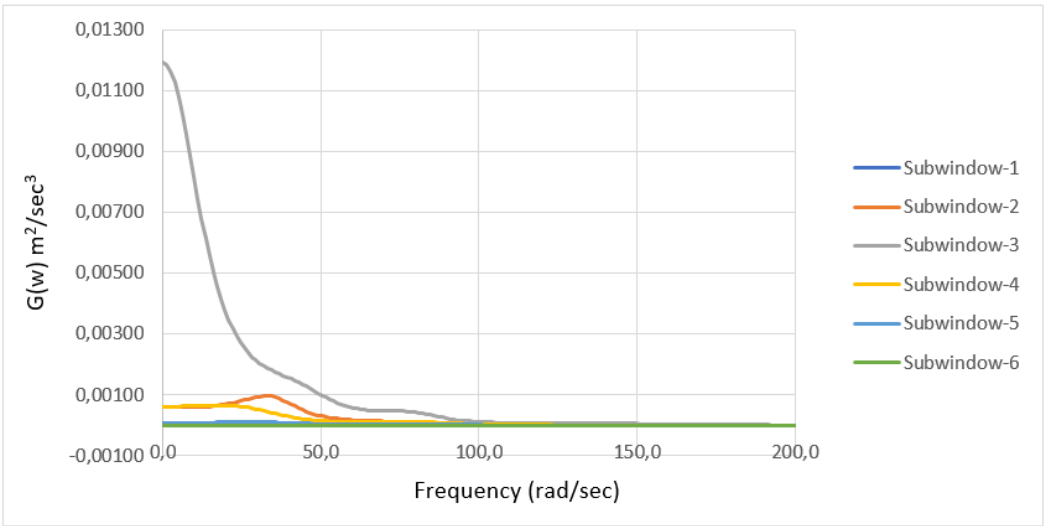

Figure 3.7. Power spectral density functions of subwindows (SGM ID: 3134).

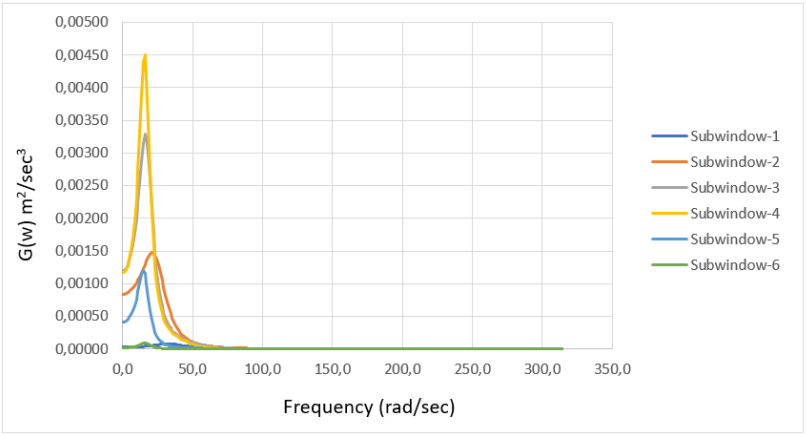

Figure 3.8. Power spectral density functions of subwindows (SGM ID: 4628).

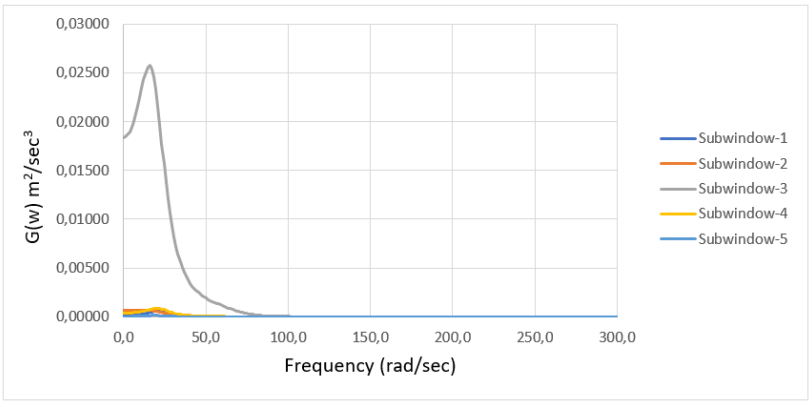

Figure 3.9. Power spectral density functions of subwindows (SGM ID: 3137).

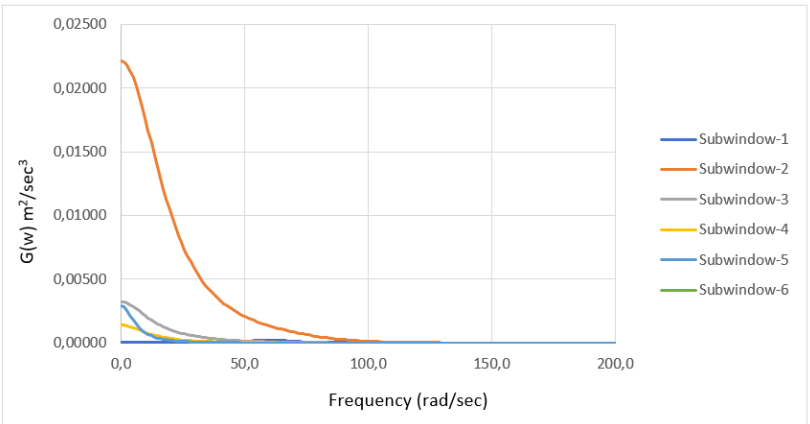

Figure 3.10. Power spectral density functions of subwindows (SGM ID: 1776).

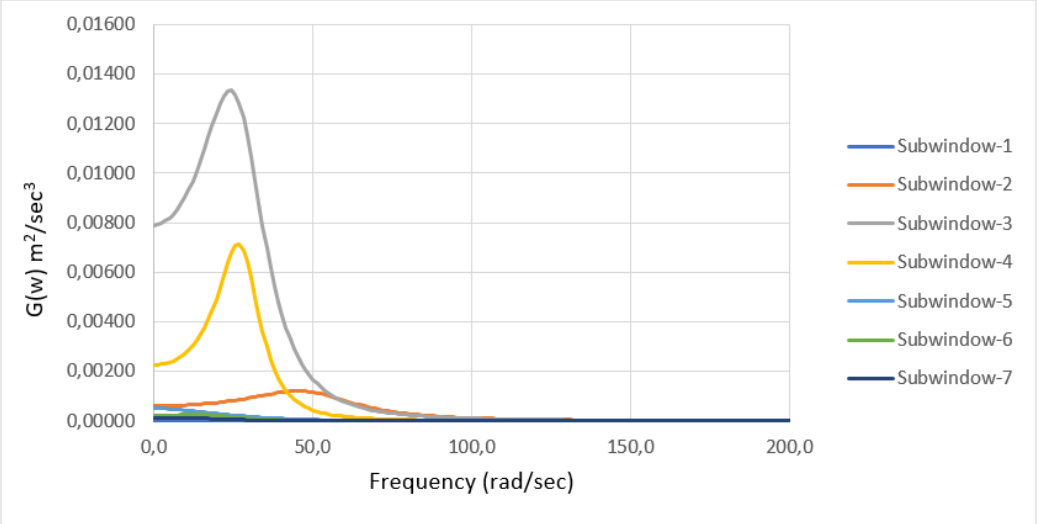

Figure 3.11. Power spectral density functions of subwindows (SGM ID: 1795).

From the graphics above, it is apparent that the highest spectral amplitudes agree with highest acceleration variations.

3.5. Generation of Time Histories

After constructing power density functions with Maximum Entropy Method, spatially correlated ground motion simulations are performed by following mathematical expressions described in Chapter 3.1. The simulations are performed for the points whose distance to each other 10 meters to provide fine grid system.

Once the power spectral density functions have been constructed using the Maximum Entropy Method, the next step is to perform spatially correlated simulations of ground motion. This is achieved by applying the mathematical expressions described in Chapter 3.1, which take into account the frequency content of the ground motion and its spatial variation. Specifically, the simulations are performed for multiple points that are spaced at 10 meters intervals, in order to create a fine grid system and provide a more accurate representation of the ground motion. By using this approach, it is possible to model the spatial variability of the ground motion and analyze its effects on structures. The resulting simulations can provide valuable insights into the behavior of the ground acceleration and displacement.

The simulations of spatially varying ground motion do not take into local site effect while considering coherency loss and wave propagation effect. It is assumed that all points where the simulations performed, located on same soil type.

3.5.1. Generation of Acceleration Histories

The evaluation of structural response to multi-support excitation requires the generation of displacement time histories. However, to obtain displacement time histories, it is necessary to first generate acceleration time histories. Therefore, in this study, spatially varying ground motion simulations were performed to obtain acceleration time histories which are then used to generate displacement time histories for structural response analysis.

Simulations at the first, middle, and last points, as well as the average acceleration histories of all simulated points, are presented in Figure 3.12 through Figure 3.26.

Moreover, following figures represent simulated acceleration histories for limited time interval to emphasize time delay and peak ground acceleration variations.

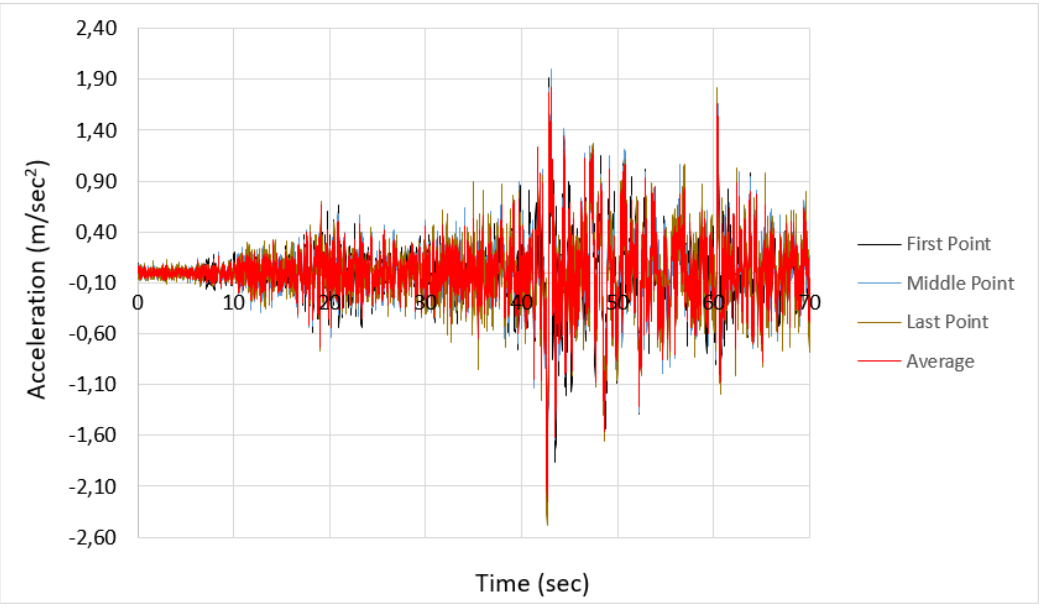

Figure 3.12. Simulated acceleration time histories (SGM ID: 3134).

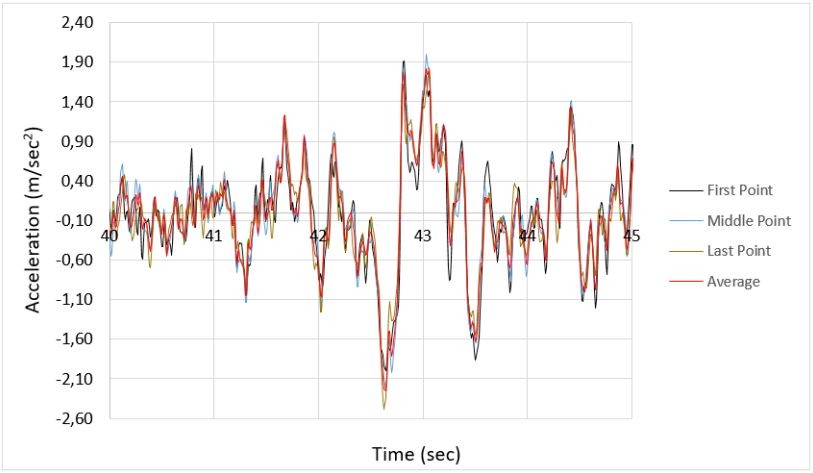

Figure 3.13. Simulated acceleration time histories for limited time interval (t_1= 40sec - t_2=45sec SGM ID: 3134).

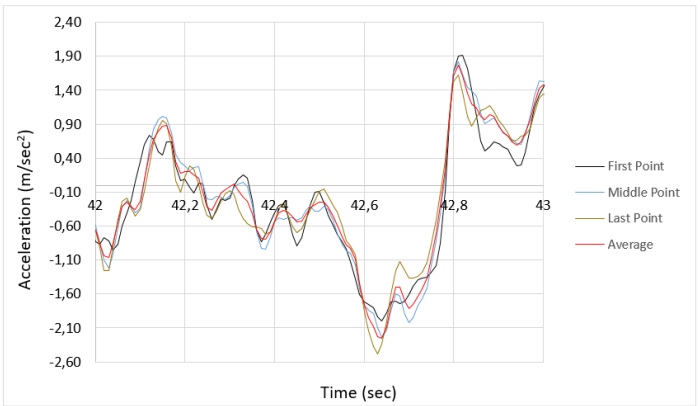

Figure 3.14. Simulated acceleration time histories for limited time interval (t_1= 42sec - t_2=43sec SGM ID: 3134).

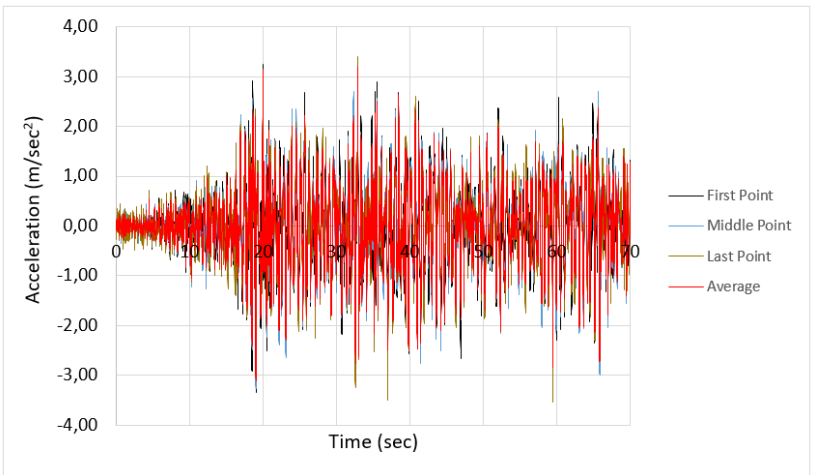

Figure 3.15. Simulated acceleration time histories (SGM ID: 4628).

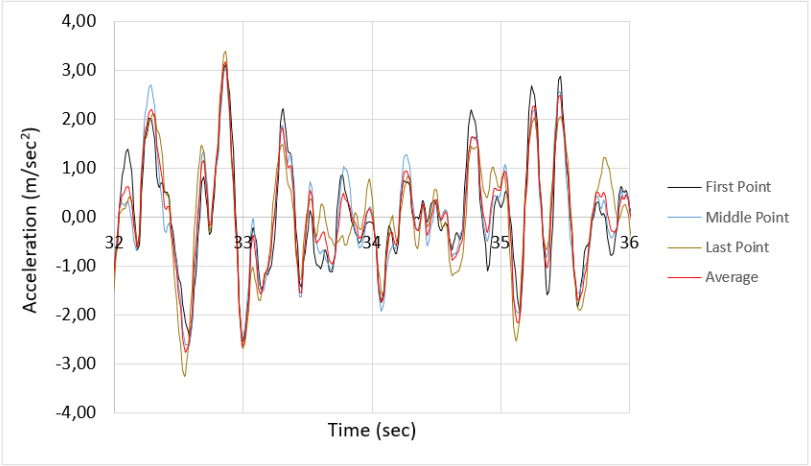

Figure 3.16. Simulated acceleration time histories for limited time interval (t_1= 32sec - t_2=36sec SGM ID: 4628).

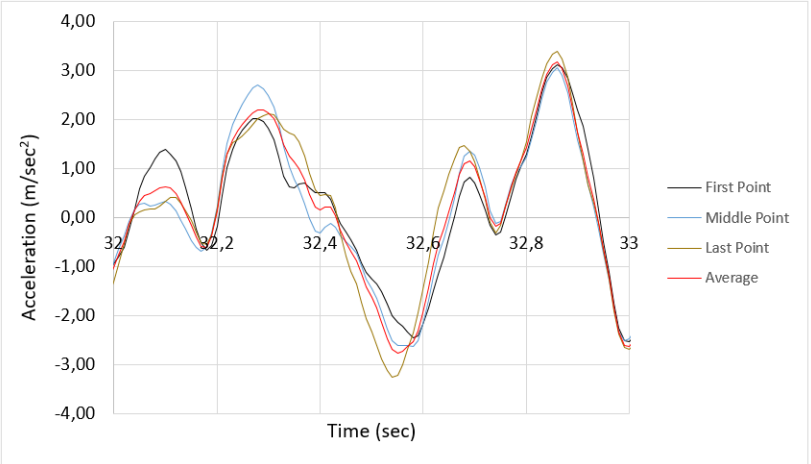

Figure 3.17. Simulated acceleration time histories for limited time interval (t_1= 32sec - t_2=33sec SGM ID: 4628).

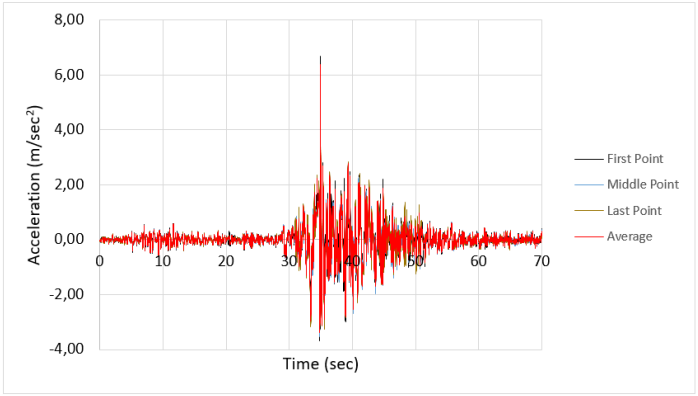

Figure 3.18. Simulated acceleration time histories (SGM ID: 3137).

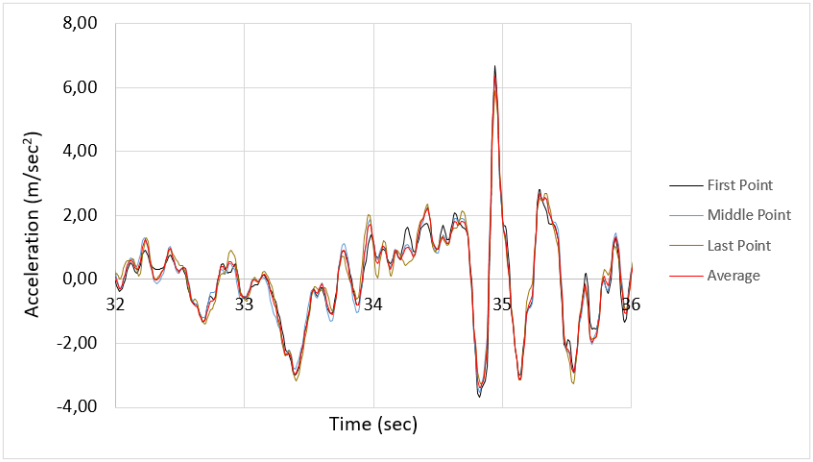

Figure 3.19. Simulated acceleration time histories for limited time interval (t_1= 32sec - t_2=36sec SGM ID: 3137).

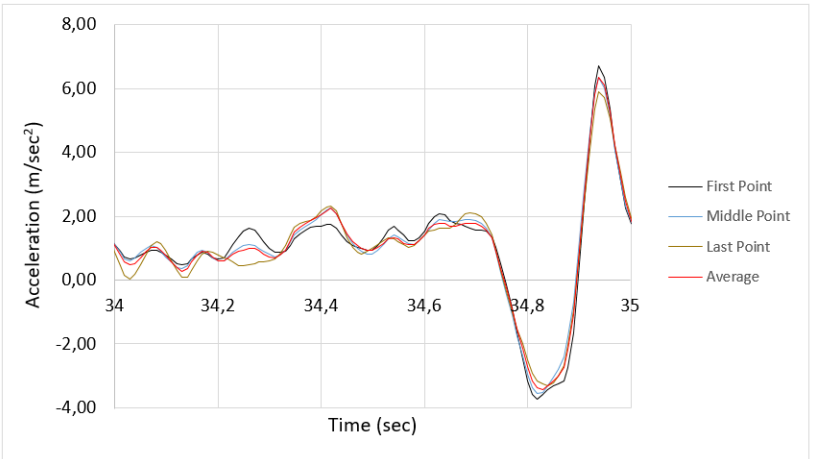

Figure 3.20. Simulated acceleration time histories for limited time interval (t_1= 34sec - t_2=35sec SGM ID: 3137).

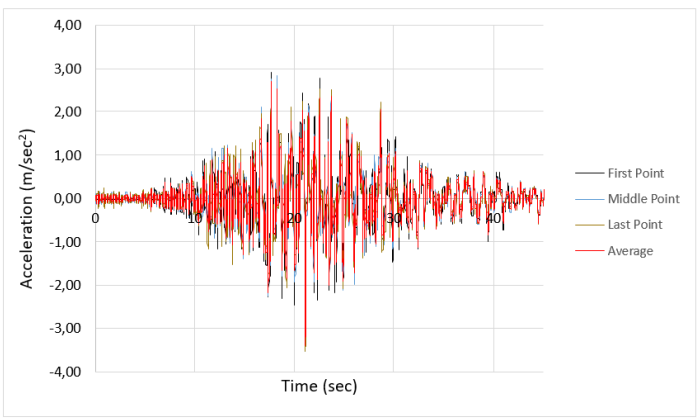

Figure 3.21. Simulated acceleration time histories (SGM ID: 1776).

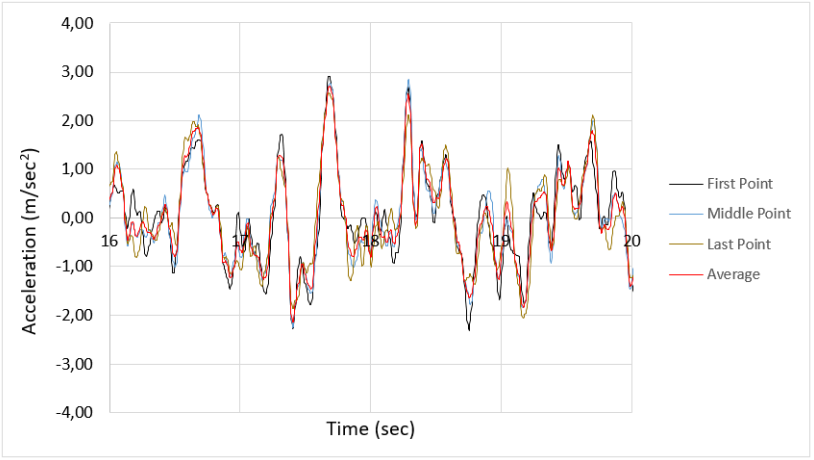

Figure 3.22. Simulated acceleration time histories for limited time interval (t_1= 16sec - t_2=20sec SGM ID: 1776).

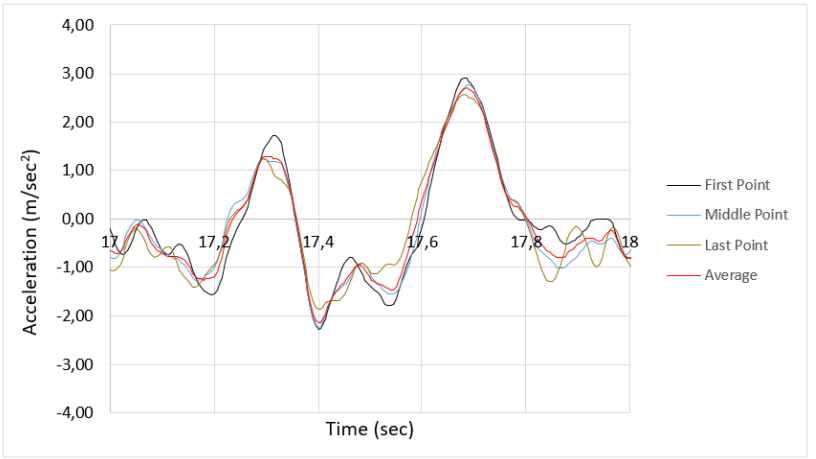

Figure 3.23. Simulated acceleration time histories for limited time interval (t_1= 17sec - t_2=18sec SGM ID: 1776).

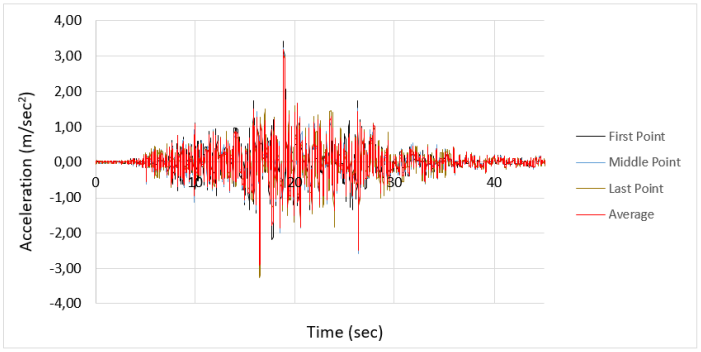

Figure 3.24. Simulated acceleration time histories (SGM ID: 1795).

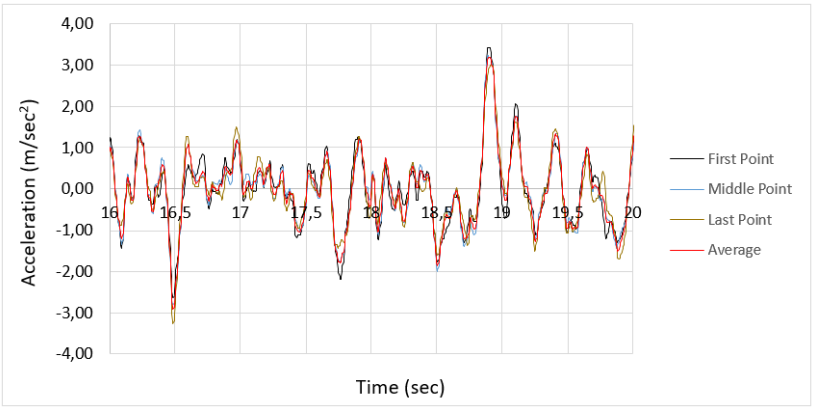

Figure 3.25. Simulated acceleration time histories for limited time interval (t_1= 16sec - t_2=20sec SGM ID: 1795).

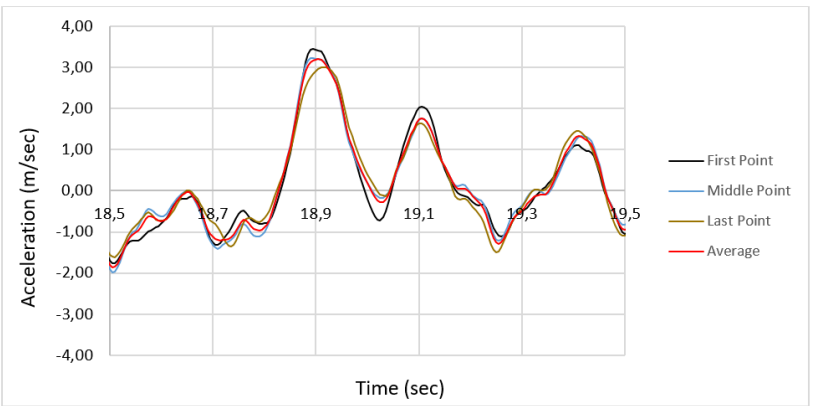

Figure 3.26. Simulated acceleration time histories for limited time interval (t_1= 18.5sec - t_2=19.5sec SGM ID: 1795).

3.5.2. Generation of Displacement Histories

After performing spatially varying ground motion simulations and obtaining acceleration histories, acceleration histories are converted to displacement histories to be used in dynamic response analysis.

To remove low-frequency noise from the simulated acceleration histories and extract frequencies of interest, a two-poles Butterworth high-pass filter with a cutoff frequency of the corner frequency is applied. This filtering operation removes the unwanted low-frequency content in the signal, leaving behind only the high-frequency content that is relevant to the analysis. The resulting filtered acceleration histories are

then used to generate displacement time histories for dynamic response analysis. The corner frequency can be calculated as

$$f_C = \frac{1}{T\left[\frac{H_0^2}{(1-H_0^2)}\right]^{\frac{1}{2n}}}. \tag{3.13}$$

The filter amplitude threshold, H_0, is selected as 0.02 which is suggested by Liao and Zerva (2006).

Simulations at the first, middle, and last points, as well as the average displacement histories of all simulated points, are presented in Figure 3.27 through Figure 3.30. Figure 3.28 and Figure 3.30 represent simulated displacement histories for limited time interval to emphasize time delay and peak ground displacement variations.

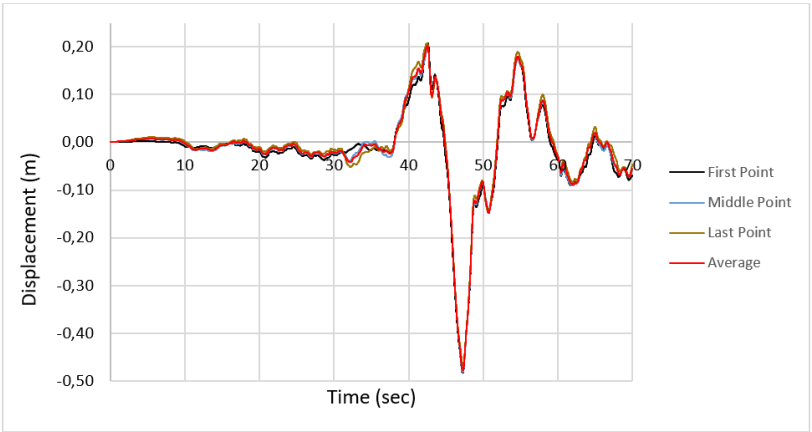

Figure 3.27. Simulated displacement time histories (SGM ID: 3134).

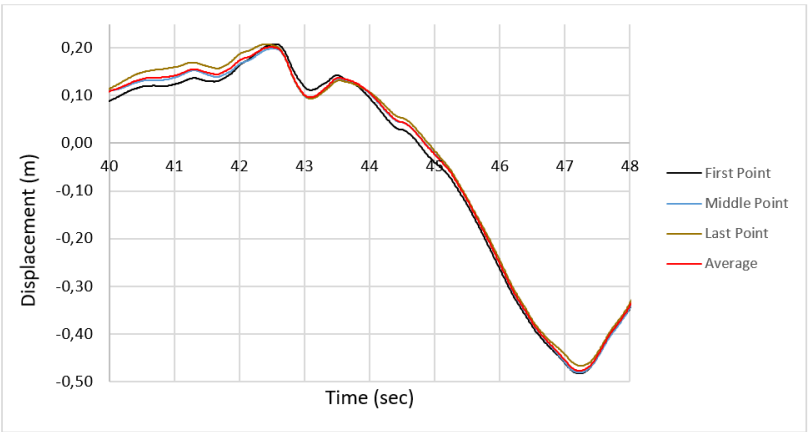

Figure 3.28. Simulated displacement time histories for limited time interval (t_1= 40sec - t_2=48sec SGM ID: 3134).

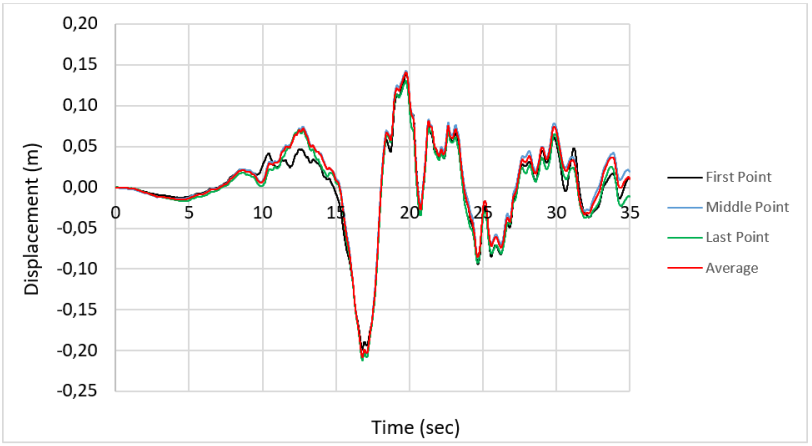

Figure 3.29. Simulated displacement time histories (SGM ID: 1776).

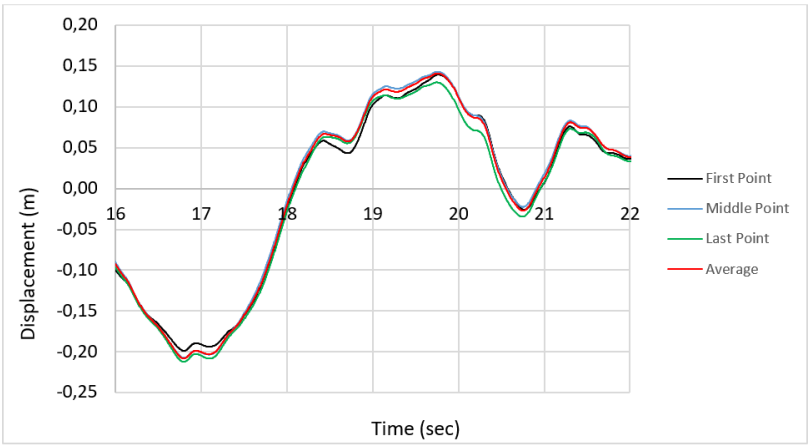

Figure 3.30. Simulated displacement time histories for limited time interval (t_1= 16sec - t_2=22sec SGM ID: 1776).

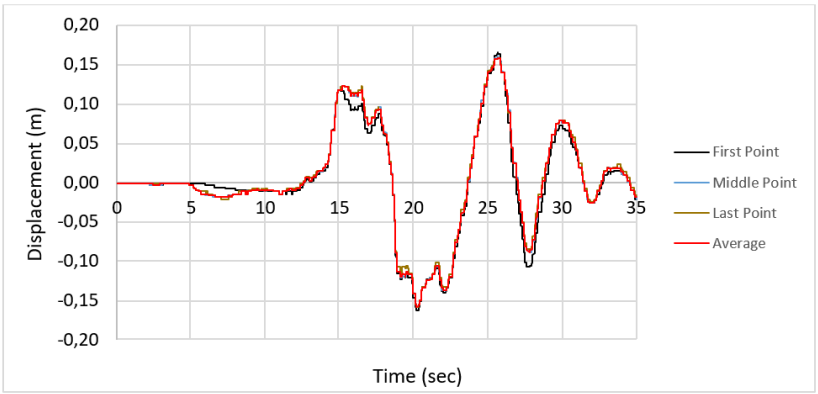

Figure 3.31. Simulated displacement time histories (SGM ID: 1795).

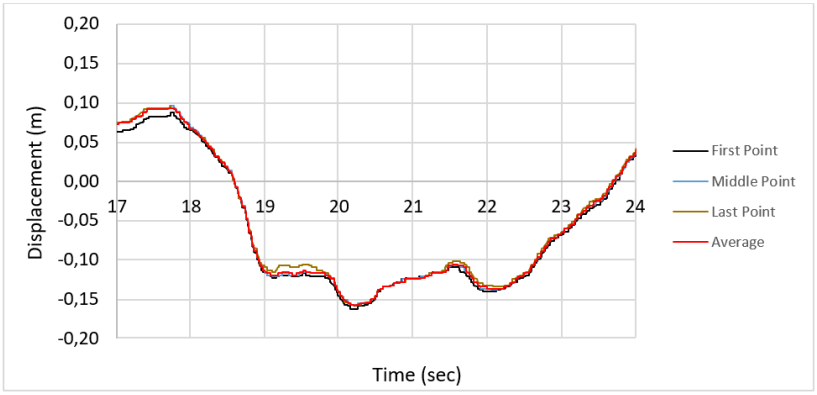

Figure 3.32. Simulated displacement time histories for limited time interval (t_1= 17sec - t_2=24sec SGM ID: 1795).

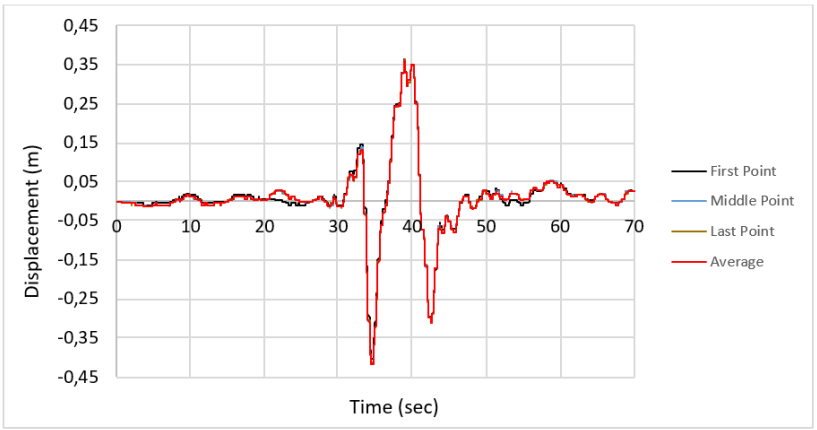

Figure 3.33. Simulated displacement time histories (SGM ID: 3137).

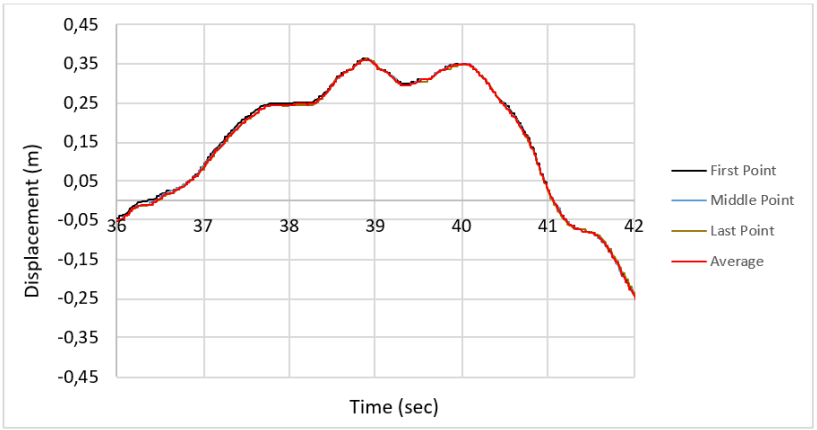

Figure 3.34. Simulated displacement time histories for limited time interval (t_1= 36sec - t_2=42sec SGM ID: 3137).

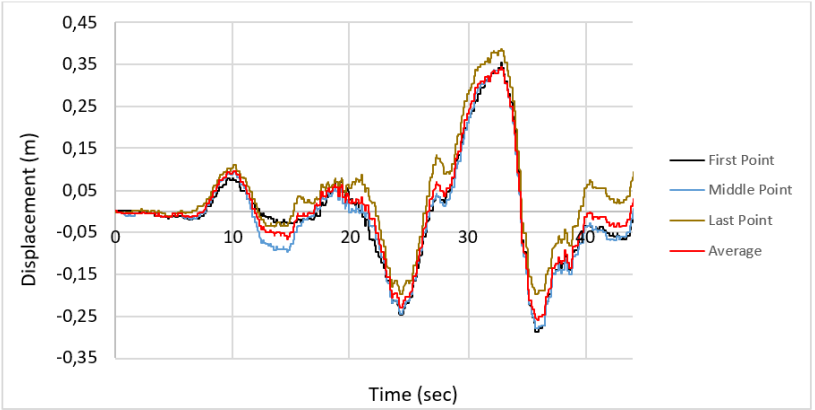

Figure 3.35. Simulated displacement time histories (SGM ID: 4628).

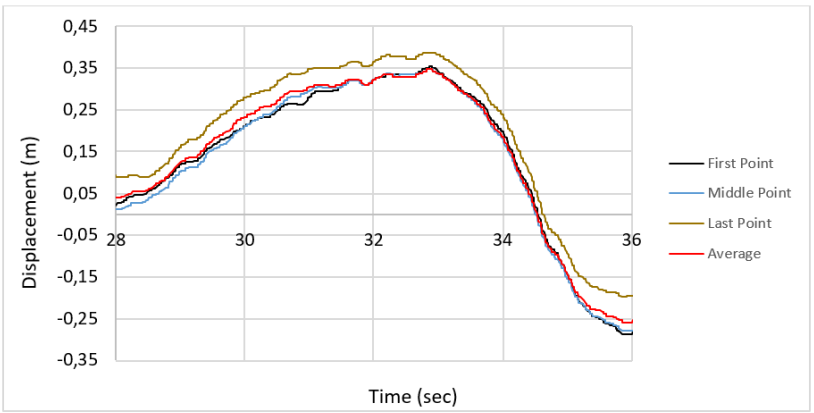

Figure 3.36. Simulated displacement time histories for limited time interval (t_1= 28sec - t_2=36sec SGM ID: 4628).

3.5.3. Application of Displacement Histories to Finite Element Model

After obtaining displacement records, the displacement responses can be defined in the structural model. In this study, earthquake records were simulated at intervals of 10 meters, and each record was defined in the structural model.

Subsequently, unit displacement loads in the desired directions (X, Y, Z) are defined. The function of the unit displacement load is set to the desired earthquake record. This allows for a separate displacement time analysis solution for each support.

By following this procedure, displacement time analyses can be performed for each support, enabling the evaluation of structural responses in different directions.

4. DYNAMIC RESPONSE ANALYSIS

A three-dimensional finite element model was developed in this study to conduct dynamic response analysis. The model was specifically designed to incorporate the nonlinear properties of friction pendulum isolators. To simulate the real conditions, the model considered the three components of earthquake ground motion, namely the horizontal components in two directions (x and y) and the vertical component. The model was able to capture the complex behavior of the structure and isolators under seismic excitations, which can provide valuable insights for total response of structure and its components.

In Chapter 3 of the study, displacement time histories were generated using spatially varying ground motion simulations. These displacement time histories were then applied to specific locations in the three-dimensional finite element model of the structure. It is important to note that the applied ground displacements included the effects of coherency loss and wave passage, which are critical factors in accurately simulating the multi-support excitation effects experienced by the building during an earthquake.

4.1. Description of Buildings

Dynamic response analyses were performed for two sample buildings with different plan lengths. Both buildings have identical features, such as friction pendulum isolator properties, section of structural elements, total height, and material properties. In this way, only the behavior of buildings with different plan lengths could be compared. For each building, multiple ground motion time histories were applied as input excitation to investigate the variability of the structural response.

Figure 4.1 illustrates the general view of the building and its main structural components, such as columns, beams, and isolators, which were modeled in the analysis.

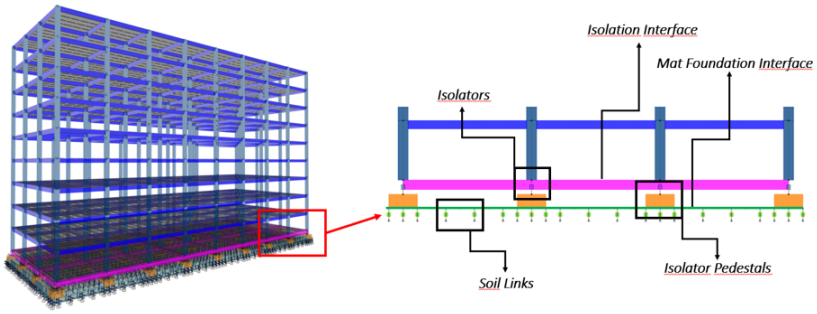

Figure 4.1. General view of structure.

Furthermore, Table 4.1 presents the geometric properties of the structural components.

Table 4.1. Geometrical properties of structural members.

Column Sections	90cm x 90cm
Beam Sections	50cm x 70cm
Slab Sections	22cm thick slab
Foundation Section	150cm thick mat slab
Height	45 meters
Concrete Grade	C40 (fck=40MPa)

In order to investigate the effect of spatial variation of ground motion on the dynamic behavior of structures, two different buildings with different plan lengths were selected for the study. The first building, referred to as SS-1, has a plan length of 120 meters, while the second building, referred to as SS-2, has a plan length of 180 meters. By comparing the dynamic responses of these two structures under the same input excitation, the effect of foundation length on spatial variation and structural response can be evaluated.

4.1.1. Dynamic Properties of Friction Pendulum Isolator

The friction pendulum type isolators are widely used in earthquake engineering to reduce the seismic response of structures. These isolators have two fundamental properties, namely the friction coefficient and the equivalent radius of curvature, which have a major role in their dynamic behavior.

In the given context, the friction coefficient and equivalent radius of curvature are specified as 0.04 and 4.5 meters, respectively. These values are typically chosen based on the design requirements and the properties of the structure and the ground motion.

Once these values are determined, the dynamic properties of the isolator can be calculated as

$$F_y = 0.04xP, \tag{4.1}$$

$$K_1 = F_y/d_y, \tag{4.2}$$

$$K_2 = P/4.5m, \tag{4.3}$$

$$T_{eff} = 2\pi\sqrt{\frac{4.5m}{g}x\frac{d_{max}}{d_{max}+0.04x4.5m}}, \tag{4.4}$$

$$\xi_{eff} = \frac{2}{\pi}x\frac{0.04x4.5m}{d_{max}+0.04x4.5m}. \tag{4.5}$$

These properties include the natural frequency, damping ratio, and effective stiffness of the isolator, which are important parameters in dynamic response analysis and can be calculated by Equation (4.1) through Equation (4.5).

4.1.2. Dynamic Stiffness of Soil Links

Mat foundations are commonly used in structural engineering to distribute the loads of a structure over a larger area of soil. Foundations are typically modelled as shell elements, and appropriate area stiffness and restraints are assigned. However, this approach is not suitable for multi support excitation analysis and can lead excessive superstructure displacement.

In order to prevent excessive displacements at mat foundation level, the soil links are applied to bottom surface of mat foundation. The dynamic stiffness of the soil links is an important parameter in the dynamic behavior of structure. It is defined as a function of the shear wave velocity and foundation length, as described by Mylonakis in 2005.

In this context, the strong ground motion data stated in Chapter 3.2 were recorded for different shear wave velocities. Therefore, different dynamic stiffness values of soil links are used for each known earthquake. By considering the specific shear wave velocity of the ground motion at each site, the appropriate dynamic stiffness values can be determined to perform multi support analysis. Soil dynamics stiffness values can be calculated as

$$K_z = \frac{2GL}{1-\vartheta}(0.73 + 1.54\chi^{0.75}) \; with \; \chi = \frac{A_b}{3L^2}, \tag{4.6}$$

$$K_y = \frac{2GL}{2-\vartheta}(2 + 2.5\chi^{0.85}), \tag{4.7}$$

$$K_x = K_y - \frac{0.2}{0.75-\vartheta}GL(1 - \frac{B}{L}), \tag{4.8}$$

where A_b is foundation are, ϑ is Poisson' ratio, B is foundation halfwidth in direction examined, L is semi-length of foundation and G is soil shear modulus.

4.1.3. Analysis Cases

In order to enhance the comprehension of the impact of the vertical component and spatial variability of strong ground motions on the dynamic behavior of structures, the present study performs the following analyses:

- Case 01: Consider only longitudinal and transverse components of earthquake as uniform (HX+HY).
- Case 02: Consider all three components of earthquake as uniform (HX+HY+HZ).
- Case 03: Consider longitudinal and transverse components of earthquake as uniform and vertical component of earthquake as non-uniform (HX+HY+SZ).
- Case 04: Consider all three components of earthquake as non-uniform (SX+SY+SZ).

4.2. Investigation of Isolator Axial Load

In the scope of this study, firstly, the effect of vertical component and spatial variation on isolators' axial load is investigated. The axial load on isolators is an

important factor in the design of isolators, as it affects their performance during an earthquake.

The vertical component of ground motion refers to the component of ground acceleration that is in the direction of gravity, and it has a significant impact on the axial load on isolators. This is because the vertical component of ground motion increases the acceleration magnitude in the direction of gravity, resulting in an increase in the axial load on isolators.

In addition, the spatial variability of ground motion can also affect the axial load on isolators. Simulated spatially varying ground motions can have time lag and coherency loss, which can introduce non-uniform displacements at the bottom joints of isolators. These non-uniform displacements can induce the transfer of axial load between adjacent isolators, resulting in an increase in the magnitude of axial load on an isolator at a certain time step during an earthquake.

Firstly, dynamic response analysis is conducted using the displacement records simulated in Chapter 3, and isolator axial load time histories are obtained. Figure 4.2 shows the isolator axial load histories for the cases described in Chapter 4.1.3.

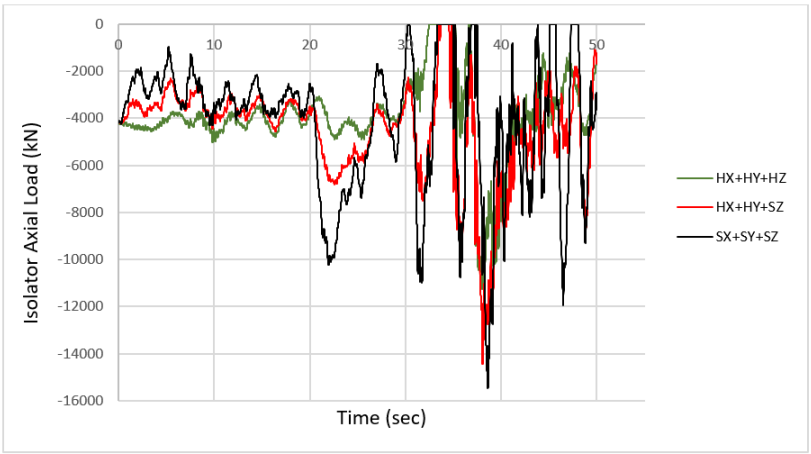

Figure 4.2. An isolator axial load histories (SGM ID: 3137 – Structure 1).

The summary results of the analyses of all cases and the two structures (SS-1 and SS-2) are presented in the following figures. The amount of increase that observed is

categorized in order to better track the increases in axial load. While Structure 1 has 75 columns, Structure 2 has 110 columns.

The graphics have been categorized into graphics “a” and “b” for ease of following. The graphics labeled “a” show the increase in axial load levels obtained in Case 3 (HX+HY+SZ) with respect to the levels obtained in Case 2 (HX+HY+HZ). The graphics labeled “b” show the increase in axial load levels obtained in Case 4 (SX+SY+SZ) with respect to the levels obtained in Case 2 (HX+HY+HZ).

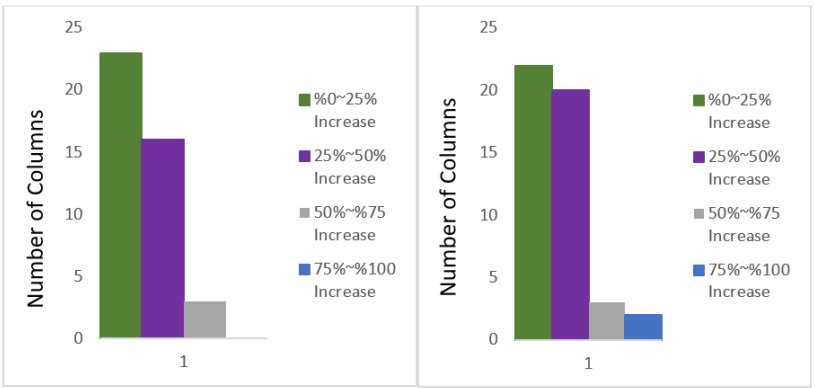

Figure 4.3. Distribution of isolator axial load increase rate (SGM ID: 3134/SS-1).

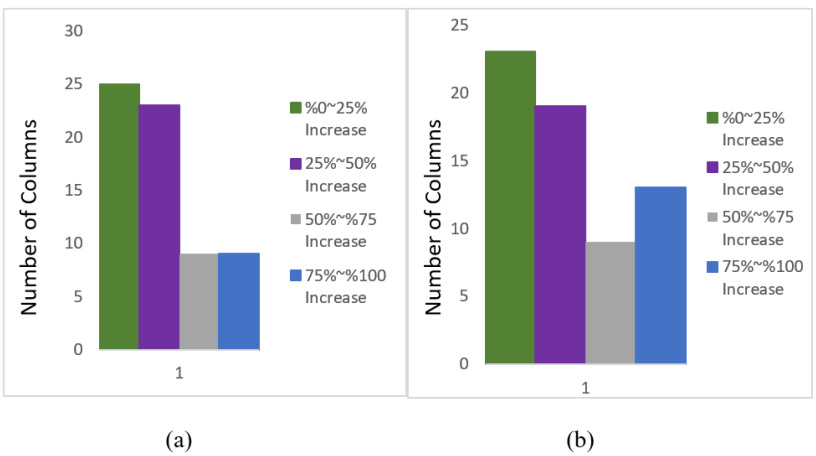

Figure 4.4. Distribution of isolator axial load increase rate (SGM ID: 3134/SS-2).

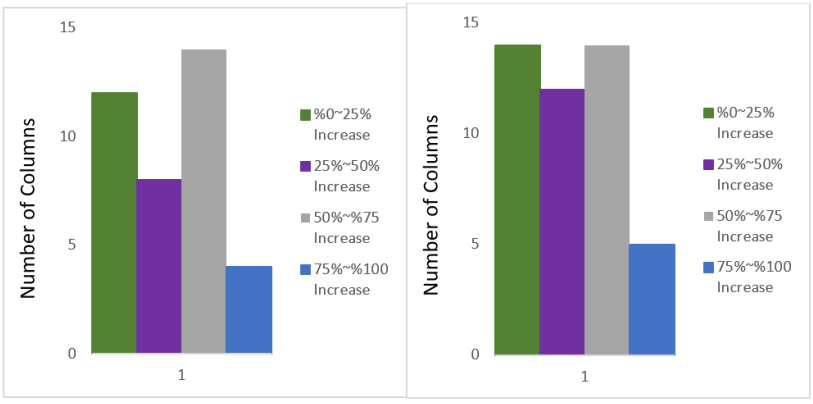

Figure 4.5. Distribution of isolator axial load increase rate (SGM ID: 4628/SS-1).

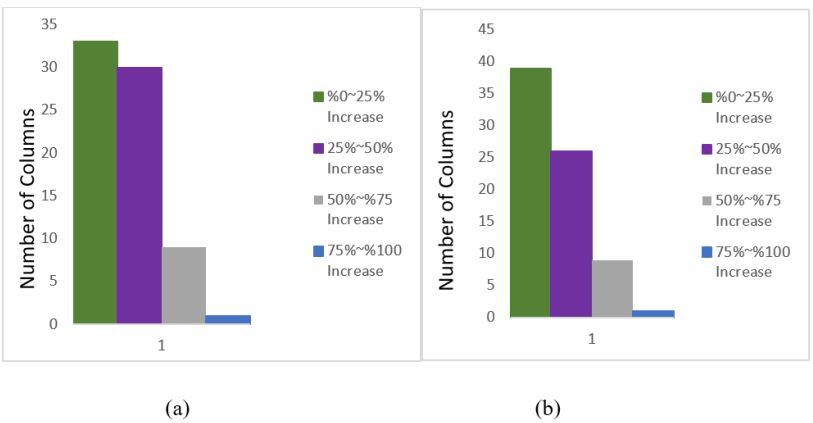

Figure 4.6. Distribution of isolator axial load increase rate (SGM ID: 4628/SS-2).

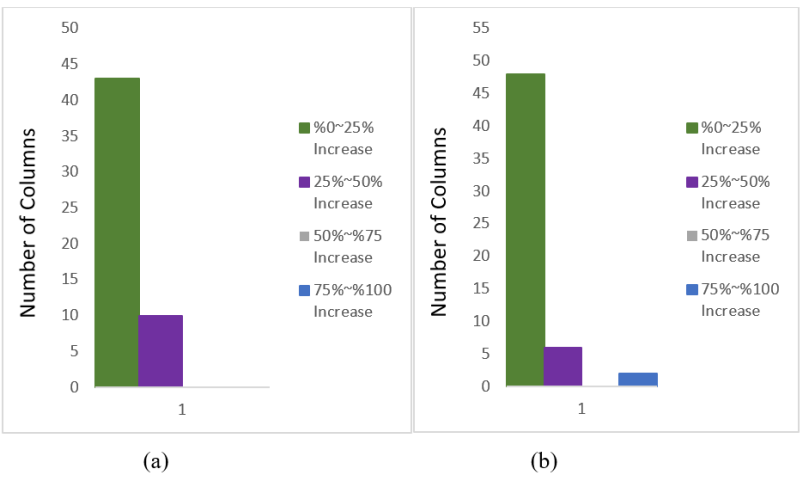

Figure 4.7. Distribution of isolator axial load increase rate (SGM ID: 1776/SS-1).

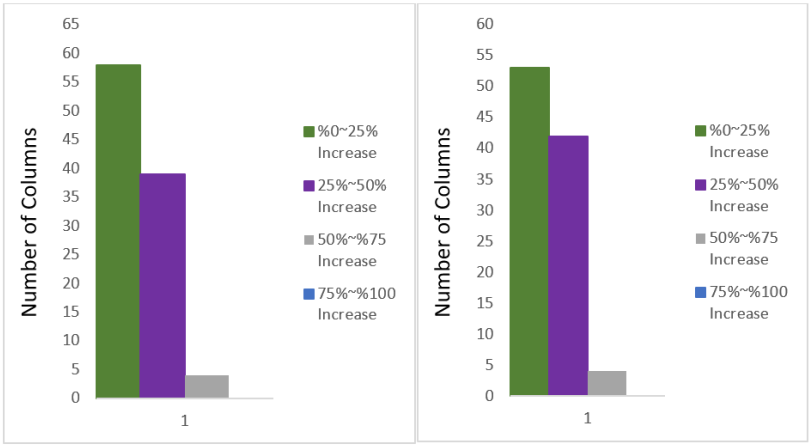

Figure 4.8. Distribution of isolator axial load increase rate (SGM ID: 1776/SS-2).

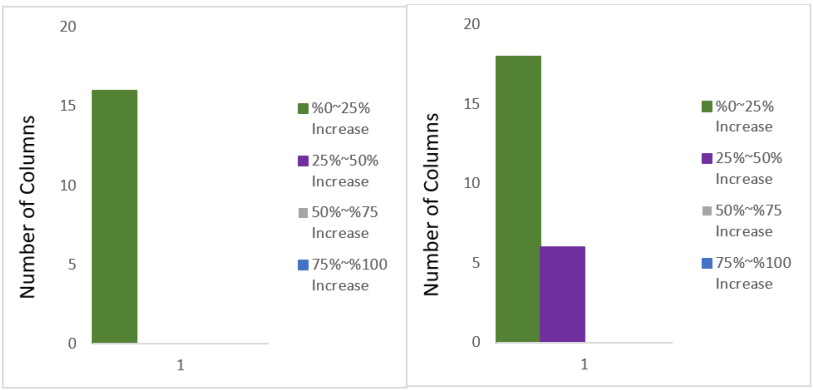

Figure 4.9. Distribution of isolator axial load increase rate (SGM ID: 1795/SS-1).

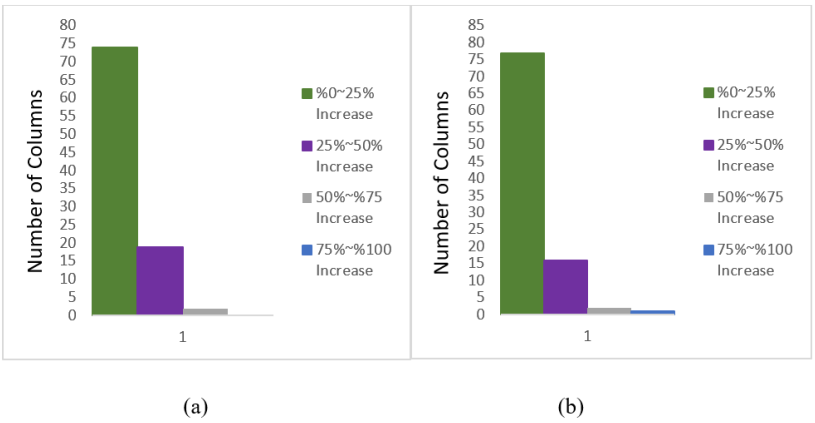

Figure 4.10. Distribution of isolator axial load increase rate (SGM ID: 1795/SS-2).

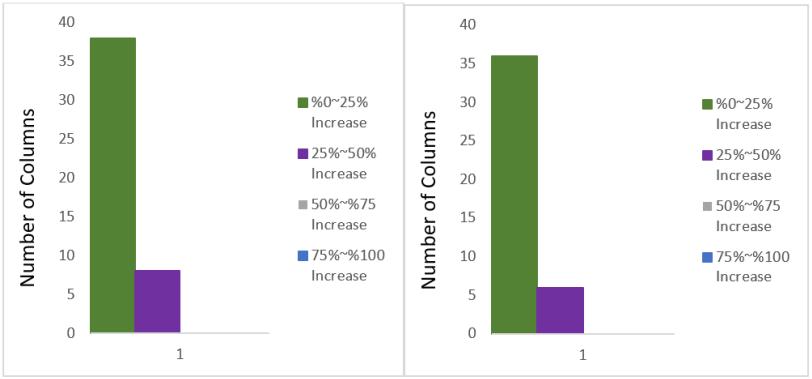

Figure 4.11. Distribution of isolator axial load increase rate (SGM ID: 3137/SS-1).

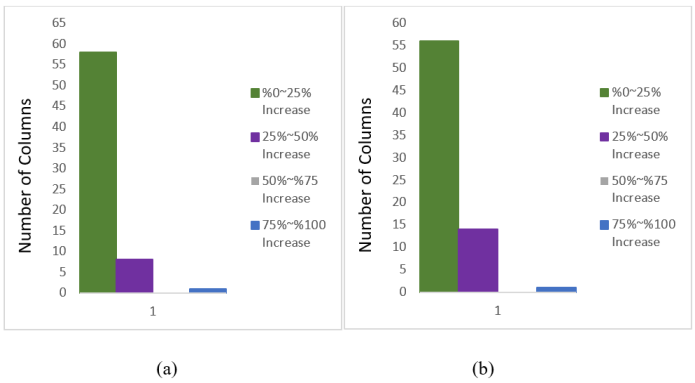

Figure 4.12. Distribution of isolator axial load increase rate (SGM ID: 3137/SS-2).

Table 4.2 and Table 4.3 provide a summary of the results presented in the preceding figures.

Table 4.2. Summary of axial load increase rate (Case 4 - Structure 1).

	Number of Columns out of 75			
SGM ID	**%0 25% Increase**	**25% 50% Increase**	**50% %75 Increase**	**75% %100 Increase**
3134	22	20	8	2
4628	14	12	4	5
1776	48	6	3	2
1795	18	6	4	0
3137	36	6	0	0

Table 4.3. Summary of axial load increase rate (Case 4 - Structure 2).

	Number of Columns out of 110			
SGM ID	**%0 25% Increase**	**25% 50% Increase**	**50% %75 Increase**	**75% %100 Increase**
3134	23	19	12	13
4628	39	26	11	1
1776	53	42	6	0
1795	77	16	3	1
3137	56	14	3	1

The findings presented in the figures and tables above demonstrate that incorporating three-dimensional spatial variation into the analysis results in a significant increase in the magnitude of the axial load on the isolators. Specifically, the axial load can increase by up to 100% when compared to the traditional analysis that considers ground displacement homogenously. The non-uniform displacements induced by the spatially varying ground motions, coupled with time lag and coherency loss, lead to the transfer of axial load between adjacent isolators, which further amplifies the magnitude of axial load on the isolators. Therefore, the inclusion of three-dimensional spatial variation is crucial for a more accurate assessment of the seismic performance of base-isolated structures.

The findings further indicate that the vertical component of spatially varying ground motion has a more significant effect on the magnitude of axial load on the isolators compared to the spatial variation of horizontal component. The impact of vertical component spatial variation tends to become more significant as the length of the structure increases, while its effect diminishes as the shear wave velocity rises. These findings highlight the importance of considering the spatial variability of both horizontal and vertical components when assessing the dynamic response of base-isolated structures, particularly for structures with larger foundation length.

To elaborate on the findings described above, Figure 4.13 is prepared.Figure 4.13 presents the isolator axial load time histories and relative vertical displacement between two near isolators, derived from both uniform and non-uniform earthquake records. To present the displacement and axial load time histories on a single plot, normalized values were employed. The normalized values were obtained by dividing the absolute maximum value of a parameter at any time step. This normalization approach allows comparing the relative variations of displacement and axial load independently of their absolute magnitudes.

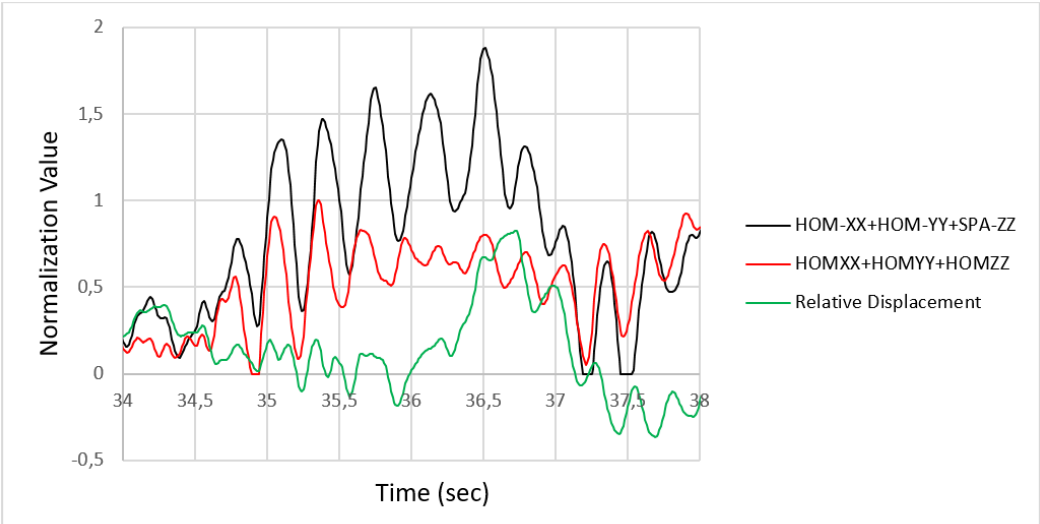

Figure 4.13. Isolator axial load and relative vertical displacement time history.

As can be observed from the Figure 4.13, there is a correlation between the increase in axial load caused by non-uniform excitation and the relative vertical displacement. In other words, as the relative displacement increases, it leads to an increase in axial load. This correlation is consistent with the expected behavior of the isolator system under non-uniform loads and demonstrates the importance of considering non-uniform loading in the design and analysis of isolator systems.

The increase in axial load represents a major concern in the design of isolators and their components. It has a direct impact on the design of crucial elements like the back plate, puck, and anchorage system, which are integral parts of the isolator assembly. Careful consideration must be given to the design of the back plate to

ensure its effectiveness in transferring the increased axial load from the superstructure to the isolator. The back plate should possess adequate strength and durability to withstand the additional load imposed on it. Optimal material selection, thickness, and strength of the back plate should be carefully determined to accommodate these increased demands.

4.3. Investigation of Column Axial Load

Secondly, considering the significant impact that it may have on the structural design of columns, the effect of vertical component and spatial variation of ground motion on the axial load of columns is examined.

The effect of vertical component and spatial variation of ground motions on column axial load is very similar to the effect on isolator axial load.

However, the increase amount is not as much as the increase on the isolator axial loads. Since, the rigid diaphragm constructed on top of the isolator balances the load distribution. The time histories of column axial forces for the uniform and spatially varying ground motion cases are presented in Figure 4.14 and Figure 4.15, respectively.

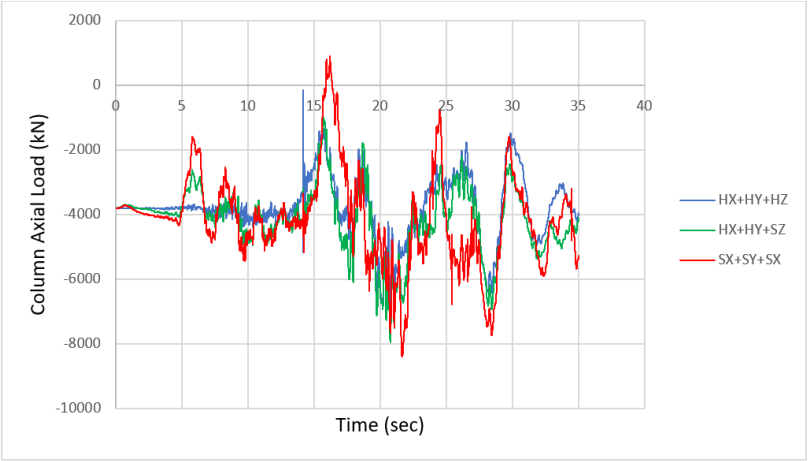

Figure 4.14. Column axial load histories (SGM ID: 1795 – Structure 1).

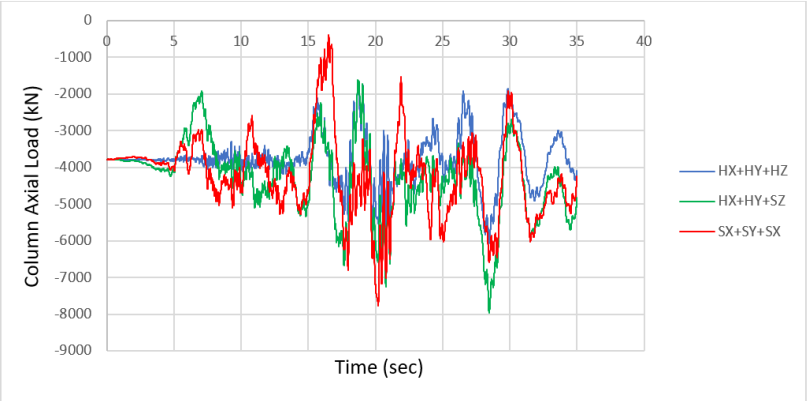

Figure 4.15. Column axial load histories (SGM ID: 1795 – Structure 2).

The figures below provide a summary of the results obtained from analyzing all cases as well as the two structures (SS-1 and SS-2. The observed increase in amount has been classified in order to more accurately monitor the increases in axial load.

The methodology described in Chaper 4.2 was followed in preparing the graphics. The graphics have been categorized into graphics “a” and “b” for ease of following. The graphics labeled “a” show the increase in axial load levels obtained in Case 3 (HX+HY+SZ) with respect to the levels obtained in Case 2 (HX+HY+HZ). The graphics labeled “b” show the increase in axial load levels obtained in Case 4 (SX+SY+SZ) with respect to the levels obtained in Case 2 (HX+HY+HZ

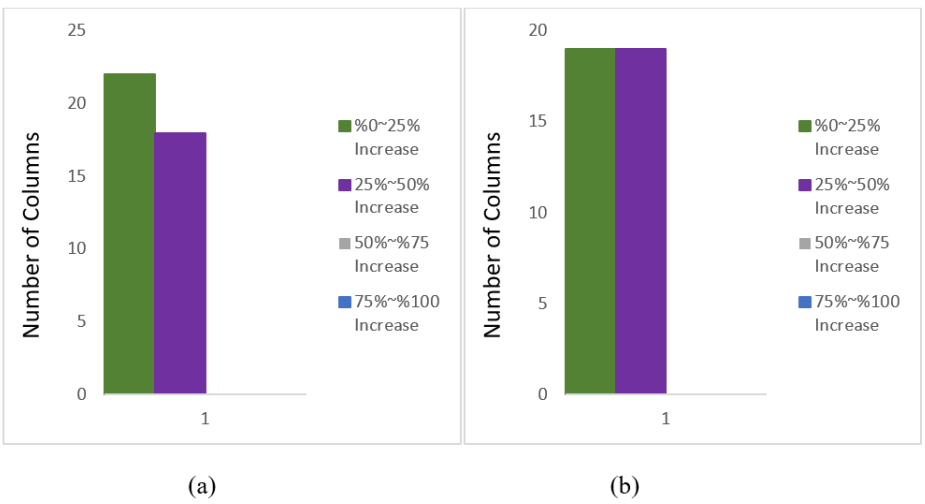

Figure 4.16. Distribution of column axial load increase rate (SGM ID: 3134/SS-1).

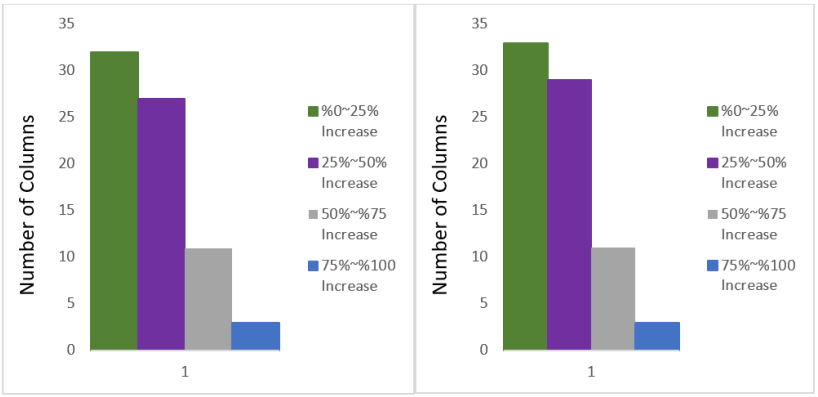

Figure 4.17. Distribution of column axial load increase rate (SGM ID: 3134/SS-2).

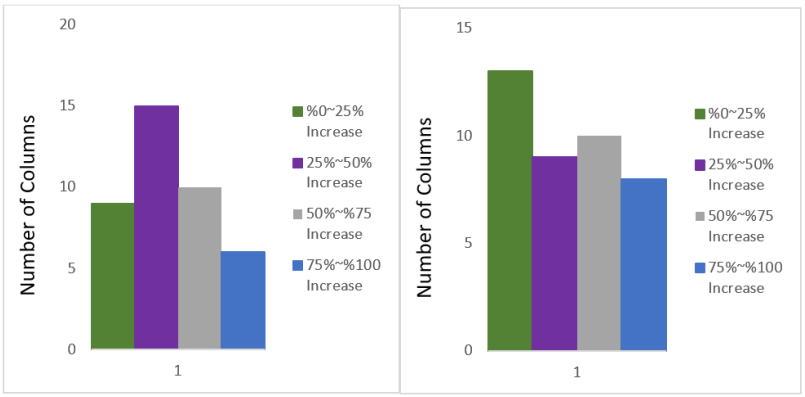

Figure 4.18. Distribution of column axial load increase rate (SGM ID: 4628/SS-1).

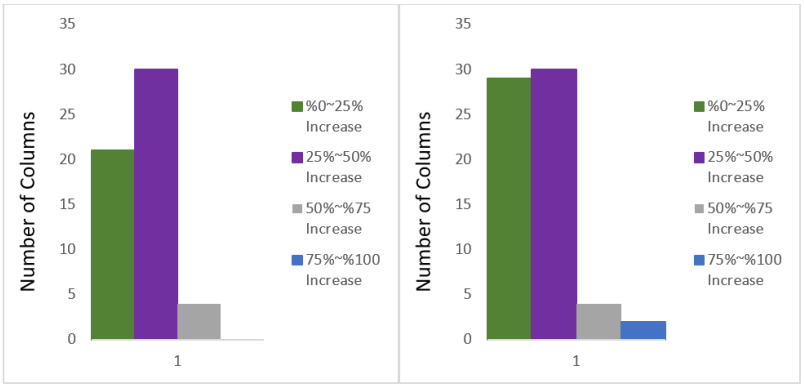

Figure 4.19. Distribution of column axial load increase rate (SGM ID: 4628/SS-2).

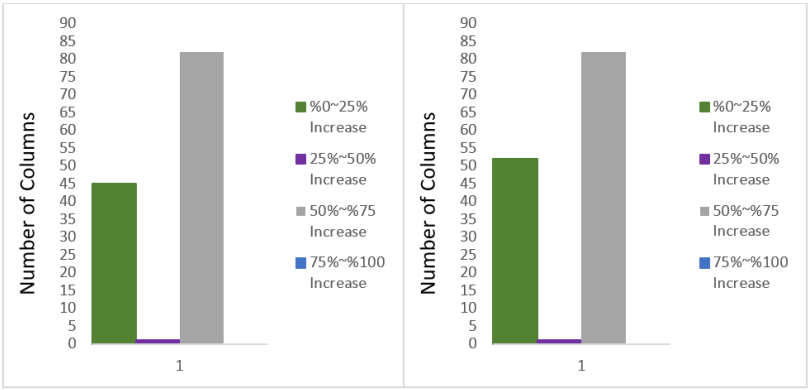

Figure 4.20. Distribution of column axial load increase rate (SGM ID: 1776/SS-1).

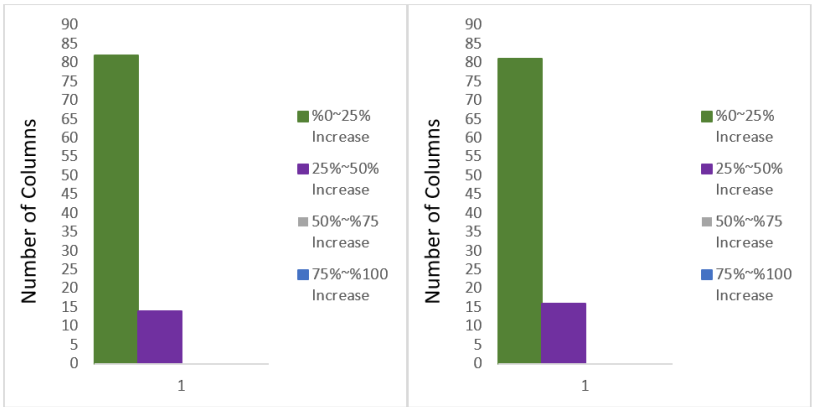

Figure 4.21. Distribution of column axial load increase rate (SGM ID: 1776/SS-2).

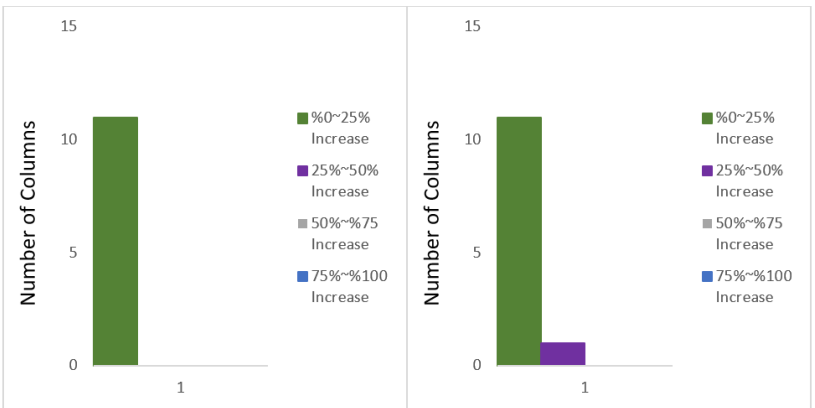

Figure 4.22. Distribution of column axial load increase rate (SGM ID: 1795/SS-1).

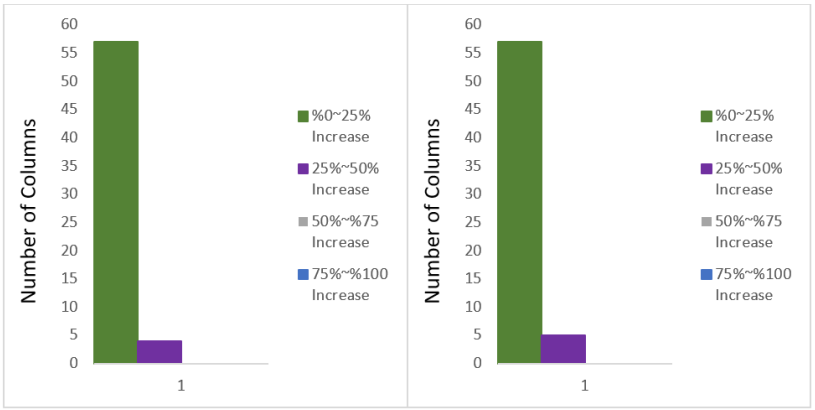

Figure 4.23. Distribution of column axial load increase rate (SGM ID: 1795/SS-2).

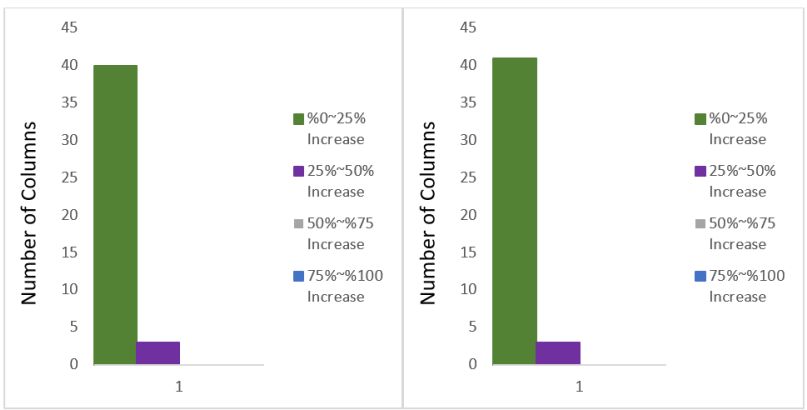

Figure 4.24. Distribution of column axial load increase rate (SGM ID: 3137/SS-1).

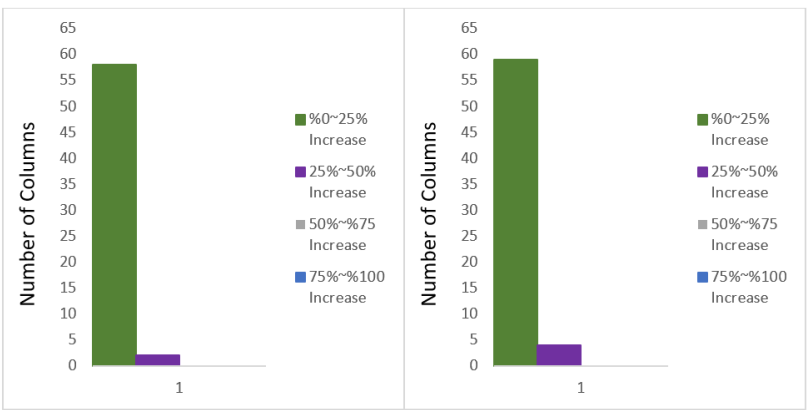

Figure 4.25. Distribution of column axial load increase rate (SGM ID: 3137/SS-2).

The following tabulated results present the outcomes of the analyses carried out for all earthquake records simulated, comprising a comprehensive overview of the response behavior of the system under various ground motions.

Table 4.4. Summary of column axial load increase rate (Case 4 - Structure 1).

	Number of Columns out of 75			
SGM ID	**%0 25% Increase**	**25% 50% Increase**	**50% %75 Increase**	**75% %100 Increase**
3134	19	19	2	0
4628	13	9	8	8
1776	52	1	0	0
1795	11	1	0	0
3137	41	3	0	0

Table 4.5. Summary of column axial load increase rate (Case 4 - Structure 2).

	Number of Columns out of 110			
SGM ID	**%0 25% Increase**	**25% 50% Increase**	**50% %75 Increase**	**75% %100 Increase**
3134	33	29	10	3
4628	13	9	8	8
1776	81	16	0	0
1795	57	5	0	0
3137	59	4	0	0

As can be observed from the presented results, similar to the increase in isolator axial loads, the shear wave velocity and foundation length remain the primary determining factors for increases in column axial loads.

The effect of increasing relative displacements between two near columns due to decreasing shear wave velocity and increasing foundation length on column axial load increase can be examined from the following figures.

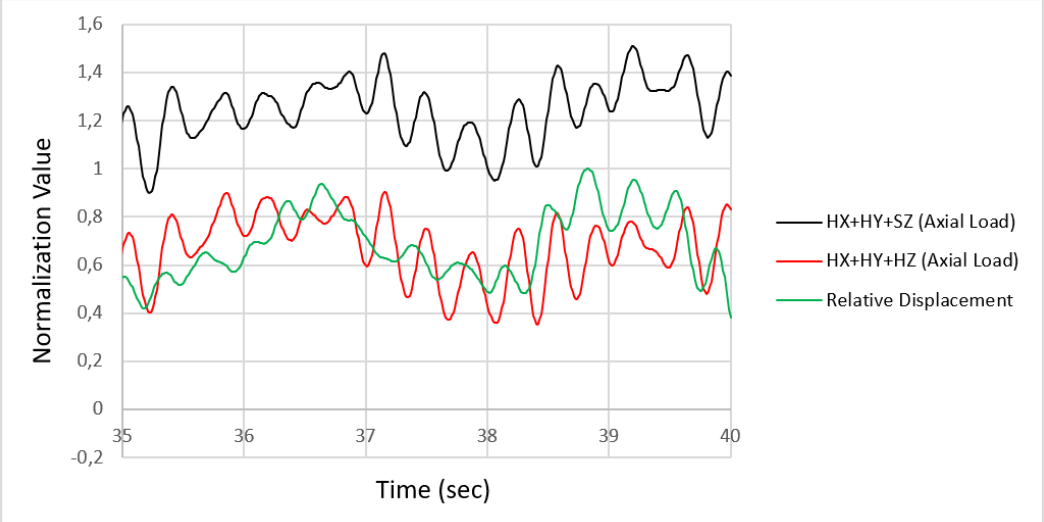

Figure 4.26. Column axial load and relative vertical displacement time history (SGM ID: 3134).

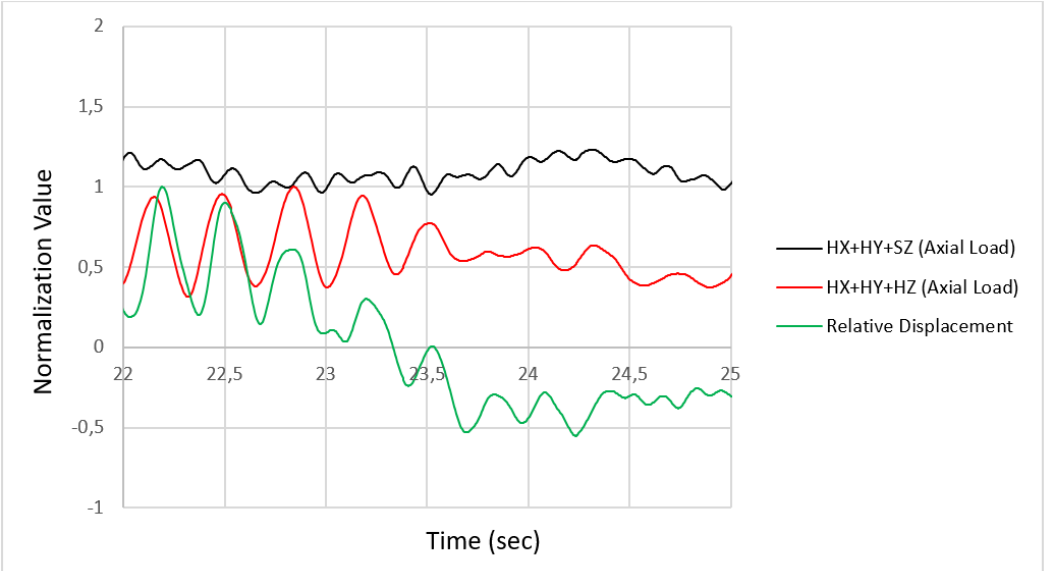

Figure 4.27. Column axial load and relative vertical displacement time history (SGM ID: 1716).

This increase in column axial load presents a significant concern in the structural design of columns. The substantial rise in axial load can lead to compressive insufficiency and a reduction in the moment capacity of the columns. The increased compression forces may surpass the column's capacity, resulting in localized compressive material failure.

Moreover, the increased axial load has a notable impact on the moment capacity of the column. As the axial load increases, the column's capacity to resist bending moments reduces. This reduction in moment capacity compromises the structural integrity of the column, making it more vulnerable to lateral deflections, excessive deformations, and potential damage.

4.4. Investigation of Base Shear

Total base shear force is one of the most important factors considered in structural design. In base isolated structures, the total base shear force is the sum of the horizontal load generated by the isolators and computed as

$$F = Dx\left(\frac{P}{R}\right) + \mu xP, \tag{4.9}$$

where F denotes the resultant horizontal force and P represents the axial load on the friction pendulum isolator. Here, D and R respectively denote the total lateral displacement and equivalent effective radius of the friction pendulum, while μ represents the coefficient of friction.

The horizontal force generated by each friction pendulum isolator is a function of the applied axial compressive load and can be represented by the Equation (4.9).

4.4.1. Effect of Vertical Component on Total Base Shear

A situation that causes an increase in the total vertical load acting on isolators would also increase the magnitude of the total horizontal load. Following that, in the case where the vertical component is taken into account, total vertical load on the isolators will increase and this increase will enlarge the total horizontal force as well.

Figure 4.28 and Figure 4.29 represents the total vertical load on the isolation system in both cases where the vertical component of strong ground is taken into account and where it is not, specifically for uniform cases.

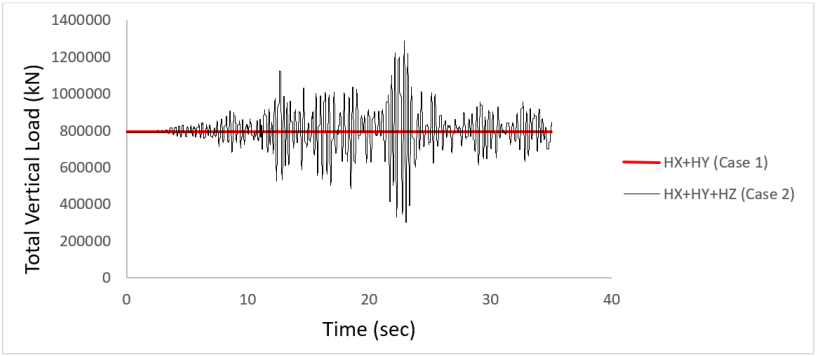

Figure 4.28. Total vertical load time histories (SGM ID: 1776).

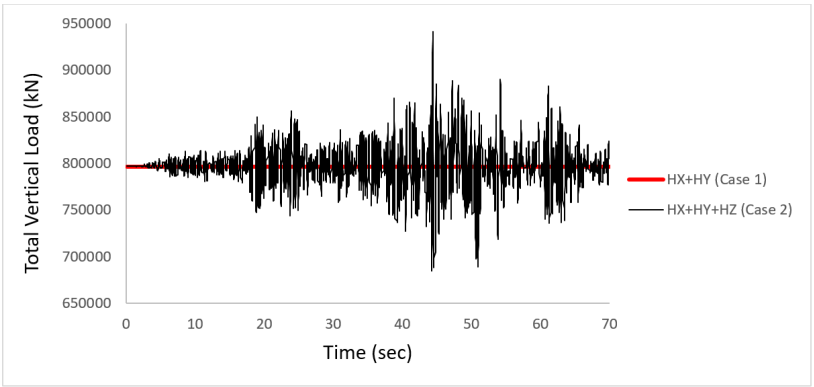

Figure 4.29. Total vertical load time histories (SGM ID: 3134).

Figure 4.30 and Figure 4.32 show the influence of the uniform vertical component on the total horizontal force. Furthermore, in order to facilitate the observation of this effect, Figure 4.31 and Figure 4.33 are provided for limited time interval.

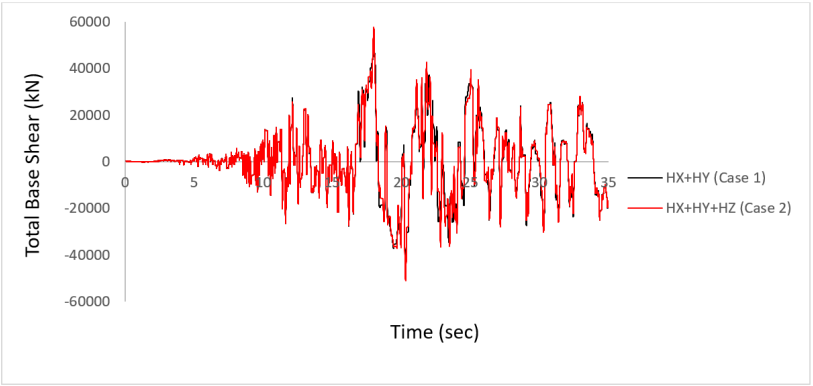

Figure 4.30. Total base shear time histories (SGM ID: 1776).

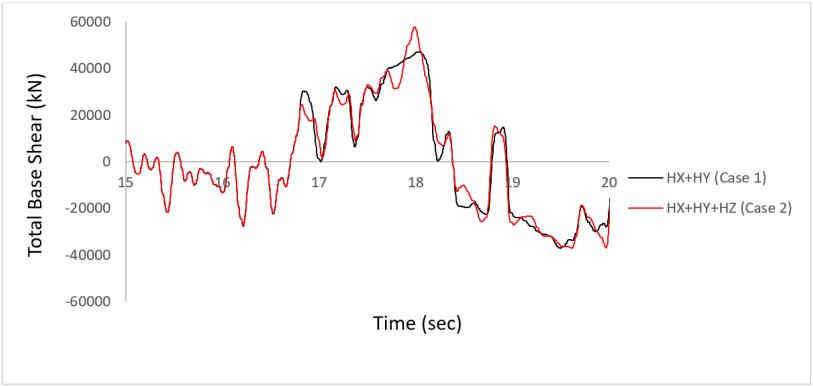

Figure 4.31. Total base shear time histories for limited time interval (SGM ID: 1776).

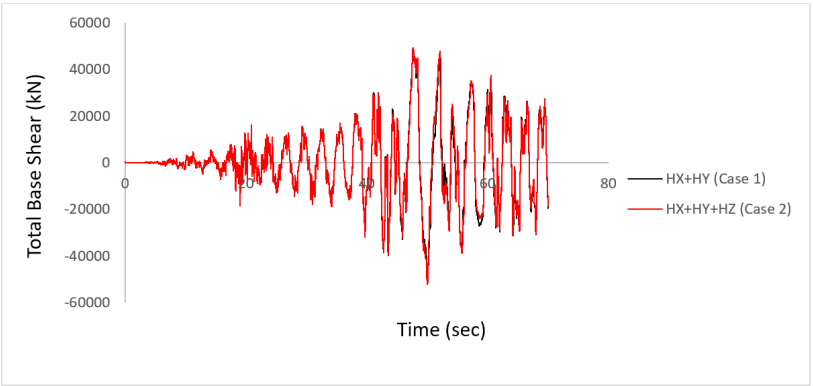

Figure 4.32. Total base shear time histories (SGM ID: 3134).

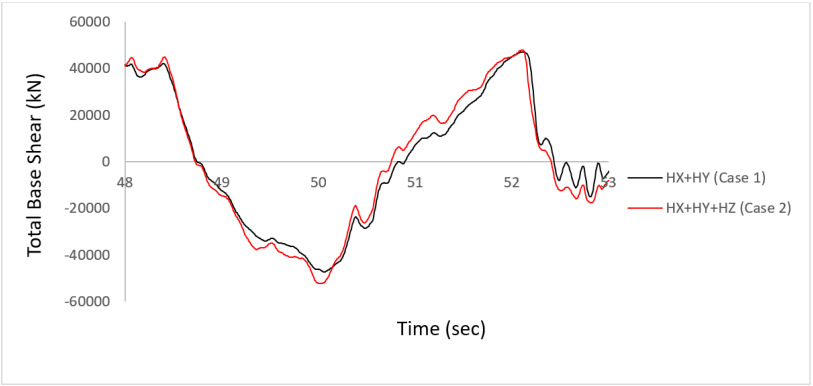

Figure 4.33. Total base shear time histories for limited time interval (SGM ID: 3134).

The total base shear force is equal to the sum of the horizontal loads that are applied to the isolators during an earthquake. This means that any change in the horizontal loads on the isolators will also affect the total base shear force.

The hysteresis curve of an isolator shows the relationship between the horizontal force applied to the isolator and the resulting displacement of the isolator. Since the total base shear force is equal to the sum of the horizontal loads on the isolators, any change in the total base shear force can also be traced on the hysteresis curve of the isolators.

Figure 4.34 and Figure 4.35 show the effect of the uniform vertical component on the isolator lateral force by using hysteresis curves.

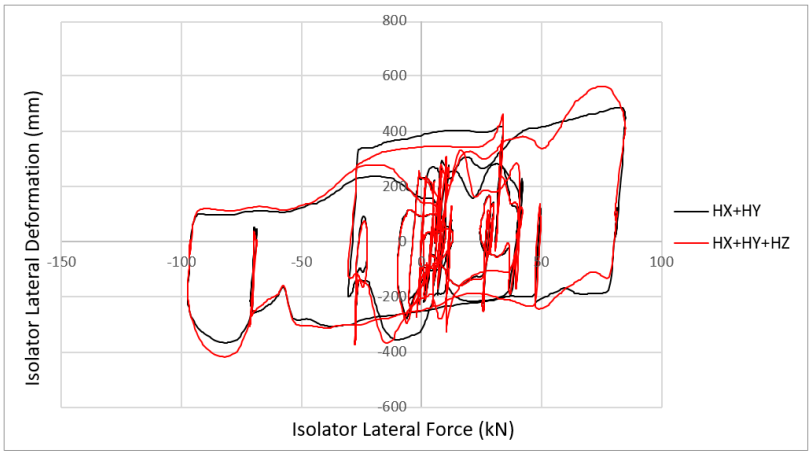

Figure 4.34. An isolator hysteresis curve (SGM ID: 1776).

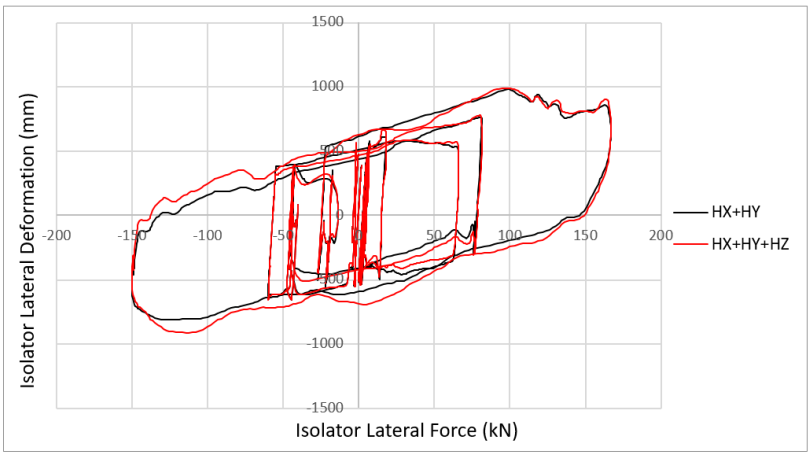

Figure 4.35. An isolator hysteresis curve (SGM ID: 3134).

In the above graphs, it can be observed that the horizontal force value shown on the Y-axis is larger when the vertical component of the earthquake is taken into account.

4.4.2. Effect of Spatial Variation on Base Shear

The impact of spatial variation on the total base shear force is investigated in cases where both the horizontal and vertical components of strong ground motion are non-uniformly propagated. Neglecting the non-uniformity of either component may result in overlooking real changes in the base shear time histories. Therefore, the effect of spatial variation on the base shear is examined for Case 1, Case 2, and Case 4.

Figure 4.36 and Figure 4.38 demonstrate the effect of spatially varying ground motion on the total base shear force. The comparison of the total base shear force is made between Case 1 (HX+HY), Case 2 (HX+HY+HAZ) and Case 4 (SX+SY+SZ).

To make it easier to observe this effect, Figure 4.37 and Figure 4.39 are presented for a limited time interval.

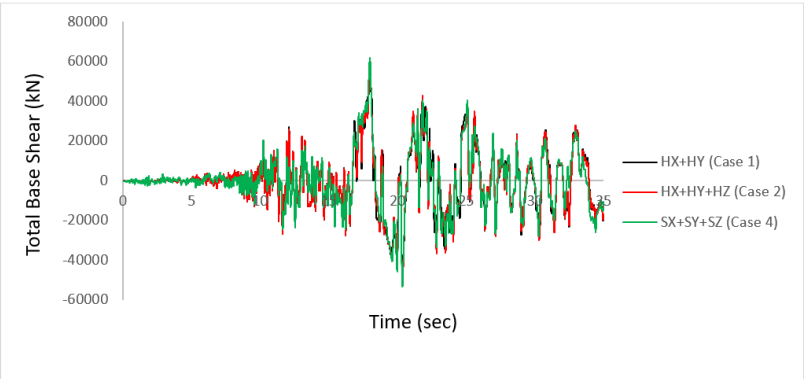

Figure 4.36. Total base shear time histories (SGM ID: 1776).

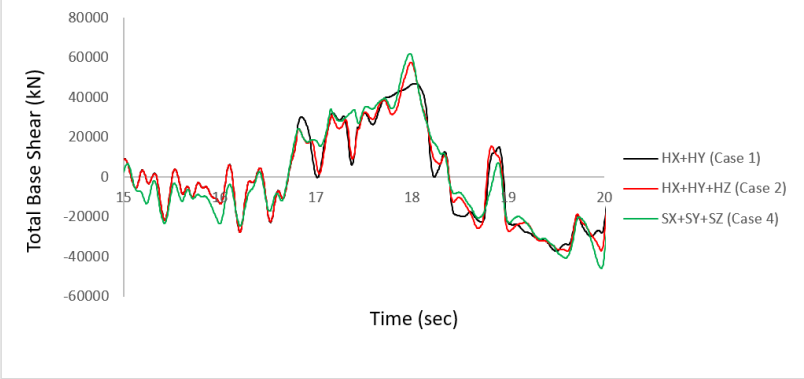

Figure 4.37. Total base shear time histories for limited time interval (SGM ID: 1776).

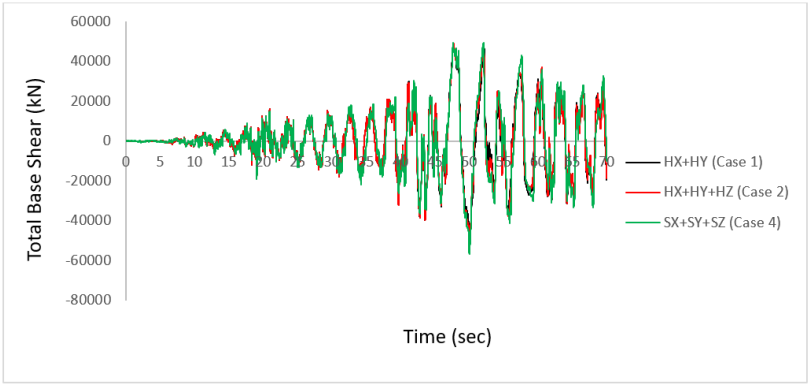

Figure 4.38. Total base shear time histories (SGM ID: 3134).

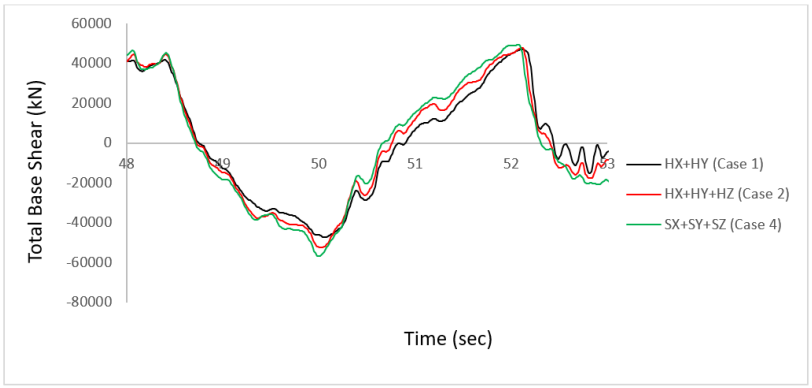

Figure 4.39. Total base shear time histories for limited time interval (SGM ID: 3134).

Similar to Section 4.4.1, the change in the total base shear force can also be followed from the hysteresis curves. Figure 4.40 and Figure 4.41 demonstrate the effect of spatial variation on the hysteresis curves.

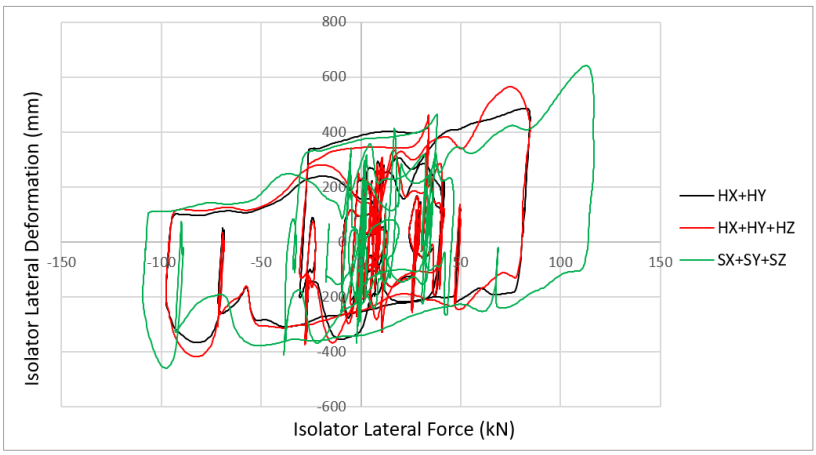

Figure 4.40. An isolator hysteresis curve (SGM ID: 1776).

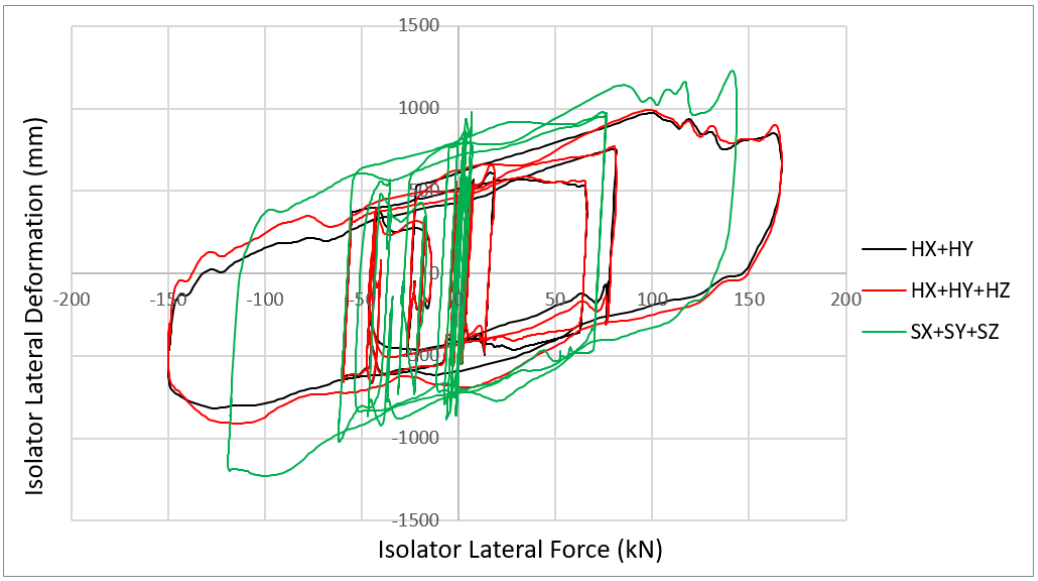

Figure 4.41. An isolator hysteresis curve (SGM ID: 3134).

The cumulative results of the analyses conducted for all simulated earthquake records are presented in the following tables, offering a comprehensive overview of the system's response behavior under varying ground motion conditions, and showing the increase in the magnitude of the total base shear under non-uniform ground motions.

To make the increase in base shear force easy to follow, the results obtained in Case 2 and Case 4 are compared to the results obtained in Case 1.

Table 4.6. Total base shear increase (Structure-1).

SGM ID	HX+HY (Case 1) / HX+HY (Case 1)	HX+HY+HZ (Case 2) / HX+HY (Case 1)	SX+SY+SZ (Case 4) / HX+HY (Case 1)
3134	100%	109%	119%
4628	100%	106%	123%
1776	100%	123%	132%
1795	100%	119%	121%
3137	100%	123%	127%

Table 4.7. Total base shear increase (Structure-2).

SGM ID	HX+HY (Case 1) / HX+HY (Case 1)	HX+HY+HZ (Case 2) / HX+HY (Case 1)	SX+SY+SZ (Case 4) / HX+HY (Case 1)
3134	100%	107%	119%
4628	100%	118%	120%
1776	100%	118%	121%
1795	100%	121%	123%
3137	100%	126%	130%

To provide further explanation for the findings described earlier, Figure 4.42 and Figure 4.43 have been created. Figure 4.42 and Figure 4.43 illustrate the time history of base shear (red line), vertical load (black line), and the sum of lateral displacements of isolators (blue and green lines) obtained from both uniform and non-uniform earthquake records. In order to present displacement and load time histories on a single plot, normalized values were used. Normalized values were calculated by dividing each parameter's absolute maximum value at any time step. This normalization method enables a comparison of the relative variations of displacement and load magnitude independent of their absolute values.

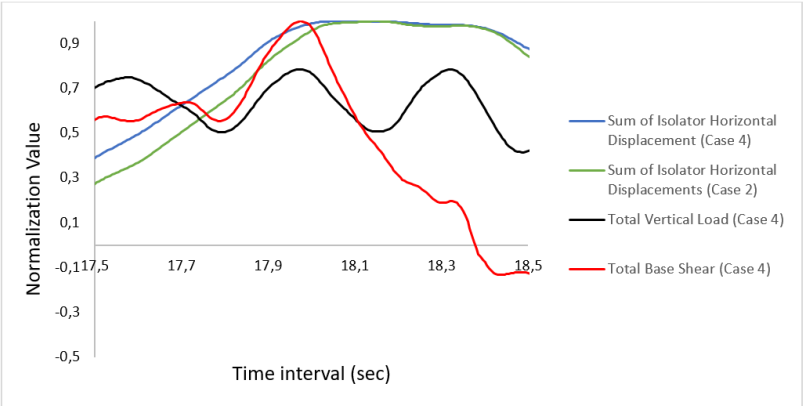

Figure 4.42. The dependance of base shear on vertical load and lateral displacement (SGM ID: 1776).

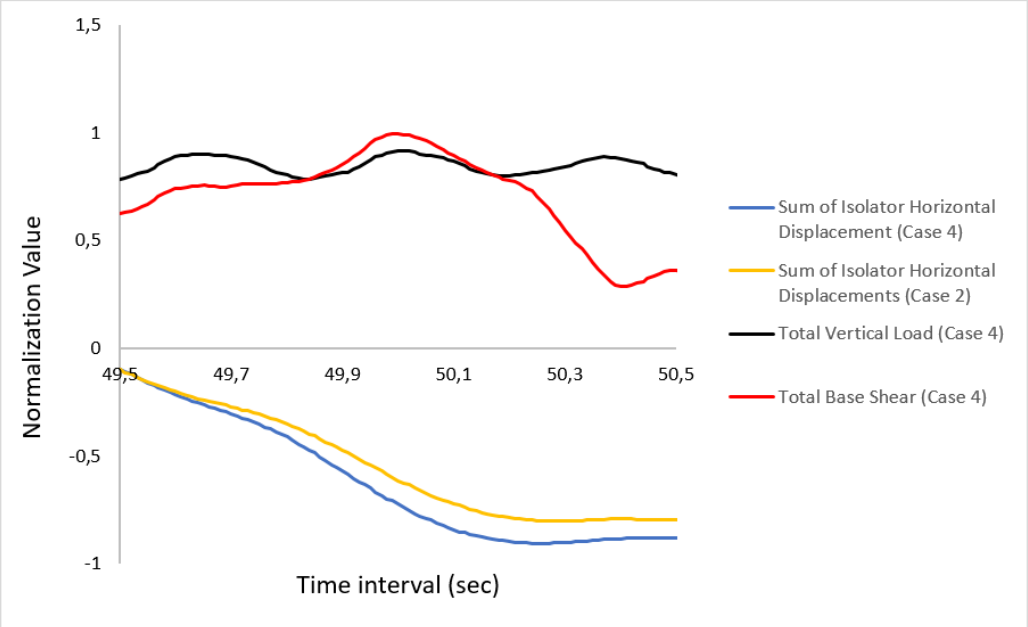

Figure 4.43. The dependance of base shear on vertical load and lateral displacement (SGM ID: 3134).

As can be observed from Figure 4.42 and Figure 4.43, if the non-uniform horizontal component causes an increase in horizontal displacement while the total axial load on the friction pendulum isolators is relatively high, this leads to an increase in the total shear force affecting the structure.

In a similar way, if the non-uniform vertical component causes an increase in total vertical load while the horizontal displacement of the friction pendulum isolators is relatively high, this can also lead to an increase in the total shear force affecting the structure.

Both situations generally result from time delay. The time delay caused by the non-uniform ground displacement distribution leads to the maximum magnitudes of two responses (maximum total vertical load and maximum isolator displacement) occurring at different times compared to the uniform ground displacement distribution. An increase in shear force can occur when the maximum isolator displacement demand of the non-uniform case is greater than the maximum isolator displacement of the uniform case even if the total vertical load remains same. Similarly, an increase in

shear force can occur when the maximum total vertical load of the non-uniform case is greater than the maximum total vertical load of the uniform case even if the maximum isolator displacement remains same.

Consequently, Case 4 results in an approximately 30% increase in total shear force compared to Case 1, and an approximately 10% increase compared to Case 2.

4.4.3. Effect of Base Shear Increase on Internal Forces of Structural Members

The increase in the base shear force explained in Chapter 4.4.1 and 4.4.2 also leads to an increase in the internal forces of structural elements. This increase in structural elements can be observed through the figures presented below. The overall increase in base shear causes an increase in the shear force and bending moment internal forces in the structural elements.

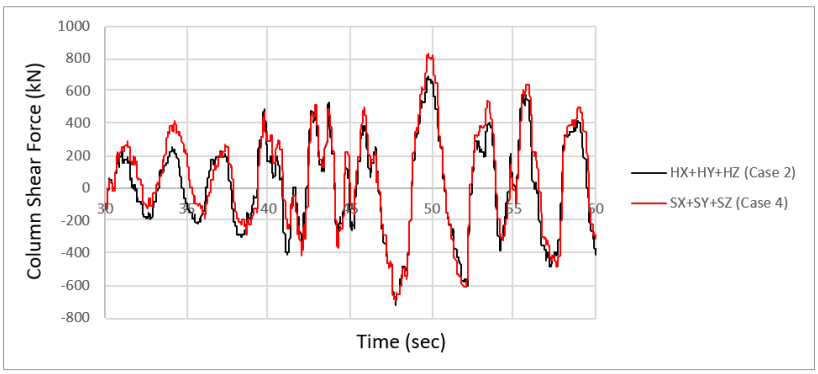

Figure 4.44. Column shear force time history (SGM ID: 3134).

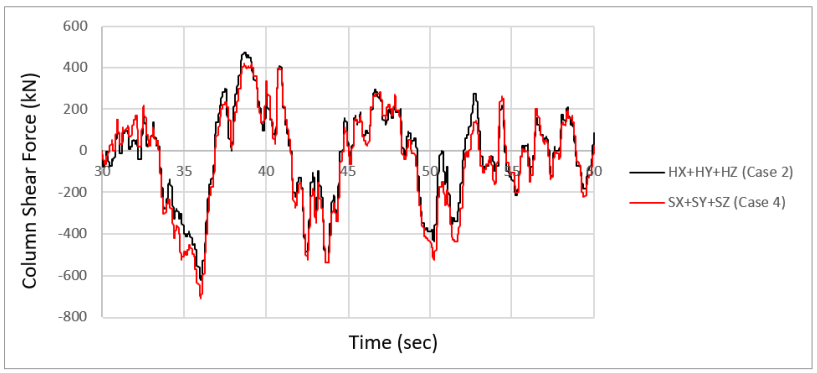

Figure 4.45. Column shear force time history (SGM ID: 1776).

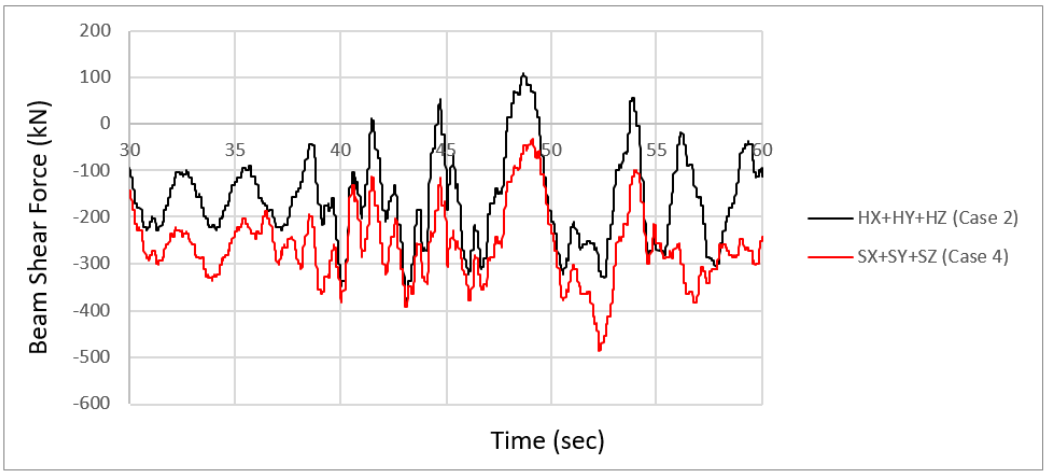

Figure 4.46. Beam shear force time history (SGM ID: 3134).

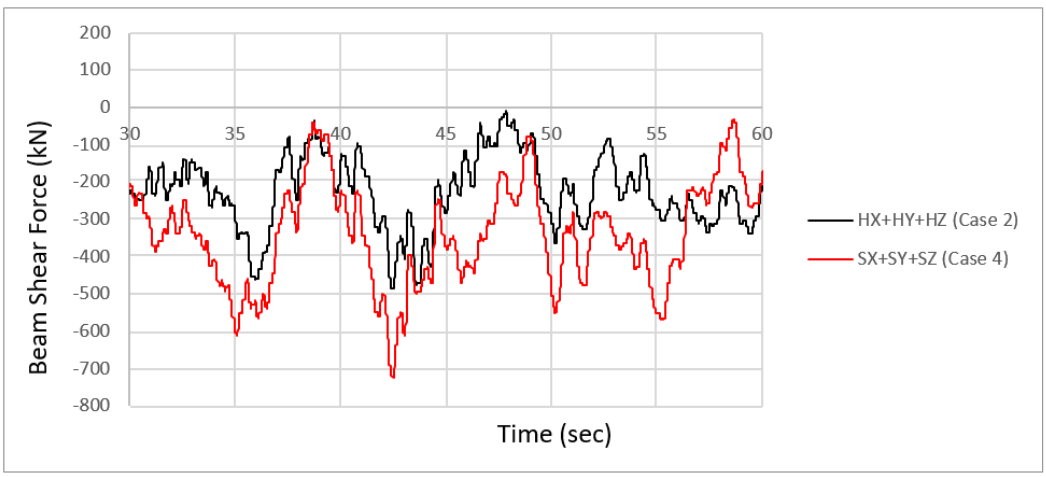

Figure 4.47. Beam shear force time history (SGM ID: 1776).

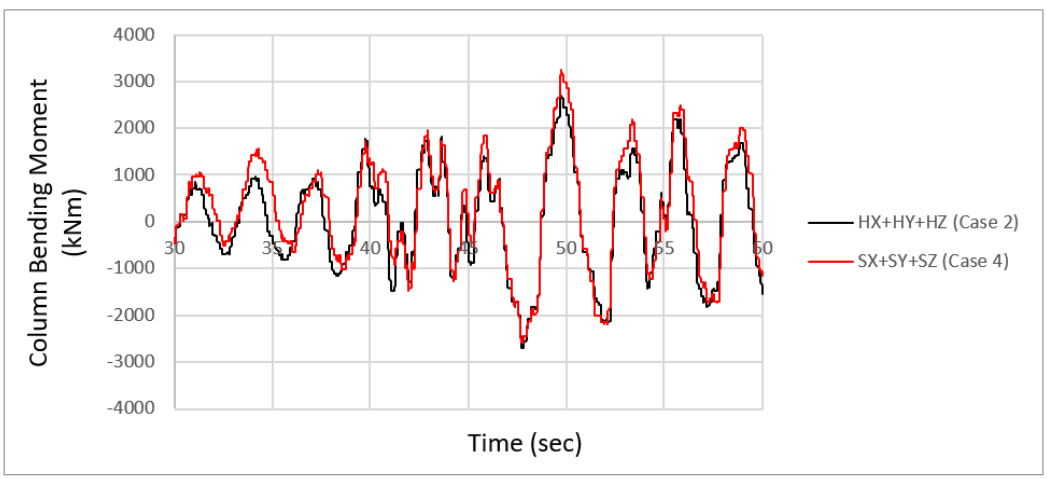

Figure 4.48. Column bending moment time history (SGM ID: 3134).

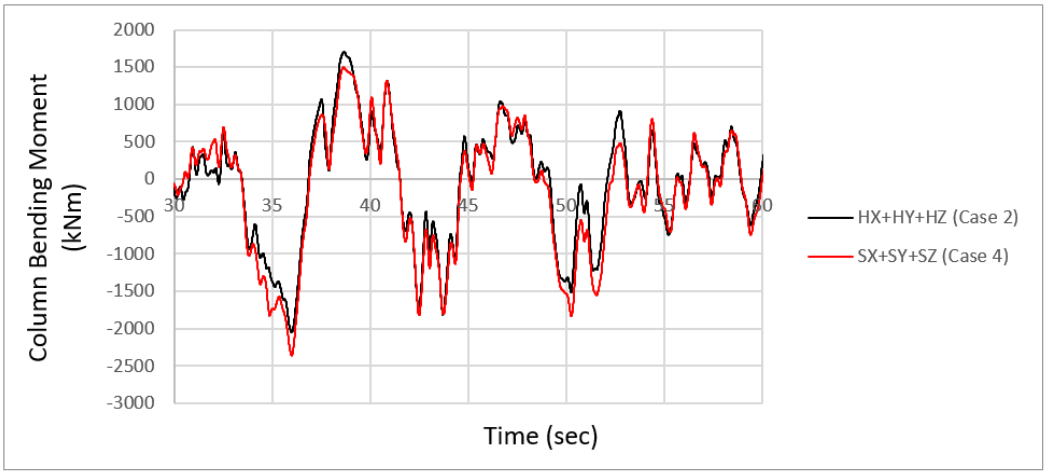

Figure 4.49. Column bending moment time history (SGM ID: 1776).

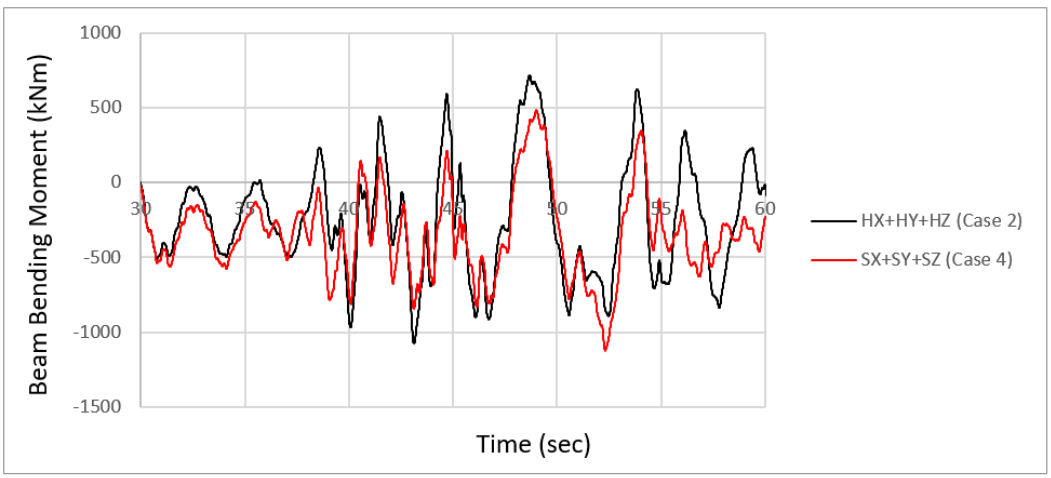

Figure 4.50. Beam bending moment time history (SGM ID: 3134).

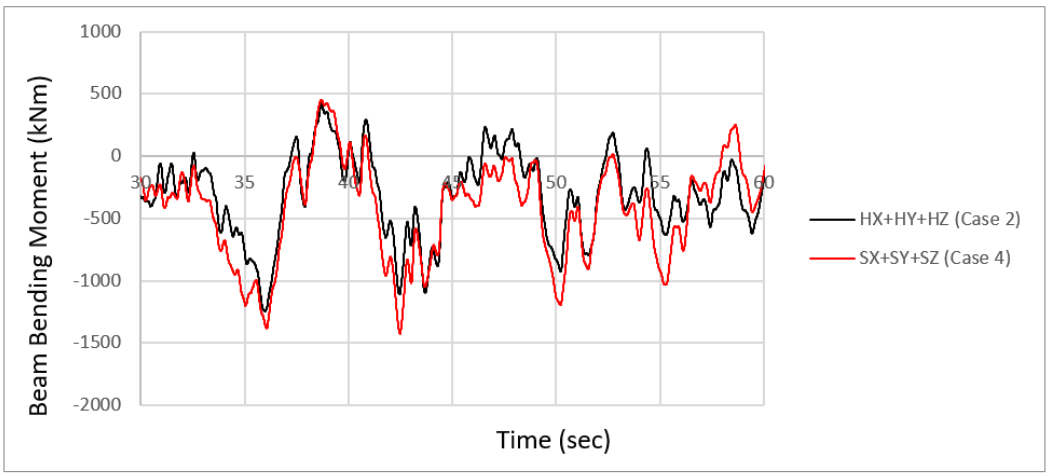

Figure 4.51. Beam bending moment time history (SGM ID: 1776).

The observed increases in internal forces can be a significant factor in the design of structural elements. This situation creates an effect that needs to be taken into consideration in structural detailing, selection of section dimensions, and design of connection joints.

4.5. Investigation of Torsional Behavior and Isolator Maximum Displacement Demand

As part of this study, the issue of torsion has been included and examined due to its critical importance in preserving the overall structural integrity and ensuring the optimal design and performance of load-bearing components in structural systems. Torsional effects can significantly impact the behavior and performance of structures, and therefore require careful consideration and analysis in the design and evaluation of structural systems.

One of the most reliable indicators of torsional effects is the measurement of lateral displacement differences between two diagonally opposite corners of the structure. This displacement difference is commonly known as the rotation of the structure. The amount of rotation is directly proportional to the magnitude of the occurred torsional force and can significantly affect the performance and behavior of the structure. Therefore, assessing the magnitude of rotation and identifying the underlying causes of torsion is essential for ensuring the safe and effective design of load-bearing structures.

The lateral displacement difference between two diagonally opposite corners of the structure can be measured through isolator movements. However, to better understand whether there is any displacement difference, the isolator resultant displacement demands in both cases (Case 2 and Case 4) were measured first.

The effect of the spatial variation of strong ground motion on the maximum resultant displacement demand of the isolator was analyzed, and Figure 4.52, Figure 4.53, Figure 4.54 and Figure 4.55 show that this variation did not have a significant effect on

the isolator maximum displacement demand. The results indicated that the isolator's maximum displacement demand remained relatively constant for spatial variations of ground motion. The resultant displacement is calculated for each time step as

$$d_t = \sqrt{d_x^2 + d_y^2}. \tag{4.10}$$

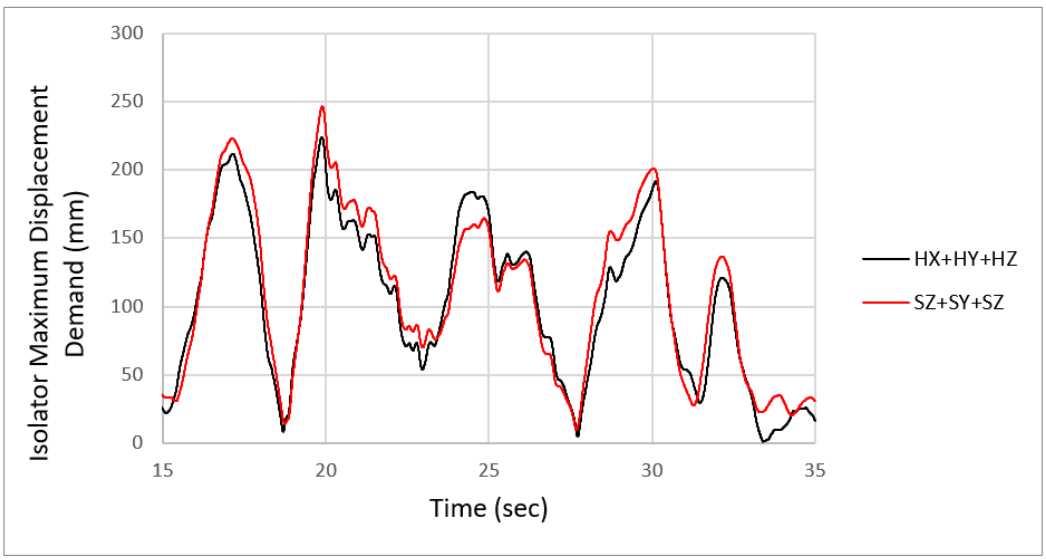

Figure 4.52. Isolator maximum resultant displacement demand (SGM ID: 1776).

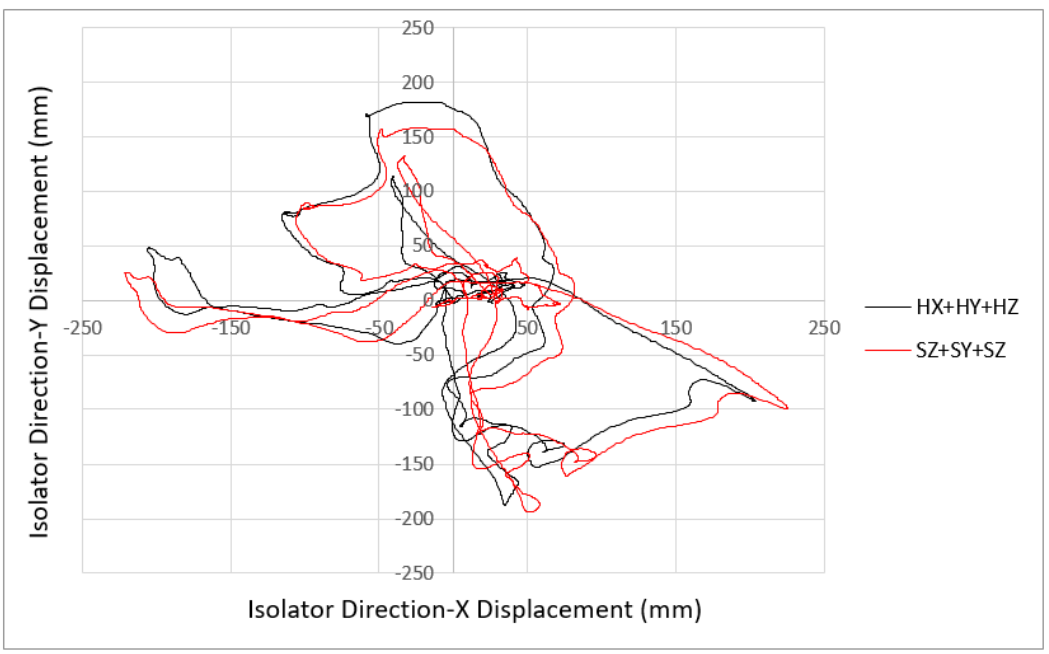

Figure 4.53. Isolator displacement track (SGM ID: 1776).

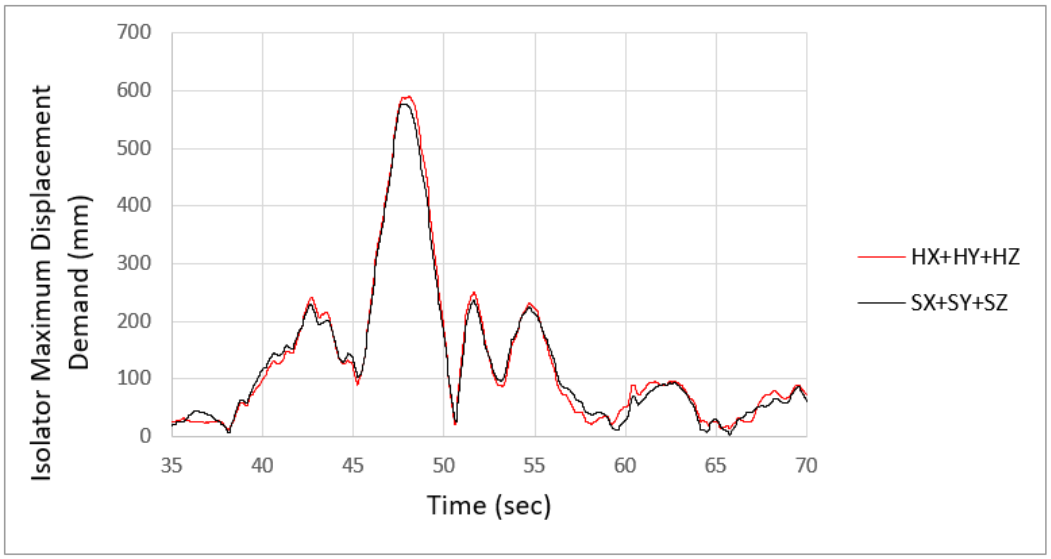

Figure 4.54. Isolator maximum resultant displacement demand (SGM ID: 3134).

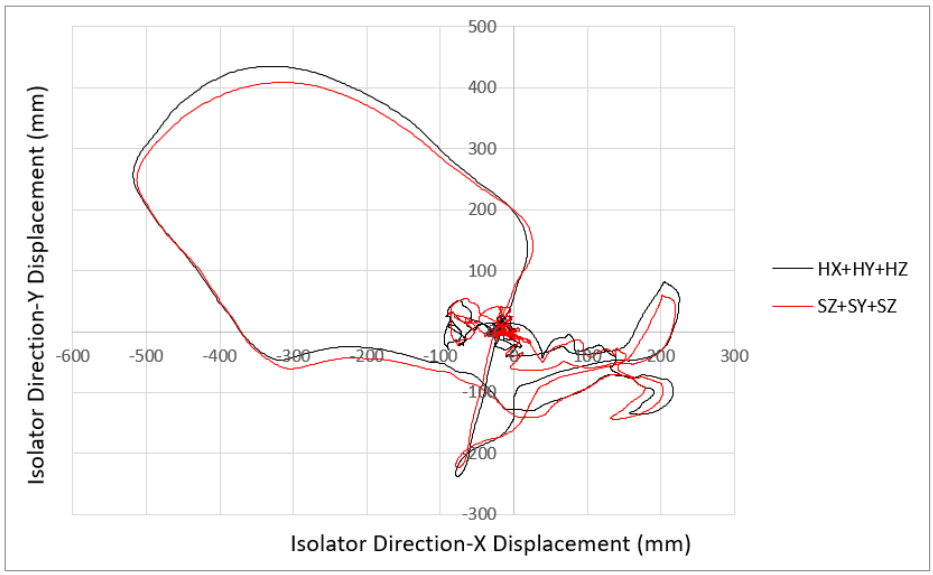

Figure 4.55. Isolator displacement track (SGM ID: 3134).

However, time delay caused by spatial variation in transverse direction can induce different isolator displacement demand at two diagonally opposite corners of structure. To investigate this issue, the relative displacement between the two points shown in Figure 4.55 and were followed.

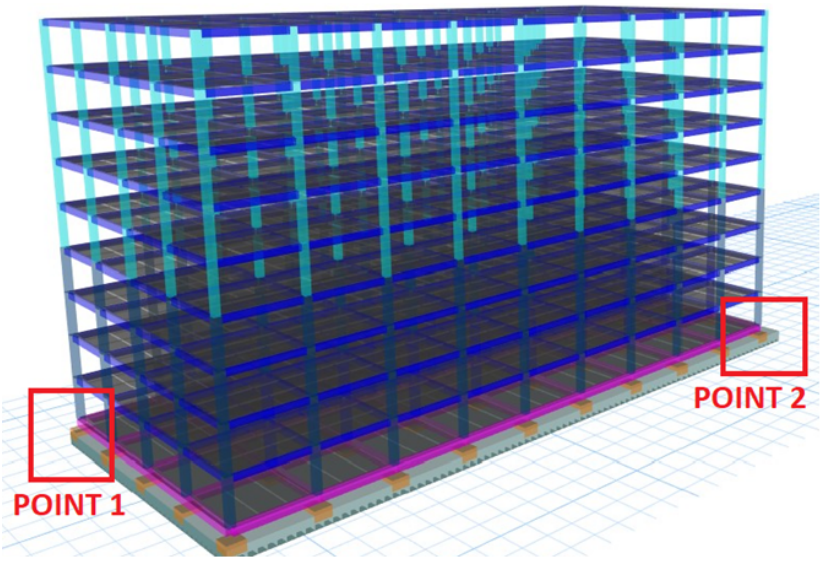

Figure 4.56. Two far points of structure.

Figure 4.57 and Figure 4.58 show the relative displacements at the two far edges of structure separately for uniform and nonuniform excitation.

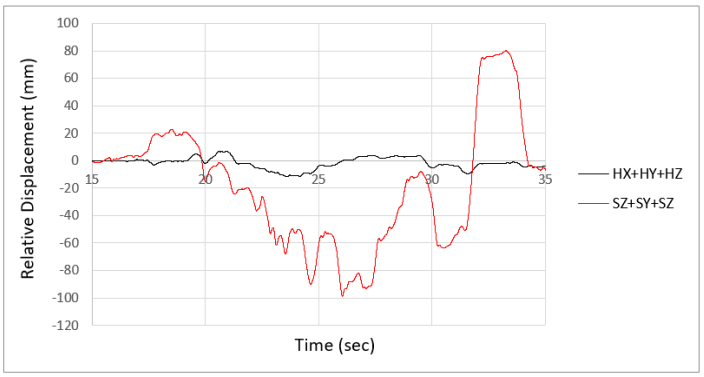

Figure 4.57. Relative displacement at far edges of structure (SGM ID: 1776).

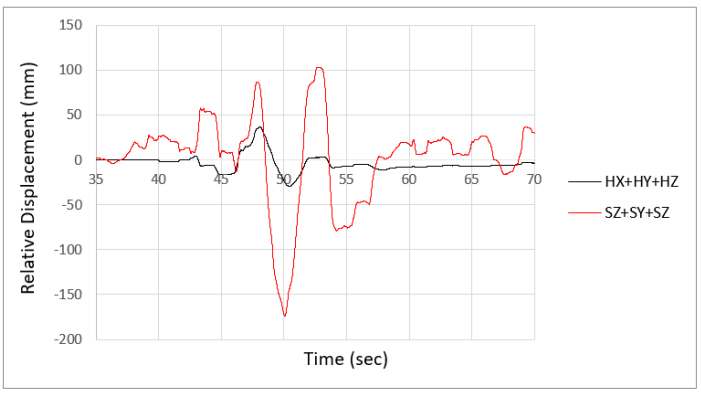

Figure 4.58. Relative displacement at far edges of structure (SGM ID: 3134).

The increasing amount of relative displacement can induce the formation of torsional forces. In Figure 4.59 and Figure 4.60, the distribution of torsional moment for both cases (Case 2 and Case 4) can be observed. There is a significant difference between the two cases. The uniform load distribution causes the entire structural system to move together (Figure 4.61), while the non-uniform distribution creates rotation in the structural system (Figure 4.62). Therewith, it would be necessary to consider torsional forces in the structural design.

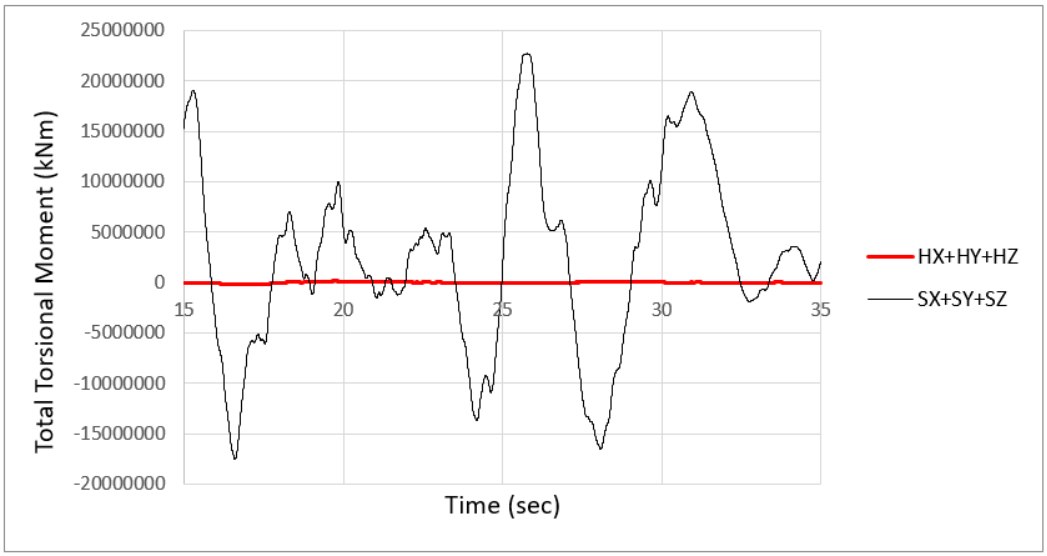

Figure 4.59. Total torsional moment time histories (SGM ID: 1776).

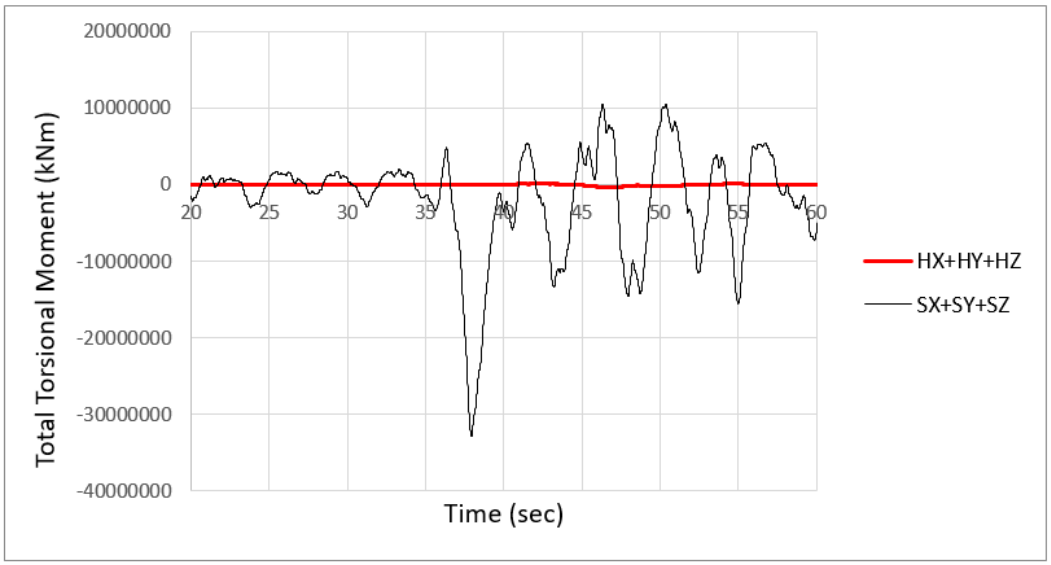

Figure 4.60. Total torsional moment time histories (SGM ID: 3134).

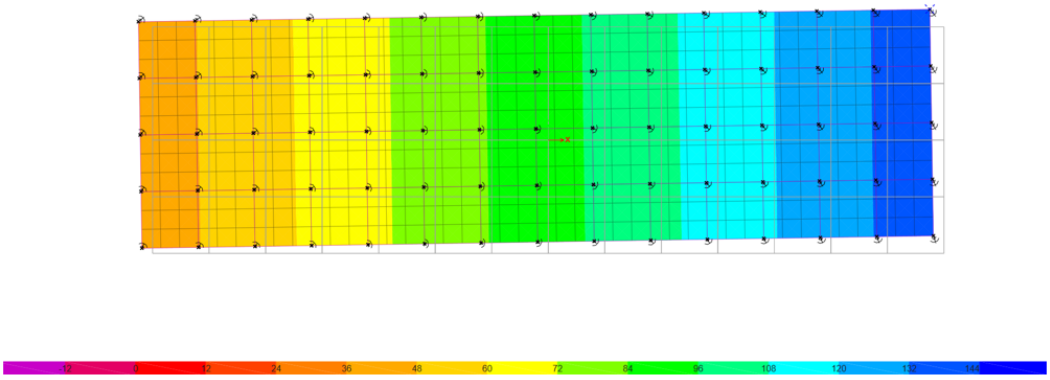

Figure 4.61. Lateral displacement in transverse direction (mm) (Structure 1 SGM ID: 1776).

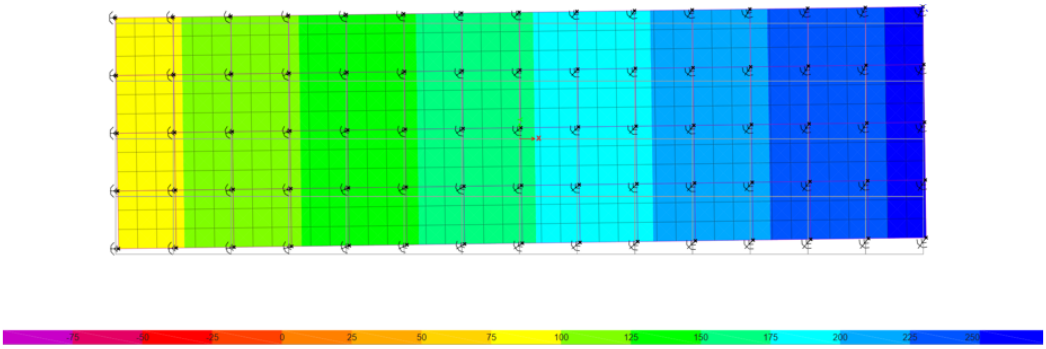

Figure 4.62. Lateral displacement in transverse direction (mm) (Structure 1 SGM ID: 3134).

The torsional forces induced by spatial variation have important role in the structural design and analysis. These forces introduce torsional moments that can significantly affect the behavior and stability of the members. Furthermore, torsional moments interact with shear forces, affecting shear design as well.

5. CONCLUSIONS AND FUTURE WORKS

This thesis presents the effect of vertical component and spatial variation of strong ground motion on base isolated structures with friction pendulum type isolators. Five known strong ground motion data are used as known acceleration histories and spatially correlated simulations are performed for the target points. It was considered that the distance between target points is 10 meters. In this way, a more accurate result was obtained.

Attention was paid to the selection of the known earthquake records with the different shear wave velocities since the effect of shear wave velocity on coherency loss is significant. Following that, two structures with different foundation lengths are studied to determine the effect of distance on spatial variation.

Three-dimensional finite element models were created to conduct dynamic response analysis of the structure. The models were designed to incorporate the nonlinear characteristics of friction pendulum isolators. The dynamic response analyses of the structures were performed using a three-dimensional finite element model, which accounted for the nonlinear properties of friction pendulum isolators. The analysis considered all three components of earthquake ground motion, including horizontal motion in two directions and vertical motion, in order to accurately identify all effects.

5.1. Conclusions

Within the scope of this study. The conclusions drawn from study are summarized as follows;

- The study findings indicate that the plan length of the building is a significant factor that affects coherency loss and phase shift. As the plan dimension of the building increases, the effect of spatially varying ground motion also increases. In

other words, larger buildings are more susceptible to non-uniform ground motion effects. To better describe this effect, studies were conducted on two buildings with different plan lengths.

- The shear wave velocity of the soil is an important parameter that can affect the coherency loss and phase shift of the structure. Specifically, lower shear wave velocity magnitudes can increase the effect of spatially varying ground motion on the structure. Therefore, the shear wave velocity should be carefully considered in the spatially varying ground motion simulations.
- Based on the dynamic response analysis results conducted with the selected five earthquake records, the spatial variation of strong ground motion can increase isolator axial load up to 95%. The effect of vertical component spatial variation increases for longer foundation length and decreases for higher shear wave velocity. The relative vertical displacements caused by coherency loss and wave passage effect result in load transfer between the isolators.

  The increase in axial load presents a significant concern for the design of isolators and their components. It has a direct impact on the design of the back plate, puck, and anchorage system, which are crucial elements of the isolator assembly. The design of the back plate needs to be carefully considered to ensure it can effectively transfer the increased axial load from the superstructure to the isolator. It should possess adequate strength and durability to withstand the additional load imposed on it. The material selection, thickness, and strength of the back plate should be optimized to accommodate the increased demands.

  Similarly, the design of the puck, which is the primary load-bearing element of the isolator, needs to be modified to account for the increased axial load. The mechanical properties and dimensions of the puck should be carefully evaluated and adjusted to ensure it can safely support the increased load.

  Additionally, the anchorage system, which connects the isolator to the foundation, should be designed to withstand the increased axial load. The selection of appropriate anchor types, their spacing, and reinforcement detailing should be carefully determined to ensure sufficient load transfer and anchorage capacity. Therefore, comprehensive design considerations, including material selection, di-

mensions, reinforcement, and connection details, should be made to accommodate the increased axial load. This approach ensures the isolator, and its components can safely and efficiently handle the additional demands, resulting in a robust and resilient base isolation system.

The impact of the spatial variation in the vertical component of strong ground motion on the variation of isolator axial load is more pronounced compared to the spatial variation in the horizontal component.

- The effect of spatial variation of ground motion on column axial load is very similar to effect on isolators. However, the rigid diaphragm on the isolators balances the axial load transfer by limiting relative displacements.

  Based on the dynamic response analysis results conducted with the selected five earthquake records, the spatial variation of ground motion can increase column axial load up to 85%.

  This increment poses a significant concern for the structural design of columns. The increase in axial load at this magnitude can result in compression failure and a reduction in the moment capacity of the columns. The high compression forces can exceed the capacity of the column, leading to localized compressive failure of the material.

  Furthermore, the increased axial load can have an important effect on the moment capacity of the column. As the axial load increases, the capacity of the column to resist bending moments decreases. This reduction in moment capacity can undermine the structural integrity of the column, making it more susceptible to lateral deflections, excessive deformations, and potential collapse.

  It is useful to address and account for this significant axial load increment in the design of columns. Adequate reinforcement, appropriate material selection, and careful consideration of cross-sectional dimensions should be employed to ensure that the columns can withstand the increased axial loads and maintain their structural integrity and performance under seismic loading conditions.

- Uniform vertical excitation has significant effect on both structural and structural elements' responses for base isolated buildings with friction pendulum. In the conducted dynamic response analysis, it has been observed that the magnitude

of the base shear increases up to %20 when the uniform vertical component is included to dynamic response analysis.

- The effect of spatially varying ground motion with three component is more significant than uniform vertical excitation. According to the dynamic response analysis results, the spatially correlated ground motion increases base shear up to 32%.

  It is difficult to measure the effect of horizontal and vertical spatial variation separately as the horizontal force of a friction pendulum is directly dependent to axial load on isolator and lateral displacement. Therefore, it should be considered that the earthquake ground motion is not uniformly distributed in all three components when calculating the base shear force.

  The increase in base shear force presents a significant concern for the design of structural elements and the overall seismic performance of structures. It has a direct impact on various aspects of structural behavior and can lead to several adverse effects.

  Firstly, the increment in base shear force affects the design of individual structural elements such as beams, columns, and walls. Proper reinforcement detailing, material selection, and sizing of structural elements are crucial to ensure they can withstand the amplified base shear forces.

  Moreover, the increase in base shear force leads to amplifications in story accelerations. This amplification in story accelerations can have detrimental effects on occupant comfort, structural damage, and overall building performance during an earthquake event.

  Additionally, the amplified base shear force contributes to increased story drifts. The lateral displacements experienced by different levels of the structure are directly proportional to the base shear force. Higher base shear forces induce larger inter-story drifts, which can impact the serviceability and functionality of the building.

  To address the implications of increased base shear force, careful attention should be given to the design of structural elements, including appropriate sizing, reinforcement, and detailing. The structural system should be adequately designed

and detailed to withstand the amplified forces and ensure the desired seismic performance.

- The spatial variation of the horizontal component of a structure can lead to the occurrence of torsional forces, which arise from the time lag along the transverse direction. When the horizontal component of a structure varies across its spatial extent, different sections experience varying degrees of displacement or acceleration at any given time. This temporal discrepancy in motion causes a time lag along the transverse direction.

  These torsional forces become a significant consideration in the design of structural members. When considering the spatial variation of ground motion, designing structural members to withstand torsional forces requires careful examination.
- It was observed that the spatial variations did not have a significant effect on the maximum displacement demands of the friction pendulum isolator. The total displacement demand did not vary significantly for different cases.

5.2. Future Works

The local soil effects have not been investigated within the scope of this study. Base isolated buildings can be very long in plan, so the soil properties can vary along the length of the foundation. It is known that changes in local soil properties can have an effect on spatially varying ground motion. The local site effect can be taken into account in future studies.

Within the scope of this study, a comprehensive investigation was conducted to assess the effects of the vertical component and spatial variation of earthquake ground motion on the overall response of a base isolated structure and its individual structural components. The primary focus was on understanding the behavior and response of the structure under these specific conditions. The study specifically examined the effect of the vertical component on the axial loads acting on isolators and columns, as well as the distribution of base shear force and the formation of torsional moments. These aspects were deemed crucial for assessing the structural integrity and performance of

the base isolated system. However, it is important to note that the study did not focus on the specific design considerations of friction pendulum isolators or other structural elements. Nevertheless, the observed increase in axial loads on isolators and columns necessitates careful consideration during the structural design phase. Based on the findings of this study, it is recommended that the design of friction pendulum isolators and other relevant structural elements should be adjusted to account for the increased loads occurred under the influence of the vertical component and its spatial variation. Future research can focus on investigating specific design modifications and strategies that can effectively address the challenges posed by the increased loads induced by the spatially varying vertical component of earthquake ground motion.

The findings of this study highlight the significant influence of the spatial variation of the vertical component of earthquakes on structural design. It has been observed that the variations in the vertical ground motion can have notable implications for the behavior and response of the structure. However, one important aspect that remains unexplored is the interaction between the spatially varying vertical component and the vertical vibration modes of the superstructure. Further investigation is required to understand how the spatially varying vertical component interacts with the vertical vibration modes of the structure. This interaction can potentially affect the dynamic characteristics and response of the system, including the distribution of internal forces. Expanding the scope of the study to include analysis of different vertical modes would be beneficial. By considering various vertical vibration modes, a more comprehensive understanding of the system's response can be achieved.

The sample structures studied on within the scope of this study do not have torsional irregularities, and they are symmetric in plan. However, as torsional irregularities can be eliminated in base isolated buildings, they can be designed in different geometric shapes. These buildings can take forms such as L-shaped, T-shaped, and so on. In buildings with such geometries, the spatial variation of the horizontal components of ground motion can have more critical implications.

REFERENCES

Ahmed, K., D. Kim, and S.H. Lee, 2018, "Effect of the Incoherent Earthquake Motion on Responses of Seismically Isolated Nuclear Power Plant Structure", *Earthquakes and Structures*, Vol. 14, No. 1, pp. 33-44.

Alam, M.I. and D. Kim, 2014, "Spatially Varying Ground Motion Effects on Seismic Response of Adjacent Structures Considering Soil-Structure Interaction", *Advances in Structural Engineering*, Vol. 17, No.1, pp. 131-142.

Bai, F., H. Hao and H. Li, 2010, "Seismic Response of a Steel Trussed Arch Structure to Spatially Varying Earthquake Ground Motions Including Site Effect", *Advances in Structural Engineering*, Vol. 13, No. 6, pp. 1089-1103.

Box, G.E., G.M. Jenkins, G.C. Reinsel and G.M. Ljung, 2015, *Time Series Analysis: Forecasting and Control*, John Wiley and Sons.

Bridgestone Corp, 2022, https://www. bridgestone. com/ products/ diversified/ anti-seismic _rubber/ product.html, accessed on April 15, 2023.

Burg, J.P., 1975, *Maximum Entropy Spectral Analysis*, Stanford University.

Constantinou M., A. Mokha and A. Reinhorn, 1990, "Teflon Bearings in Base Isolation II: Modeling", *Journal of Structural Engineering*, Vol. 116, No. 2, pp. 455-474.

Constantinou M., A. Mokha, A. Reinhorn and V.A. Zayas, 1991, "Experimental Study of Friction Pendulum Isolation System", *Journal of Structural Engineering*, Vol. 117, No. 4, pp. 1201-1217.

Dacheng Rubber Co., 2023, http://www.zqdcrubber.com/Products/, accessed on March 17, 2023.

Deodatis, G., 1996, "Non-Stationary Stochastic Vector Processes: Seismic Ground Motion Applications", *Probabilistic Engineering Mechanics*, Vol. 11. No. 3, pp. 149-168.

Deodatis, G., 1996, "Simulation of Ergodic Multivariate Stochastic Processes", *Journal of Engineering Mechanics*, Vol. 122, No. 8, pp.1378-1399.

EPS Corp., 2023, https://www.earthquakeprotection.com/triple-pendulum, accessed on February 17, 2022.

Fujita, K., S. Yoshitomi, M. Tsuji and I. Takewaki, 2008, "Critical Cross-Correlation Function of Horizontal and Vertical Ground Motions for Uplift of Rigid Block", *Engineering Structures*, Vol. 30, No. 5, pp. 1199-1213.

Hao, H., 1989, *Effects of Spatial Variation of Ground Motions on Large Multiply-Supported Structures*, Earthquake Engineering Research Center, University of California Berkeley, CA.

Hao, H., C.S. Oliveira, J. Penzien, 1989, "Multiple-station Ground Motion Processing and Simulation Based on Smart-1 Array Data", *Nuclear Engineering and Design*, Vol. 111, No. 3, pp. 293-310.

Harichandran, R.S. and E.H. Vanmarcke, 1986, "Stochastic Variation of Earthquake Ground Motion in Space and Time", *Journal of Engineering Mechanics*, Vol. 112, No. 2, pp. 154-174.

Heysami, A. S.A. Razavi and N. Farasat, 2015, "Evaluation of Seismic Performance for Bridges Isolated with Lead-Rubber Seismic Isolator Bearing", *Journal of Applied Environmental and Biological Sciences (JAEBS)*, Vol. 5, No. 12, pp. 804-810.

Jankowski, R., 2012, "Non-Linear FEM Analysis of Pounding-Involved Response of Buildings Under Non-Uniform Earthquake Excitation", *Engineering Structures*, Vol. 37, pp. 99-105.

Kameda, H. and H. Morikawa, 1994, "Conditioned Stochastic Processes for Conditional Random Fields", *Journal of Engineering Mechanics*, Vol. 120, No. 4, pp. 855-875.

Kelly J.M., 1994, *The Implementation of Base Isolation in the United States*, Earthquake Engineering Tenth World Conference, California at Berkley, USA.

Konakli, K. and A. Der Kiureghian, 2012, "Simulation of Spatially Varying Ground Motions Including Incoherence, Wave-Passage and Differential Site-Response Effects", *Earthquake Engineering and Structural Dynamics*, Vol. 41 No. 3, pp. 495-513.

Landi, L., G. Grazi and P.P. Diotallevi, 2015, "Comparison of Different Models for Friction Pendulum Isolators in Structures Subjected to Horizontal and Vertical Ground Motions", *Soil Dynamics and Earthquake Engineering*, Vol. 81, pp. 75-83.

Liao, S. and A. Zerva, 2006, "Physically Compliant, Conditionally Simulated Spatially Variable Seismic Ground Motions for Performance[U+2010]Based Design", *Earthquake Engineering and Structural Dynamics*, Vol. 35, No. 7, pp. 891-919.

Loghman, V., F. Khoshnoudian and M. Banazadeh, 2015, "Effect of Vertical Component of Earthquake on Seismic Responses of Triple Concave Friction Pendulum Base Isolated Structures", *Journal of Vibration and Control*, Vol. 21, No. 11, pp. 2099-2113.

Mylonakis, G., S. Nikolaou, and G. Gazetas, 2006, "Footings Under Seismic Loading: Analysis and Design Issues with Emphasis on Bridge Foundations", *Soil Dynamics and Earthquake Engineering*, Vol. 26, No. 9, pp. 824-853.

Naderzadeh, A. 2009, "Historical Aspects of Seismic Base Isolation Application", *Proceedings of the 15th International Symposium on Seismic Response Controlled Buildings for Sustainable Society*, Vol. 16, pp. 18-39.

Naeim F. and J.M. Kelly, 1999, *Design of Seismic Isolated Structures: From Theory to Practice*, Wiley and Sons.

Oiles Corp., 2022, https://www2.oiles.co.jp/en/menshin/building/, accessed on November 15, 2022.

Rao B.P. and R.S. Jangid, 2001, "Experimental Study of Base Isolated Structures", *ISET Journal of Earthquake Technology*, Vol. 38, No. 1, pp. 1-15.

Rodda, G.K. and D. Basu, 2020, "Spatially Correlated Vertical Ground Motion for Seismic Design", *Engineering Structures*, Vol. 206, pp. 191-222.

Ryan K.L. and Dao D., 2015, "Influence of Vertical Ground Shaking on Horizontal Response of Seismically Isolated Buildings with Friction Bearings", *Journal of Structural Engineering*, Vol. 142, No. 1, pp. 15089-15102.

Sayed, M.A., S. Go, S.G. Cho and D. Kim, 2015, "Seismic Responses of Base-Isolated Nuclear Power Plant Structures Considering Spatially Varying Ground Motions", *Structural Engineering and Mechanics*, Vol. 54, No. 1, pp. 169-188.

Shama, A.A., 2007, "Simplified Procedure for Simulating Spatially Correlated Earthquake Ground Motions", *Engineering Structures*, Vol. 29, No. 2, pp. 248-258.

Shinozuka, M. and C.M. Jan, 1972, "Digital Simulation of Random Processes and its Applications", *Journal of Sound and Vibration*, Vol. 25, No. 1, pp. 111-128.

Shinozuka, M. and D. George, 1991, "Simulation of Stochastic Processes By Spectral Representation", *Shinozuka, Masanobu and Deodatis, George*, Vol. 1, pp. 191-204.

Tan R.Y., 1996, "Identification of Dynamic Properties of Isolated Structures", *Engineering Structures*, Vol. 18, No. 3, pp. 240-246.

Teknolojik İzolatör Sistemleri (TIS), 2022, https://www.tis.com.tr/en/products/, ac-

cessed on May 15, 2022.

Ulrych, T.J. and R.W. Clayton, 1976, "Time Series Modelling and Maximum Entropy", *Physics of the Earth and Planetary Interiors*, Vol. 12, No. 2-3, pp. 188-200.

Vanmarcke E.H., E.H. Zavoni, G.A. Fenton, 1989, "Conditional Simulation of Spatially Correlated Earthquake Ground Motion", *Journal of Engineering Mechanics*, Vol. 119, No. 11, pp. 2333-2352.

Ye, J., J. Pan and X. Liu, Vertical, 2011, "Coherency Function Model of Spatial Ground Motion", *Earthquake Engineering and Engineering Vibration*, Vol. 10, No. 3, pp. 403-410.

Zentner, I. 2013, "Simulation of Non-Stationary Conditional Ground Motion Fields in the Time Domain", *Georisk: Assessment and Management of Risk for Engineered Systems and Geohazards*, Vol. 7, No. 1, pp. 37-48.

Zerva, A. and V. Zervas, 2002, "Spatial Variation of Seismic Ground Motions: An Overview", *Applied Mechanics Reviews*, Vol. 55, No. 3, pp. 271-297.